Spring 3-21-2014

Broad Ligand Specificity in the Small Multidrug Resistance Transporter EmrE

Emma Antonina Morrison
Washington University in St. Louis

Recommended Citation

Morrison, Emma Antonina, "Broad Ligand Specificity in the Small Multidrug Resistance Transporter EmrE" (2014). *All Theses and Dissertations (ETDs)*. 1254.
https://openscholarship.wustl.edu/etd/1254

WASHINGTON UNIVERSITY IN ST. LOUIS

Division of Biology & Biomedical Sciences
Molecular Biophysics

Dissertation Examination Committee:
Katherine A. Henzler-Wildman, Chair
Eric A. Galburt
Kathleen B. Hall
Christopher J. Lingle
Timothy M. Lohman
Paul Schlesinger

Broad Ligand Specificity in the Small Multidrug Resistance Transporter EmrE

by

Emma Antonina Morrison

A dissertation presented to the
Graduate School of Arts and Sciences
of Washington University in
partial fulfillment of the
requirements for the degree
of Doctor of Philosophy

May 2014

St. Louis, Missouri

Table of Contents

List of Figures

Chapter I.

Chapter II.

Chapter III.

Chapter IV.

Chapter V.

List of Tables

Chapter II.

Chapter III.

Chapter IV.

Acknowledgements

My graduate experience has been a fulfilling one, owing in large part to the scientific community around me. The Department has offered a great environment for developing scientists. The faculty members are genuinely interested in graduate training, and I would like to thank them, especially the members of my thesis committee, for helpful discussions and equipment usage.

Most importantly, I would like to thank my advisor and mentor. I feel honored to have been Katie’s first graduate student. Katie has a true enthusiasm for science that is infectious. She not only has deep expertise in her area, but also a knowledge that extends widely in the biomedical and basic sciences that I can only strive to emulate. While the lab has grown over the years, Katie has always made the time to discuss scientific research and career concerns with me. Under Katie’s guidance, I feel that I have developed into a much more independent scientist, prepared to take on the next stage in my scientific training. A big thanks to the entire Wildman family for being so welcoming to me over the years. I am thankful to have gotten the chance to be a part of Martha and Tommy’s lives.

As the lab has grown over the years, I have gotten more colleagues in my research. Greg has been instrumental in the training of all NMR students and post docs. Greg, Supratik, and Josh have become good friends as well as lab mates, and I have appreciated all of the scientific and non-scientific conversations that we have had.

I would additionally like to acknowledge the sources that funded my research over the years, which included funds from the Division of Biology and Biomedical Sciences, the Department of Biochemistry and Molecular Biophysics, the National Science Foundation

Graduate Research Fellowship Program (DGE-1143954 to EAM), the National Institute of General Medical Sciences (1R01GM095839 to KAHW), and the Searle Scholars Program (to KAHW).

I have been fortunate to have a number of wonderful scientific mentors over the years. My Dad has always been a major inspiration. He showed my sister and I the fun of science from a young age and has always supported us in whatever direction we might choose to take, even if that was science for both of his daughters. Thank you to Joel Tolman, who took me into his lab when I was only a freshman and a novice. Thank you to Bertrand García-Moreno and David Draper, who mentored and advised me in my scientific path in college and beyond. Thank you to Tim Lohman and Rohit Pappu, whose labs I rotated through. I am deeply appreciative of the support that Dr. Lohman continued to give me in Katie's lab—for the scientific discussions and the usage of a whole host of lab equipment.

I would like to thank my St. Louis friends for just being awesome. I would not have made it through graduate school without them, especially Jay, Joe, Josh, and Stephanie. They are a wonderful group of supportive people and we have had a lot of fun times together. Climbing has given me an outlet for stress and the opportunity to meet a diverse group of amazing people. I have had the opportunity to travel to many incredible places with these friends. The friends that I have made in St. Louis make it extremely difficult to leave the city.

Finally, I would like to thank my family for their constant support. I am very fortunate to be a part of a close, loving family. Although distance has separated us over the years, it has only strengthened our family, and I owe everything to them.

Dedication

To my parents, who have always supported and inspired me. They are the two people in my life who have always been there for me and always will be, no matter where life takes us.

ABSTRACT OF THE DISSERTATION

Broad Ligand Specificity in the Small Multidrug Resistance Transporter EmrE

by

Emma Antonina Morrison

Doctor of Philosophy in Biology and Biomedical Sciences

Molecular Biophysics

Washington University in St. Louis, 2014

Professor Katherine A. Henzler-Wildman, Chair

EmrE, an *E. coli* small multidrug resistance transporter, effluxes a diverse range of toxic polyaromatic cations, thus imparting resistance to drug compounds of this type. Transporters must interconvert between inward- and outward-facing structures during the transport cycle to alternate access of its binding site between the two sides of the membrane. As a secondary active antiporter, EmrE must couple drug binding to this conformational exchange and its energy source, the proton gradient across the inner membrane. The transport cycle involves the import of two protons to drive the export of one substrate molecule. As a multidrug resistance transporter, EmrE has particularly broad specificity and a large variation in affinities for these transported substrates, yet all substrates must trigger the same conformational change between inward- and outward-facing states in order for transport to occur. My research focuses on this coupling between substrate binding and conformational exchange and the functional outcome of this coupling, transport.

As one of the smallest transporters, EmrE serves as an ideal system to study the minimal requirements for multidrug recognition and transport. EmrE transports polyaromatic cations that vary in geometry (i.e. planar vs. tetrahedral), charge (i.e. $^{+}1$ vs. $^{+}2$), and overall size. By combining a variety of biophysical techniques, I have investigated the thermodynamics and kinetics of broad substrate recognition and the conformational interconversion that it triggers. In particular, I have focused on two ligand series: i) a series of related tetrahedral ligands with an identical charge of $^{+}1$, and ii) a series of planar ligands that vary in size and charge. EmrE binds these substrates with affinities that span several orders of magnitude and transports them with varying efficiency. We have directly monitored conformational exchange in substrate-bound EmrE using ZZ-exchange NMR spectroscopy and found that the rate of this key step in transport varies considerably with the identity of the bound ligand. These studies have interesting implications for the energetics of the transport cycle. Substrate binding alters both the ground and transition state energies of EmrE. A common theme has emerged in the literature suggesting that enzymes pre-sample their functional motions in the absence of substrate. However, to be a functional antiporter, EmrE cannot interconvert in the absence of substrate. Thus, the protein alone cannot determine the barrier to exchange between the inward- and outward-facing states, and substrate must play an important role.

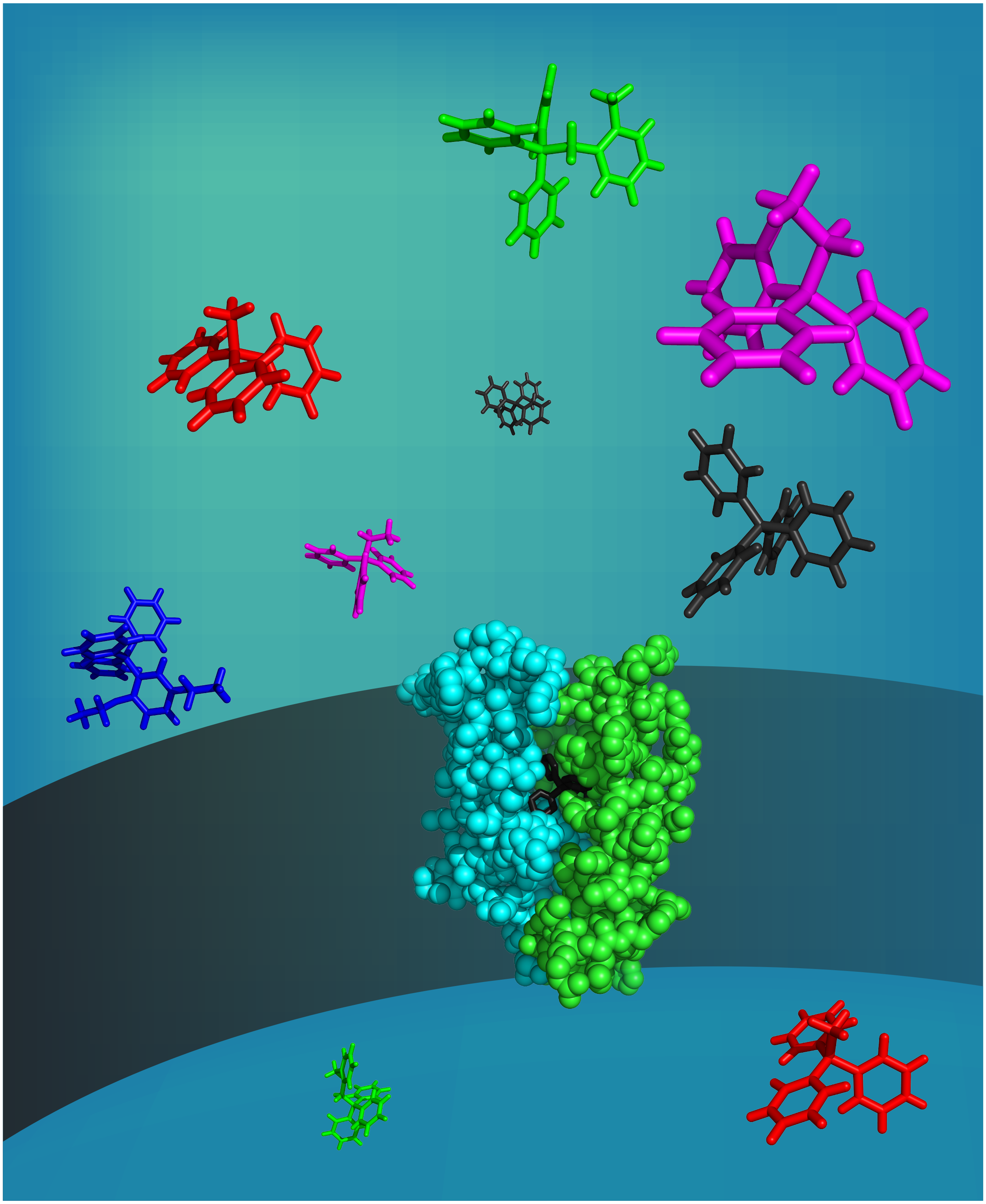

Chapter I. Introduction: The small multidrug resistance transporter EmrE.

Drug resistance, especially multidrug resistance, is a significant challenge to global health[1,2]. The main mechanisms of drug resistance include modification of the target protein, metabolism of the drug, and decrease in drug uptake, either through decreased permeability or through active efflux[1,3]. Multidrug resistance (MDR) transporters fit into this last category and play an essential role in the development of some forms of clinical drug resistance, especially multidrug resistance[1]. To gain insight into the mechanism of multidrug efflux, I have focused my studies on the MDR transporter EmrE. As one of the smallest known transporters, EmrE serves as an ideal system to study the minimal requirements for multidrug recognition and transport.

Single-Site Alternating-Access Transport

In order to efflux drug molecules from the cytoplasm, MDR transporters, as with most transporters, must move the substrate against its concentration gradient. As a protein open to both sides of the membrane simultaneously would dissipate this gradient and in effect import drugs into the cell, the transporter must alternate the access of its binding site between the two sides of the membrane[4]. In addition, these transporters must have an energy source to move these compounds against their concentration gradient, either the hydrolysis of ATP (primary active transport) or an ion gradient (secondary active transport). Structures exist for MDR transporters of four different superfamilies: the ATP-binding cassette (ABC) family, driven by ATP hydrolysis, and the major facilitator superfamily (MFS), resistance-nodulation-division (RND), and small multidrug resistance (SMR) families, all driven by ion gradients[1]. MDR transporters must be able to tightly couple the binding of substrate to the conformational change and the energy source in order to perform active transport.

Secondary active transporters use the downhill movement of an ion (H^+ or Na^+) as the driving force for the uphill movement of the substrate. These transporters can either be symporters or antiporters, which move the substrate and driving-force ion across the membrane in the same or opposite directions, respectively. These two types of transport have different mechanistic requirements within the alternating-access model[5]. To carry out successful symport, a transporter must only undergo a conformational interconversion when bound to none or both of its substrates (**Fig. 1A**). On the other hand, to carry out successful antiport, a transporter must be able to undergo its conformational interconversion when bound to either its substrate or the driving-force ion but not in its truly apo state (**Fig. 1B**). This latter mechanism is also referred to as the single-site alternating-access model for transport.

Multidrug Recognition

Multidrug recognition evolved independently into the structural framework of a handful of different superfamilies of transporters in addition to the transcription factors that regulate their expression[1]. The mechanism of multidrug recognition has intrigued researchers for decades. Most well-studied protein-ligand interactions involve highly specific recognition: a ligand with a well-defined chemical moiety binds in a well-defined protein cavity in a well-defined orientation. But multidrug proteins recognize a wide range of chemically and structurally diverse compounds without being entirely nonspecific or promiscuous. Each transporter or regulator does have a limit to which drug compounds it can bind, and transport activity can vary significantly between structurally related compounds, so there must be some form of recognition[6]. Are there common principles governing ligand recognition across the MDR transporters and MDR regulators?

Limited structural studies have provided insight into the mechanism of multidrug recognition. Due to the technical difficulties associated with structural investigations of membrane proteins, many important insights have been gained from the soluble MDR regulators in addition to studies of MDR transporters[1,6,7]. The canonical MDR protein has a large, flexible binding pocket, with multiple subsites for coordinating different drugs[7]. This is typified by the transcription factor QacR, which has been shown to bind different drugs, including proflavin and ethidium, at distinct subsites wherein the different compounds interact with distinct residues[1]. QacR can even accommodate these two ligands concurrently within the single, large pocket[1,8] (**Fig. 2A**). The RND transporter AcrB has also been crystallized with multiple drugs. These structures indicate that monocyline and doxorubicin bind in distinct but overlapping subsites (**Fig. 2B**)[9]. Several members of the ABC and MFS transporter families have also been shown to be capable of binding multiple drug molecules simultaneously in different subsites[1], offering additional support for the canonical view of MDR ligand recognition by a large, flexible binding pocket.

Hydrophobic interactions and electrostatic interactions with active-site acidic residue(s), in addition to the architecture of the protein binding site and the structure of the small molecule, all play a role in the broad substrate specificity[6]. There is a high content of aromatic residues in the binding pockets of MDR transporters and regulators. These key residues are involved in π-hydrophobic, π-π, and π-cationic interactions[1,7]. Polar and charged residues are key in stabilizing drug charge and polar moieties. Studies of QacR have revealed that the sidechains of these residues adopt different rotameric states depending upon the bound drug[7].

Proteins that bind hydrophilic compounds must form specific hydrogen bonds and electrostatic and hydrophobic interactions in order for the small molecule to bind the protein preferentially over water, which in effect creates a highly specific binding site[6]. On the other hand, there are fewer demands placed on a protein that needs to out-compete water for binding of a hydrophobic molecule[6].

As described above, the canonical MDR transporter has a large, hydrophobic binding pocket with multiple, potentially overlapping, subsites[1,6], but what about a small transporter? As described in more detail below, the small multidrug resistance transporters, typified by EmrE, have a single, smaller binding site. How can a single small protein accommodate a wide range of ligands in its binding pocket and transport them all?

EmrE, an *E. coli* Small Multidrug Resistance Transporter

EmrE is a representative member of the small multidrug resistance (SMR) family of transporters. This family comprises the smallest multidrug transporters, and its members are found only in prokaryotes[1]. SMR transporters have 100-140 amino acids that form four transmembrane (TM) helices connected by short loops and lacking any significant extramembrane domains[1,10]. Members of this family have minimal functional units of dimers and form either homo- or heterodimers. SMRs provide resistance to quaternary ammonia compounds and other lipophilic cations[10].

EmrE is a homodimeric SMR that is native to *E. coli* and exploits the proton gradient across the inner membrane to drive efflux of polyaromatic cations via the single-site alternating-access model for transport[11]. These substrates span a range of traits: they can be $^{+}$1- or $^{+}$2-

charged, planar or tetrahedral, and a range of overall sizes. The transport stoichiometry is 2 H^+:1 drug molecule stoichiometry, regardless of ligand charge[12].

Biochemical studies have determined the functional relevance of many key residues in EmrE (**Fig. 3**). An active site glutamate is essential for transport function. Glu14, located in TM1, is the only one of eight charged residues to be located within the transmembrane domain and is conserved across all SMRs. E14D is the only mutant of this critical residue that is known to retain any function, and it has highly compromised activity[11]. This membrane-imbedded glutamate has a highly elevated pK_a, variously estimated to lie between 7.3 and 8.5[13-15], which poises proton binding and release around physiological pH. TM1 contains a handful of other residues on the same helical face as Glu14 that are key in substrate binding and transport. The residues Leu7, Ala10, Ile11, Gly17, and Thr18 are important in binding, and Ala10 is also important in coupling proton and drug transport[11]. Aromatic residues are also important for substrate binding. They are thought to stabilize substrate interactions by stacking with aromatic regions of the drugs and through cation/π interactions[11]. Trp63, Tyr40, and Tyr 60 are key aromatic residues for the binding of substrate, and Tyr4 is important in proton-drug coupling in transport[11].

As previously mentioned, the minimal functional unit of EmrE is a dimer, which is supported by a variety of biochemical experiments[11]. A glycine motif in TM4 is essential for dimerization. Gly90 and Gly97 are separated by six non-glycine residues, forming a GG7 motif. Within this motif, residues 93 and 94 are large hydrophobic amino acids in most SMRs, including EmrE. This GG7 motif is instrumental in forming contacts between the two monomers[11,16].

Structural Studies of EmrE

The existing structures for EmrE are of only medium resolution. The first structure of EmrE was determined bound to TPP^+ using electron cryomicroscopy (cryo-EM), with a resolution of 7.5 Å in the plane of the membrane bilayer and 16 Å perpendicular to the bilayer plane[17,18]. A 3.8 Å x-ray crystal structure of TPP^+-bound EmrE overlays well with the cryo-EM density map[19] (**Fig. 4A,C**). EmrE was crystallized in nonylglucoside for the x-ray crystal structure, but EmrE solubilized in this detergent has compromised activity. The binding affinity for TPP^+ is weakened by an order of magnitude when compared with the DDM-solubilized reference state[19]. On the other hand, the cryo-EM structure was determined in a crystalline DMPC bilayer, which binds substrate properly[20]. For this reason, despite its low resolution, the cryo-EM structure is considered the "gold-standard" for the EmrE structure[21,22].

Fleishman, et al. computationally designed a C_α model of the transmembrane region of EmrE based on the cryo-EM data and sequence conservation data (**Fig. 4B**)[23]. The individual amino acids were not resolved in the cryo-EM structure, nor could the TM helices be assigned ambiguously. However, Fleishman, et al. used the quasi symmetry relationship between six of the eight TM helices of the dimer, along with the single connection between two TM helices apparent in the cryo-EM density map and the spatial positions of the eight helices. They combined these features of the cryo-EM structure with evolutionary conservation, i.e. that conserved residues are buried in the protein core while variable positions are exposed to lipid, in order to predict a C_α structural model[23].

The structure determined via x-ray crystallography is strikingly similar to the Fleishman computational model, as shown by the 1.4 Å average rmsd over equivalent C_α [19]. From both structures, it is clear that EmrE crystalized as an asymmetric homodimer, with six transmembrane (TM) helices forming the substrate binding pocket and the remaining two helices forming a dimerization arm[17-19]. ^{13}C chemical shift data from solid state NMR studies indicates that the active site residue Glu14 has two sets of peaks, supporting this structural asymmetry[24]. Although the topology could not be determined from the cryo-EM structure with certainty, the only symmetry relationship in that data is the pseudo-two-fold rotation axis in the bilayer plane, which implies an antiparallel dimer[17]. Three TM helices from each monomer overlay well with each other after a 160° rotation about this pseudo-two-fold axis of symmetry. The two TM helices that form the dimerization arm have a 20° tilt at this point[18,22]. The x-ray crystal structure showed clear electron density for the loops connecting the four helices in each monomer. In addition, selenomethionine labeling confirmed an antiparallel topology, as the positions of the labels on the two monomers were related by a pseudo two-fold rotation axis[19].

Although the majority of the side chains were not resolved in the x-ray crystal structure, the position of the backbone places biochemically important residues in the active site[19]. The structure of the dimer showed that it allowed access to substrate from either one water-exposed face of the protein or the membrane leaflet on the same side of the bilayer while shutting off access to the other leaflet[17], suggesting that EmrE was captured in the open-in or open-out state of the alternating-access mechanism.

The model proposed by Fleishman, et al. suggests a mechanism of conformational interconversion. The two monomers swap conformations upon conversion of the dimer from the inward- to outward-facing structure. In this model, the open-in and open-out states are identical structures that differ only in which side of the membrane they are open to. These two states are related by a 180° rotation around an axis in the plane of the membrane bilayer. During exchange between open-in and open-out states, TM1-TM3 from the two monomers move as a single unit.

On the other hand, the two TM4s form a stable pair, stabilized in part by G90 and G97 packing, and do not appear to move much during the conformational exchange. The interface between TM3 and TM4, representing the connection between the substrate binding pocket and translocation pathway and the dimerization arm, is smaller than the other helix-helix interactions. The crossing-angles between TM3 and TM4 change by approximately 20° upon conformational interconversion as TM3 alternates between a kinked and straightened structure. There is a small translation of the TM1-TM3 bundle with respect to TM4 between the two states. As keenly noted by Fleishman, et al., the dual topology of EmrE has distinct advantages for transport mechanism. Dual topology allows the open-in and open-out structures to be identical, which requires the evolution of only a single optimized low energy structure[23].

Attempts have also been made to acquire structural information on drug-free forms of EmrE. 2D crystals in DMPC for cryo-EM studies were obtained for both drug-free and TPP^+-bound forms of EmrE, but the crystals formed in the presence of substrate were more highly ordered[17]. The cryo-EM 2D projection map is very similar in the presence and absence of TPP^+ [17,25] and suggests that binding of drug results in movement of at least one helix[25]. However, there is not a full 3D cryo-EM structure for drug-free EmrE. The only full structure for a drug-free form of EmrE is a 4.5 Å x-ray crystal structure that is widely considered to be non-physiological (**Fig. 4D**)[19,22]. This structure was acquired on EmrE that was crystallized in nonylglucoside at pH 4. The protein is thought to be acid-denatured, but still has 4TM helices per monomer. TM1-TM3 form a three helix bundle, which packs with the three-helix bundle from a second monomer. However, TM4 lies within the bilayer plane rather than passing through it[19]. As this helix forms the bulk of the crystal contacts in the eight-monomer asymmetric unit, it is still seen as an indication that TM4 is the key player in dimerization[22].

EPR studies were carried out to investigate the structure and dynamics of both the drug-free and TPP^+-bound forms of EmrE in a full lipid bilayer[26]. Spin labels were systematically placed on each residue in the protein using single cysteine mutants to assess spin label dynamics, lipid and water accessibility, and pairwise short range distances. The periodicity in the accessibility data supports four TM helices per monomer, and dipolar coupling between spin labels within the dimer support the packing of TM1-TM3 from each monomer, as seen in the crystal structures. However, the data is not consistent with tight packing between TM4s, which is thought to be the driving force for dimerization. The EPR data indicates that the drug-free state is highly dynamic with at least two spin label populations, one that is consistent with an antiparallel dimer. This TPP^+-free state was identified as the protonated form, but with samples collected at pH 7.5, it was likely to be a mixture of protonated and deprotonated EmrE. Perhaps this mixture accounts for the two observed populations. Nevertheless, the flexibility in the drug-free state supports that idea that a dynamic apo state may contribute to broad ligand specificity. The EPR data indicates that, upon binding TPP^+, EmrE undergoes conformational changes including a repacking of TM1, a tilting of TM2, and changes in the backbone of TM3 and the TM3-TM4 loop. No significant changes were observed in TM4, which is consistent with the idea that ligand does not interact directly with TM4. In addition, the EPR data is consistent with a kink in TM3, as observed in the x-ray crystal structure and Fleishman's model. Despite the general agreement with some of the broad structural features of the crystal structure, the EPR data has significant differences from the crystal structure of TPP^+-bound EmrE, some of which might be explained by the low resolution of the crystal structure[26].

Recently, an *in vivo* tryptophan scan was carried out to test features of the structures derived from EmrE crystallized out of membrane mimetic environments[27]. Mutation of single residues within the TM helices to bulky tryptophan side chains will perturb structure and negatively affect function if placed in a buried (rather than lipid-exposed) region of the protein. A total of 60 individual mutations were made across all four TM helices. Tryptophan-scanning mutagenesis was accompanied by ethidium-resistance assays to assess function *in vivo*. The functional results were in good agreement with lipid exposure determined from coarse-grained MD simulations based on the x-ray crystal structure. All but one of the instances where the functional effects of the mutation did not correlate with lipid accessibility could be explained by location within the predicted structural and other biochemical data. The results were not compatible with the only parallel structural model that has been published, which was based on sequence conservation and crosslinking data, because residues that were predicted to be essential for the dimer interface in the model are not affected by mutation to tryptophan[27,28].

Topology of the EmrE Dimer is Controversial

Although the existing structural data consistently suggests an antiparallel topology, the biochemical evidence has variously suggested parallel or antiparallel topology. The concept of dual topology, or an antiparallel homodimer, is highly controversial, in part due to the implications for the synthesis and insertion of integral membrane proteins and membrane protein evolution.

Several decades ago, von Heijne noted the bias for more positively charged residues (lysine and arginine) to be on interior loops and termini over exterior loops and termini and introduced the ‘positive-inside rule’[29] for topology determination of integral membrane proteins. The von Heijne lab has explored the *in vivo* relation of topology to charge distribution in small bacterial membrane proteins, including SMRs, using the C-terminal fusion reporters GFP (fluorescent in the cytoplasm) and PhoA (active in the periplasm). Single charge mutations were shown to alter the reporter activity and thus the topology of predicted dual topology homodimers such as EmrE. As a control, the paired gene SMR YdgE/YdgF, which has a strong and opposite charge bias between the two proteins, did not change topology with single charge mutations. Genes in the SMR family, as well as a few other families, occur as pairs in close proximity or singletons. The paired genes have strong topological charge determinants, with the members of each pair biased for opposite orientations. In contrast, the singletons do not have a strong charge bias, and thus likely have dual topology[30].

Ethidium resistance assays were carried out to investigate which topological forms of EmrE, created by altering the charge bias, are functional. EmrE was mutated to change the K+R charge bias and form N_{in}-C_{in} and N_{out}-C_{out} forms. Expressed alone, each charge-biased mutant no longer offered resistance to ethidium. However, co-expression of the two mutants recovered resistance, suggesting that the engineered heterodimer formed a functional antiparallel dimer, but that each mutant alone was not capable of forming a functional unit[31]. Even the addition of a single positively charged residue to various positions on EmrE can alter the topology[32].

Additionally, the Schuldiner lab has carried out various biochemical assays, such as crosslinking, tagging, and genetic fusions, to investigate the topology of EmrE. Schuldiner has asserted that the biochemical equivalence of residues between the two monomers, indicated by the accessibility of active-site residue Glu14 and cysteines introduced in the TM region to chemical modification in the presence and absence of ligand, implies a parallel topology[11]. To assess the topology in cells, membrane permeable and impermeable sulfhydryl reagents were added to cells expressing single-cysteine mutants of EmrE. A cysteine-reactive fluorescent probe was then added to EmrE purified out of these samples to detect any unreacted cysteines.

These assays indicated that EmrE exits only in an N_{in}-C_{in}, and thus parallel, orientation[33]. To assess functionality, purified EmrE crosslinked with o-PDM, which has a short linker and should only cross-link single-cysteine EmrE mutants if they have parallel topology, binds and transports substrate properly[11].

Genetically fused dimers were designed to force either a parallel or antiparallel dimer and allow the functionality of each topology to be tested. Parallel fusions were made by inserting a short, hydrophilic linker between the C-terminus of the first repeat and the N-terminus of the second repeat. Antiparallel fusions were designed by inserting a ninth TM helix (from glycophorin A) between the C-terminus of the first repeat and the N-terminus of the second repeat. Both the parallel- and antiparallel-fused dimers transport monovalent and divalent substrates properly[11,34]. To reconcile these mixed results, it has more recently even been proposed that EmrE can function as both a parallel, in both N_{in}-C_{in} and N_{out}-C_{out} forms, and antiparallel homodimer[35]. Another recent paper has supported this claim that both parallel and antiparallel forms can exist, but that the antiparallel homodimer is more stable and is the functional form[36]. It is difficult to envision how a protein can function in both topological forms, taking into account the location of the active site and dimerization residues. The functionally relevant residues for ligand binding are on one face of the TM1-TM3 helices and TM4 is important in dimerization.

Both sides of the topology debate can argue for lack of controls or misinterpretation of the biochemical data. It is clear that EmrE topology is highly sensitive to exact sequence and likely also environment. Thus, studies carried out on a mutant may not report on the native topology of EmrE and results may be skewed by the various C-terminal tags commonly used for expression or as topological reporters[11,32]. In addition, the contradictory results arise from experiments performed in different environments. The topological investigations were carried out *in vivo* or on protein purified under different conditions and assayed in detergent or reconstituted into lipids. It has been established that the structure and function of membrane proteins, including EmrE, are sensitive to environment[37-39]. It is clear that more definitive experiments are required to clear up the topological controversy.

Dynamics are Important in Protein Function

How do proteins involved in activities such as signaling and catalysis move between different functionally relevant structures, or conformations? Structural techniques such as X-ray crystallography, cryo-EM, NMR, and small-angle X-ray scattering capture static structures or ensembles of static structures. Adding ligands and changing solution conditions can capture alternative static structures. These different structures may represent distinct low-energy conformational states along a functional pathway. The relative populations, or the relative free energies, of the conformational states describe the thermodynamics of the system, while the energetic barriers describe the kinetics of the system[40]. Proteins that undergo large domain motions move, or exchange, between conformational states that are separated by energetic barriers of several *kT*. These large domain motions occur on the timescale of microseconds-to-seconds and are considered slow timescale motions (**Fig. 5A**). This is the same timescale as most biological processes, and thus these motions may affect functional rates. Each conformational state is actually a collection of substates that are related by local flexibility, such as loop motions, side chain rotations, and bond vibrations. Significantly smaller energetic barriers separate these substates, such that they occur much faster than the larger concerted motions, on the femtosecond-to-nanosecond timescales[40].

NMR spectroscopy is an ideal technique for studying the kinetics of slow and fast timescale motions because it provides atomic resolution and can be carried out under native solution conditions at equilibrium. Microsecond-to-second timescale motions are characterized by the NMR timescale of their exchange. Practically speaking, the NMR timescale determines whether two peaks with intensities proportional to the relative populations of the two states (slow exchange), a single population-weighted peak (fast exchange), or something in between (intermediate exchange) is observed in a spectrum (**Fig. 5B**). The NMR timescale is a comparison of the conformational exchange rate (the sum of the forward and reverse rates, k_{ex}) against the difference in the chemical shifts of the two states ($\Delta\nu$): $k_{ex} \ll \Delta\nu$ (slow exchange), $k_{ex} \approx \Delta\nu$ (intermediate exchange), or $k_{ex} \gg \Delta\nu$ (fast exchange).

My studies focused on the large domain motions necessary to alternate access of the EmrE binding pocket between the intracellular and extracellular sides of the membrane, which is the key motion for transport. As this is a large domain motion, it falls into the millisecond-to-second time regime that can be accessed via NMR experiments such as relaxation dispersion and ZZ-exchange spectroscopy, depending on the exact timescale of the dynamics. As will be described in **Chapters 3 and 4** in more detail, ZZ-exchange spectroscopy was the primary technique used to measure the rate of conformational exchange in ligand-bound EmrE.

ZZ-exchange spectroscopy is used to quantify the rate of two-state exchange occurring on the millisecond-to-second timescale when two peaks are observed in the spectrum[41-43]. For two-state exchange between arbitrary states A and B, the system can be represented by the simple reaction scheme $A \underset{k_{BA}}{\overset{k_{AB}}{\Leftrightarrow}} B$. In the ZZ-exchange experiment, magnetization is initially transferred from the amide ^{1}H to the attached ^{15}N, and the amide nitrogen chemical shift is recorded. A variable-time delay is inserted before transfer of magnetization back to ^{1}H, and the chemical shift of the attached proton is then recorded (**Fig. 6A,C**). During the variable-time delay, magnetization is stored as in-phase magnetization along *z* (i.e. parallel to the magnetic field)[41] so that it is only subject to the slower longitudinal (T1) relaxation. This permits extended mixing times to be used for the measurement of slow dynamics.

2D planes are recorded with increasing delay times. In the absence of exchange, the spectrum looks identical to that of a ^{15}N/^{1}H HSQC, with the peak for state A at $^{15}N_A/^1H_A$ and the peak for state B at $^{15}N_B/^1H_B$ (**Fig. 6A,B**). When proper care is taken to eliminate other forms of relaxation (i.e. due to cross-correlation between ^{1}H-^{15}N dipole and ^{15}N CSA), magnetization decays monoexponentially according to T1 during the mixing time. If the system is in exchange, then there is the possibility that the amide will convert from state A to state B (or vice versa) before the magnetization is transferred from the amide nitrogen to its attached proton (*i.e.* during the mixing time). The probability that this event will take place prior to the magnetization transfer is related to the delay time and the rate of exchange. If this exchange occurs, then a peak for this amide will appear at $^{15}N_A/^1H_B$ (or $^{15}N_B/^1H_A$ in the alternative case). Thus, auto-peaks ($^{15}N_A/^1H_A$, $^{15}N_B/^1H_B$) will decay and cross-peaks ($^{15}N_A/^1H_B$, $^{15}N_B/^1H_A$) will grow in as the delay time increases (**Fig. 6A,B**).

A TROSY-selected ZZ-exchange experiment by Li and Palmer extends the application of ZZ-exchange experiments to large systems (**Fig. 6C**)[43]. In this version of the experiment, the slowly relaxing narrow TROSY component of the ^{15}N magnetization, $S_Z I_\beta$ (where S is ^{15}N and I is ^{1}H), is selected for in both the mixing and frequency encoding periods of the pulse sequence. During the mixing period, the selected spin state, $S_Z I_\beta$, is longitudinal magnetization as before, and evolves as:

$$\frac{d}{dt}\begin{bmatrix} S_Z I_\beta{}^A \\ S_Z I_\beta{}^B \end{bmatrix} = \begin{bmatrix} -R^{*A} - k_{AB} & k_{BA} \\ k_{AB} & -R^{*B} - k_{BA} \end{bmatrix} \begin{bmatrix} S_Z I_\beta{}^A \\ S_Z I_\beta{}^B \end{bmatrix}$$

where the intrinsic relaxation for each state is given by $R^* = \overline{R_1} - \eta_Z$. Here, $\overline{R_1}$ is the average of the ^{15}N and two-spin order relaxation rates, and η_Z is the longitudinal ^{15}N-^{1}H dipole/^{15}N chemical shift anisotropy cross-correlated relaxation rate. The pulse sequence is designed to ensure that, in the absence of exchange, the decay of the selected $S_Z I_\beta$ magnetization is essentially monoexponential. Thus, in the presence of exchange, the full solutions to the time-dependent change in autopeak intensity (I_{AA} and I_{BB}) and crosspeak intensity (I_{AB} and I_{BA}) from their initial intensities (I_A^0 and I_B^0) are given by:

$$I_{AA}(t) = I_A^0 \left[(R^{*A} + k_{AB}) \left(\frac{e^{-\lambda_1 t} - e^{-\lambda_2 t}}{\lambda_1 - \lambda_2} \right) + \left(\frac{\lambda_1 e^{-\lambda_2 t} - \lambda_2 e^{-\lambda_1 t}}{\lambda_1 - \lambda_2} \right) \right]$$

$$I_{BB}(t) = I_B^0 \left[(R^{*B} + k_{BA}) \left(\frac{e^{-\lambda_1 t} - e^{-\lambda_2 t}}{\lambda_1 - \lambda_2} \right) + \left(\frac{\lambda_1 e^{-\lambda_2 t} - \lambda_2 e^{-\lambda_1 t}}{\lambda_1 - \lambda_2} \right) \right]$$

$$I_{AB}(t) = I_A^0 \left[\left(\frac{k_{AB} e^{-\lambda_2 t} - k_{AB} e^{-\lambda_1 t}}{\lambda_1 - \lambda_2} \right) \right]$$

$$I_{BA}(t) = I_B^0 \left[\left(\frac{k_{BA} e^{-\lambda_2 t} - k_{BA} e^{-\lambda_1 t}}{\lambda_1 - \lambda_2} \right) \right]$$

where

$$\lambda_1 = \frac{(R^{*A} + R^{*B} + k_{AB} + k_{BA})}{2} + \frac{1}{2}\sqrt{(R^{*A} - R^{*B} + k_{AB} - k_{BA})^2 + 4k_{AB}k_{BA}}$$

$$\lambda_2 = \frac{(R^{*A} + R^{*B} + k_{AB} + k_{BA})}{2} - \frac{1}{2}\sqrt{(R^{*A} - R^{*B} + k_{AB} - k_{BA})^2 + 4k_{AB}k_{BA}}$$

This allows the quantification of two-state exchange in a large system, such as a membrane protein in a membrane-mimetic environment.

Scope of Thesis

In the chapters that follow, I will detail the bulk of the work that I have performed during my graduate studies, in conjunction with some supporting studies carried out by colleagues in the lab. I will start by describing a modification to the EmrE reconstitution procedure that made my thesis work feasible, and then continue on to describe my biochemical and biophysical investigations into the mechanism of multidrug resistance in EmrE. We first directly observed the conformational interconversion between inward- and outward-facing states of EmrE bound to the commonly studied ligand TPP^+, characterized the interconverting states, and carried out our own definitive topological studies. We then proceeded to explore the broad ligand specificity of EmrE by expanding the ligand profile used in our studies and connecting binding, transport, and conformational interconversion. Together, these findings on the EmrE model system provide insight into multidrug efflux.

References:

1. Higgins, C. F. Multiple molecular mechanisms for multidrug resistance transporters. *Nature* **446,** 749–757 (2007).
2. Li, X.-Z. & Nikaido, H. Efflux-mediated drug resistance in bacteria: an update. *Drugs* **69,** 1555–1623 (2009).
3. Hawkey, P. M. The origins and molecular basis of antibiotic resistance. *BMJ* **317,** 657–660 (1998).
4. Jardetzky, O. Simple allosteric model for membrane pumps. *Nature* **211,** 969–970 (1966).
5. Forrest, L. R. & Rudnick, G. The rocking bundle: a mechanism for ion-coupled solute flux by symmetrical transporters. *Physiology (Bethesda)* **24,** 377–386 (2009).
6. Neyfakh, A. A. Mystery of multidrug transporters: the answer can be simple. *Mol. Microbiol.* **44,** 1123–1130 (2002).
7. Wade, H. MD recognition by MDR gene regulators. *Curr Opin Struct Biol* **20,** 489–496 (2010).
8. Schumacher, M. A., Miller, M. C. & Brennan, R. G. Structural mechanism of the simultaneous binding of two drugs to a multidrug-binding protein. *EMBO J* **23,** 2923–2930 (2004).
9. Murakami, S., Nakashima, R., Yamashita, E., Matsumoto, T. & Yamaguchi, A. Crystal structures of a multidrug transporter reveal a functionally rotating mechanism. *Nature*

443, 173–179 (2006).

10. Bay, D. C., Rommens, K. L. & Turner, R. J. Small multidrug resistance proteins: a multidrug transporter family that continues to grow. *Biochim Biophys Acta* **1778,** 1814–1838 (2008).
11. Schuldiner, S. EmrE, a model for studying evolution and mechanism of ion-coupled transporters. *BBA - Proteins and Proteomics* 1–15 (2009). doi:10.1016/j.bbapap.2008.12.018
12. Rotem, D. & Schuldiner, S. EmrE, a multidrug transporter from Escherichia coli, transports monovalent and divalent substrates with the same stoichiometry. *J Biol Chem* **279,** 48787–48793 (2004).
13. Muth, T. R. & Schuldiner, S. A membrane-embedded glutamate is required for ligand binding to the multidrug transporter EmrE. *EMBO J* **19,** 234–240 (2000).
14. Soskine, M., Adam, Y. & Schuldiner, S. Direct evidence for substrate-induced proton release in detergent-solubilized EmrE, a multidrug transporter. *J Biol Chem* **279,** 9951–9955 (2004).
15. Adam, Y., Tayer, N., Rotem, D., Schreiber, G. & Schuldiner, S. The fast release of sticky protons: kinetics of substrate binding and proton release in a multidrug transporter. *Proc Natl Acad Sci USA* **104,** 17989–17994 (2007).
16. Poulsen, B. E., Cunningham, F., Lee, K. K. Y. & Deber, C. M. Modulation of Substrate Efflux in Bacterial Small Multidrug Resistance Proteins by Mutations at the Dimer Interface. *J Bacteriol* **193,** 5929–5935 (2011).
17. Ubarretxena-Belandia, I., Baldwin, J. M., Schuldiner, S. & Tate, C. G. Three-dimensional structure of the bacterial multidrug transporter EmrE shows it is an asymmetric homodimer. *EMBO J* **22,** 6175–6181 (2003).
18. Tate, C. G. Comparison of three structures of the multidrug transporter EmrE. *Curr Opin Struct Biol* **16,** 457–464 (2006).
19. Chen, Y. J. *et al.* X-ray structure of EmrE supports dual topology model. *Proc Natl Acad Sci USA* **104,** 18999–19004 (2007).
20. Ubarretxena-Belandia, I. & Tate, C. G. New insights into the structure and oligomeric state of the bacterial multidrug transporter EmrE: an unusual asymmetric homo-dimer. *FEBS Lett* **564,** 234–238 (2004).
21. Rapp, M., Seppala, S., Granseth, E. & Heijne, Von, G. Controversy over EmrE structure: response. *Science* **317,** 749–750 (2007).
22. Korkhov, V. M. & Tate, C. G. An emerging consensus for the structure of EmrE. *Acta Crystallogr D Biol Crystallogr* **65,** 186–192 (2009).
23. Fleishman, S. J. *et al.* Quasi-symmetry in the cryo-EM structure of EmrE provides the key to modeling its transmembrane domain. *J Mol Biol* **364,** 54–67 (2006).
24. Lehner, I. *et al.* The key residue for substrate transport (Glu14) in the EmrE dimer is asymmetric. *J Biol Chem* **283,** 3281–3288 (2008).
25. Tate, C. G., Ubarretxena-Belandia, I. & Baldwin, J. M. Conformational changes in the multidrug transporter EmrE associated with substrate binding. *J Mol Biol* **332,** 229–242 (2003).
26. Amadi, S. T., Koteiche, H. A., Mishra, S. & McHaourab, H. S. Structure, dynamics and substrate-induced conformational changes of the multidrug transporter emre in liposomes. *J Biol Chem* (2010). doi:10.1074/jbc.M110.132621
27. Lloris-Garcerá, P. *et al.* In Vivo Trp Scanning of the Small Multidrug Resistance Protein

EmrE Confirms 3D Structure Models. *J Mol Biol* (2013). doi:10.1016/j.jmb.2013.07.039

28. Gottschalk, K.-E., Soskine, M., Schuldiner, S. & Kessler, H. A structural model of EmrE, a multi-drug transporter from Escherichia coli. *Biophysical Journal* **86,** 3335–3348 (2004).
29. Heijne, G. The distribution of positively charged residues in bacterial inner membrane proteins correlates with the trans-membrane topology. *EMBO J* **5,** 3021–3027 (1986).
30. Rapp, M., Granseth, E., Seppälä, S. & Heijne, von, G. Identification and evolution of dual-topology membrane proteins. *Nature Publishing Group* **13,** 112–116 (2006).
31. Rapp, M., Seppala, S., Granseth, E. & Heijne, Von, G. Emulating Membrane Protein Evolution by Rational Design. *Science* **315,** 1282–1284 (2007).
32. Seppala, S., Slusky, J. S., Lloris-Garcera, P., Rapp, M. & Heijne, Von, G. Control of Membrane Protein Topology by a Single C-Terminal Residue. *Science* **328,** 1698–1700 (2010).
33. Ninio, S., Elbaz, Y. & Schuldiner, S. The membrane topology of EmrE – a small multidrug transporter from Escherichia coli. *FEBS Lett* **562,** 193–196 (2004).
34. Steiner-Mordoch, S. *et al.* Parallel topology of genetically fused EmrE homodimers. *EMBO J* **27,** 17–26 (2008).
35. Schuldiner, S. Undecided membrane proteins insert in random topologies. Up, down and sideways: it does not really matter. *Trends Biochem Sci* **37,** 215–219 (2012).
36. Lloris-Garcera, P. *et al.* Antiparallel Dimers of the Small Multidrug Resistance Protein EmrE Are More Stable Than Parallel Dimers. *Journal of Biological Chemistry* **287,** 26052–26059 (2012).
37. Seddon, A. M., Curnow, P. & Booth, P. J. Membrane proteins, lipids and detergents: not just a soap opera. *Biochim Biophys Acta* **1666,** 105–117 (2004).
38. Tillman, T. S. & Cascio, M. Effects of membrane lipids on ion channel structure and function. *Cell Biochem Biophys* **38,** 161–190 (2003).
39. Charalambous, K., Miller, D., Curnow, P. & Booth, P. J. Lipid bilayer composition influences small multidrug transporters. *BMC Biochem* **9,** 31 (2008).
40. Henzler-Wildman, K. & Kern, D. Dynamic personalities of proteins. *Nature* **450,** 964–972 (2007).
41. Farrow, N. A., Zhang, O., Forman-Kay, J. D. & Kay, L. E. A heteronuclear correlation experiment for simultaneous determination of 15N longitudinal decay and chemical exchange rates of systems in slow equilibrium. *J Biomol NMR* **4,** 727–734 (1994).
42. Kleckner, I. R. & Foster, M. P. An introduction to NMR-based approaches for measuring protein dynamics. *Biochim Biophys Acta* **1814,** 942–968 (2011).
43. Li, Y. & Palmer, A. G. TROSY-selected ZZ-exchange experiment for characterizing slow chemical exchange in large proteins. *J Biomol NMR* **45,** 357–360 (2009).

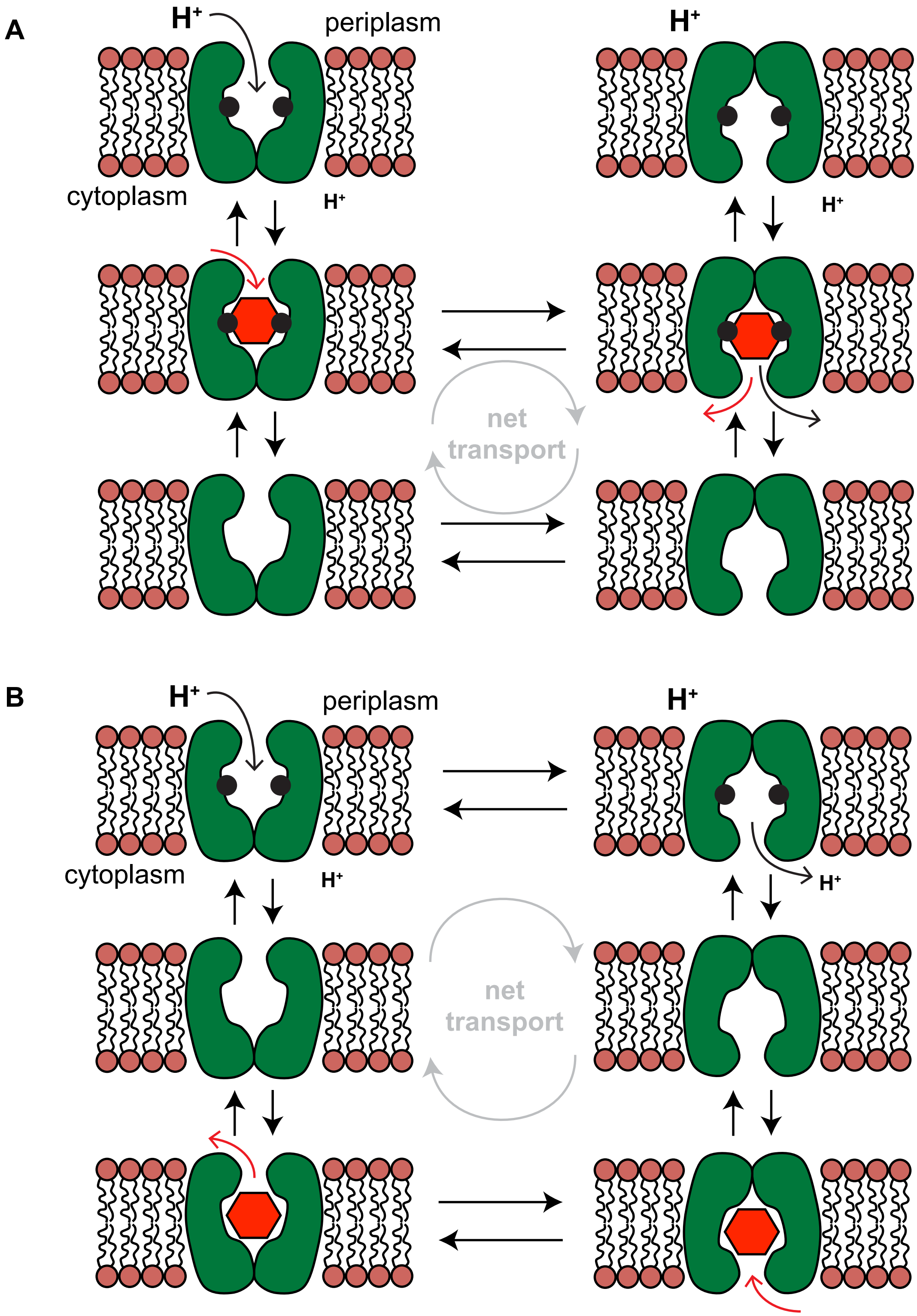

Figure 1. Secondary active transport is is divided into symport (**A**) and antiport (**B**). The cartoon diagrams here depict protons (black circles when bound) as the ion driving transport of substrate (red hexagon) by the transporter (green) across the membrane bilayer (salmon and black). Note the forbidden transitions in each model.

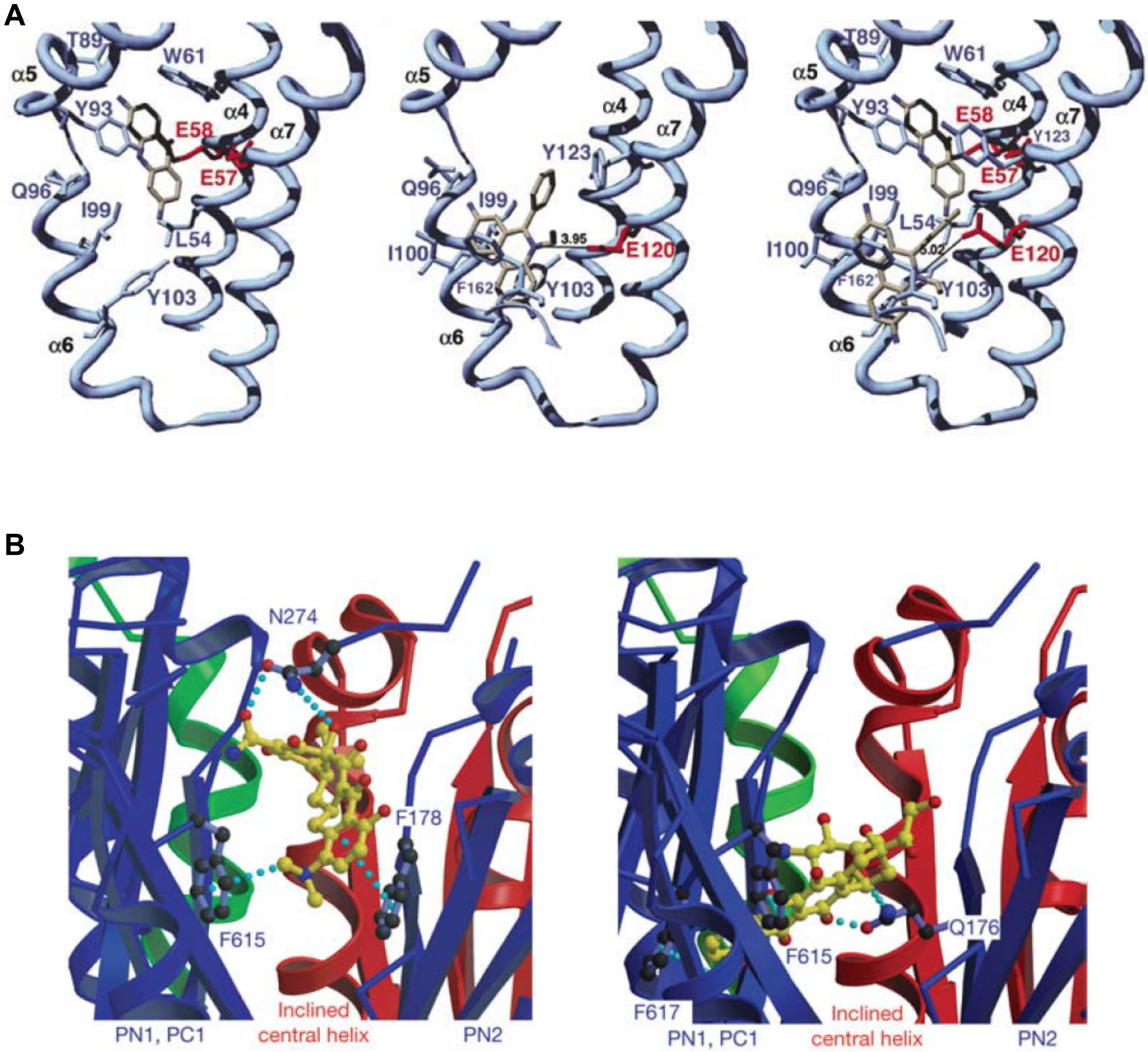

Figure 2. Canonical multidrug recognition in transcription factors and transporters. **A.** The MDR regulator QacR binds proflavin (left) and ethidium (center) in different subsites and can even bind the two simultaneously (right). Figure from Schumacher, et al., 2004. **B.** The MDR transporter AcrB binds minocycline (left) and doxorubicin (right) in separate but overlapping subsites. Part of the protein was removed for clear visualization. Figure from Murakami, et al., 2006 (ref. 9). The proteins are depicted as ribbons, with key residues represented as sticks.

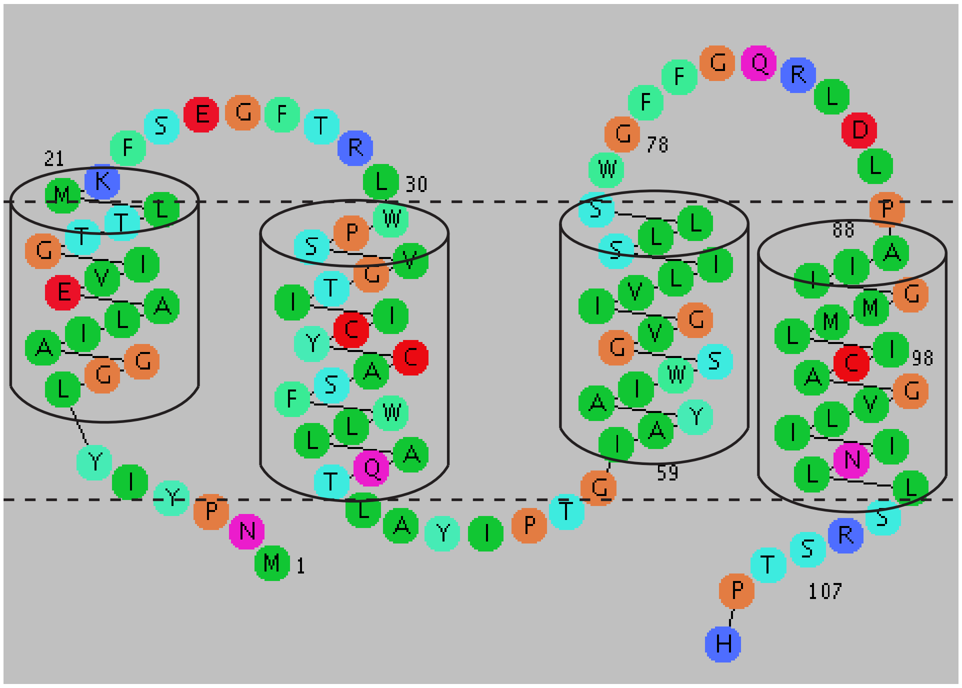

Figure 3. Secondary structure diagram of EmrE. Helix boundaries are based on the crystal structure of TPP$^+$-bound EmrE. The amino acid color guideline is as follows: hydrophobic in green, acidic and cysteine in red, polar in magenta, serine and threonine in cyan, basic in blue, and glycine and proline in orange. Figure made using RbDe: Konvicka, et al. *Protien Engineering* (2000) **13:** 395-6.

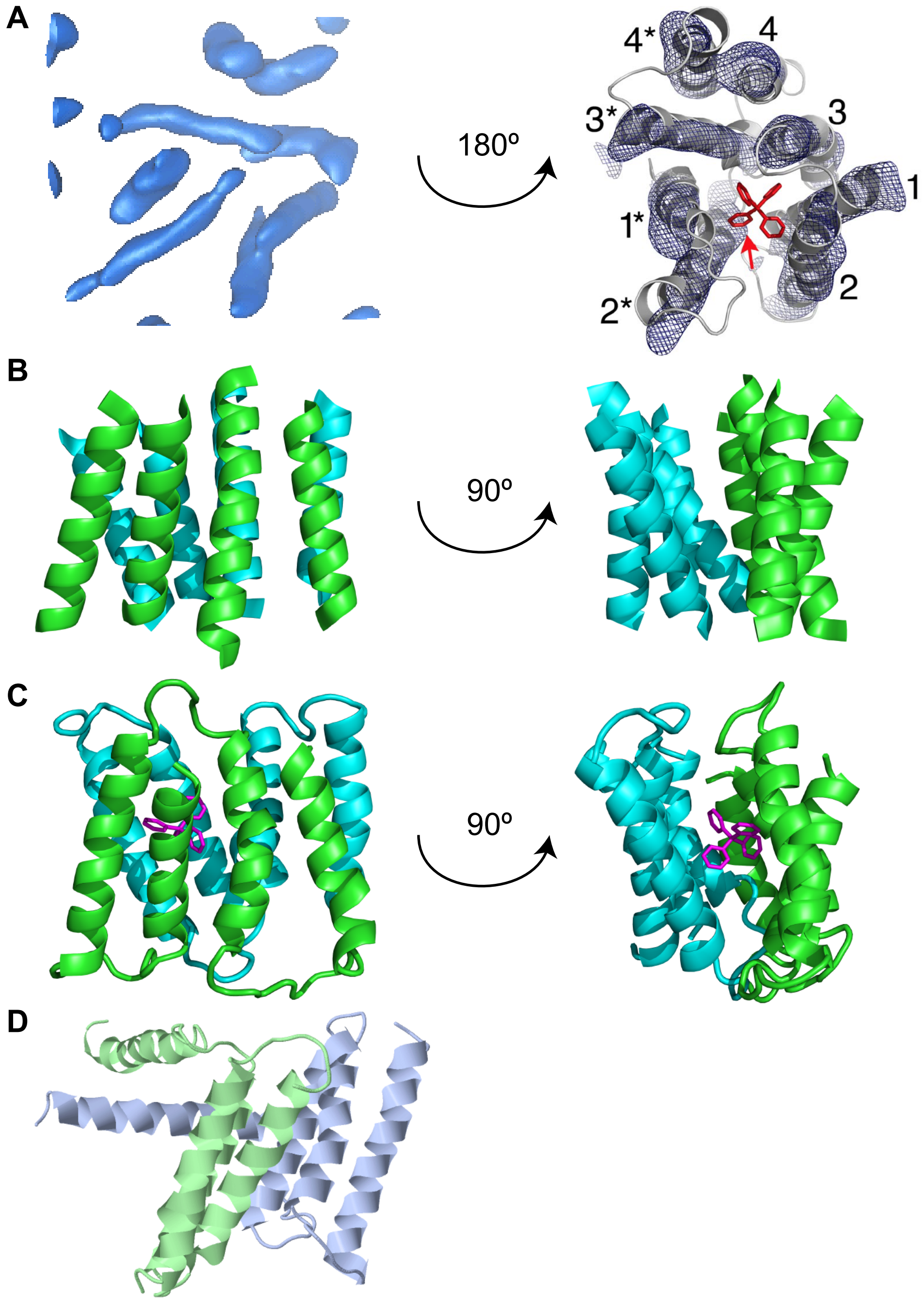

Figure 4. Structures of EmrE. **A.** A 7.5 Å resolution cryoEM electron density map of TPP$^+$-bound EmrE, with density contoured at 59.7 and viewed down the normal to the membrane bilayer (left). Image from EMDataBank (EMD-1087). A view rotated by 180° (right) shows the cryoEM density contoured at 1.2σ in mesh overlayed with the X-ray crystal structure (ribbon representation) shown in (**C**). Figure from Chen, et al. 2007 (ref. 19). **B.** Fleishman's model of TM helices, based on cryoEM data from (**A**). The TPP$^+$ is not explicitly shown. Image made in PyMOL using PDB 2I68. **C.** The TPP$^+$-bound X-ray crystal structure at 3.8 Å resolution (PyMOL, PDB 3B5D). **D.** The drug-free X-ray crystal structure at 4.5 Å resolution (PyMOL, PDB 3B61). Corresponding monomers are colored identically in (**B**) and (**C**). (**B**)-(**D**) are viewed within the bilayer plane.

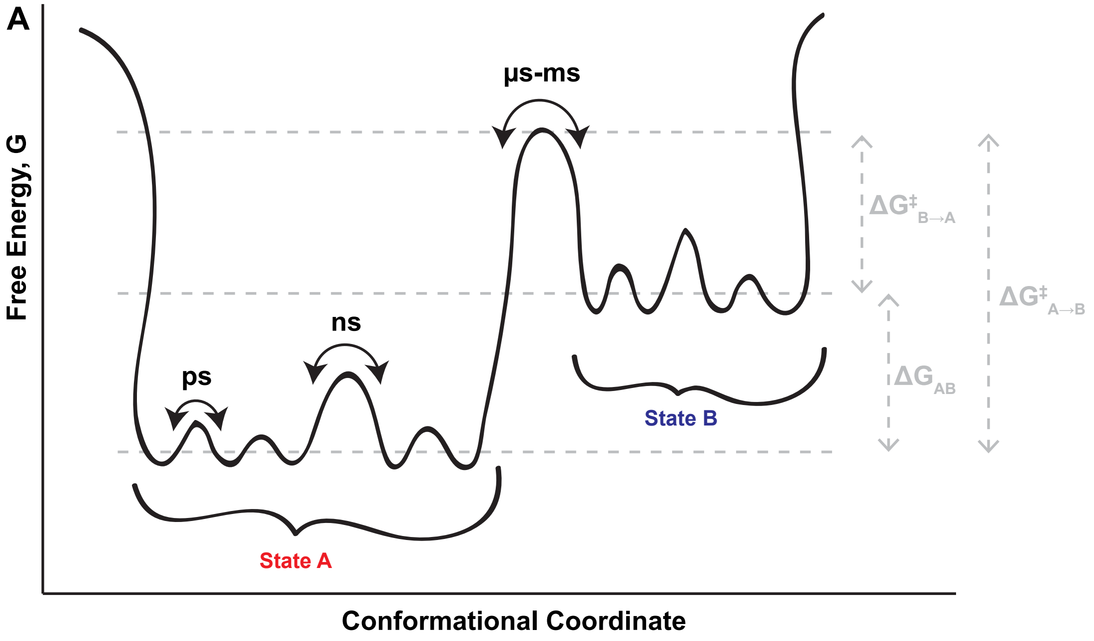

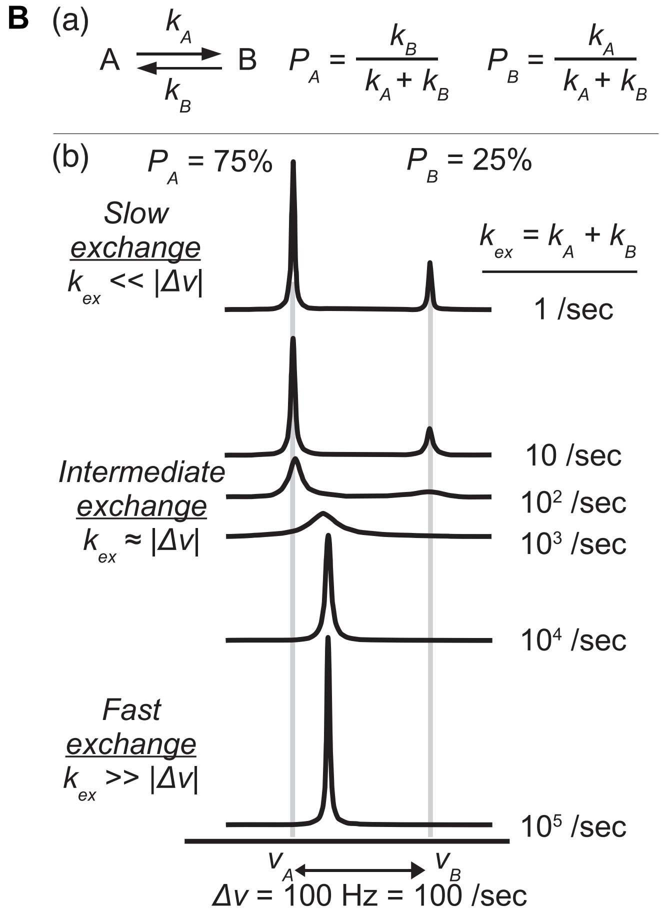

Figure 5. Protein dynamics via solution NMR. **A.** A simplified energy diagram illustrates that dynamics occur on different timescales. A protein undergoing a large domain motion will exchange between multiple states (states A and B). However, each state is an ensemble of closely related substates. These substates are separated by smaller energy barriers. Movement between states A and B occurs on the µs-ms timescale. These states are separated in energy by ΔG_{AB}, but movement between the two states is met by the energetic barriers $\Delta G^{\ddagger}_{A\rightarrow B}$ and $\Delta G^{\ddagger}_{A\rightarrow B}$. Figure inspired by Henzler-Wildman and Kern, 2007 (ref. 40). **B.** Slow, global motions occur in different regimes on the NMR timescale, depending on the relationship between the exchange rate (k_{ex}) and the chemical shift difference between the two states ($\Delta\nu$). This relationship determines whether a separate peak is observed for each state or a population-weighted average. Figure from Kleckner and Foster, 2011 (ref. 42).

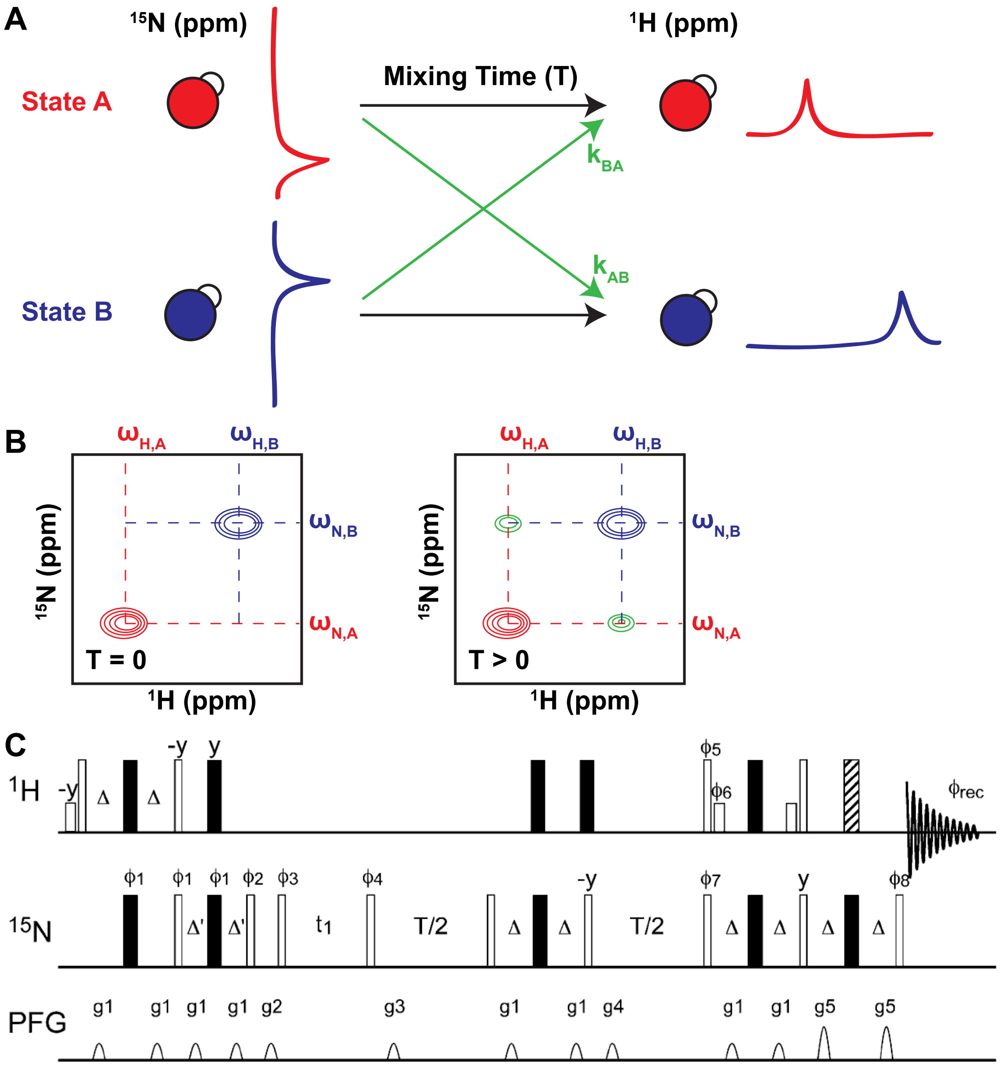

Figure 6. ZZ-exchange spectroscopy. **A.** A cartoon description of a ZZ-exchange experiment illustrates that chemical shift evolves on the amide nitrogen, followed by a delay, and then the magnetization is transferred to proton, where the chemical shift is recorded. If the system is in slow exchange, the amide converts from state A to state B and vice versa during the delay time, with a probability proportional to the exchange rate. **B.** The resulting 2D spectrum shows only autopeaks when *T* = 0. Cross peaks build in when *T* > 0. Figures (**A**-**B**) inspired by Mittermaeir and Kay, 2009. **C.** Diagram of TROSY-selected ZZ-exchange pulse sequence. The pulse representations are as follows: open bars are 90° pulses; filled bars are 180° pulses; short, open bars are rectangular, water-selective 90° pulses; and the striped bar is a 3-9-19 pulse. The time delays are given by Δ = 2.7 ms, Δ' = 1.35 ms, and T is the variable mixing time. Unless labeled otherwise, all pulses have a phase of *x*. The phase cycle (for Bruker) is: $\Phi_1 = \Phi_3 = 4$(x, -x, -y, y); $\Phi_2 = 2$ (135°, 315°, 45°, 225°), 2 (315°, 135°, 225°, 45°); $\Phi_4 = 4$ (x, -x, y, -y); $\Phi_5 = 2$ (y, y, y, y, -y, -y, -y, -y); $\Phi_6 = 2$ (-y, -y, -y, -y, y, y, y, y); $\Phi_7 = 4$(-x, x, -y, y); $\Phi_8 = 2$ (x, x, x, x, -x, -x, -x, -x); Φ_{rec} = (x, -x, y, -y, x, -x, -y, y, -x, x, -y, y, -x, x, y, -y). Phase Φ_4 is incremented using States-TPPI to achieve quadrature detection in the indirect dimension. The *z* gradients (PFG) have sine profiles with the parameters: G1 = 7.5 G/cm for 1.5 ms; G2 = G4 = 10 G/cm for 0.5 ms; G3 = 10 G/cm for 1.5 ms; and G5 = 22.5 G/cm for 1.0 ms. Figure from Li and Palmer, 2009 (ref. 43).

Chapter II. Reconstitution of integral membrane proteins into isotropic bicelles with improved sample stability and expanded lipid composition profile.

Optimization of the sample preparation for EmrE was key in making the bulk of my thesis work possible because solution NMR and other biophysical studies of EmrE require the production of stable, reproducible samples. The purification of EmrE in the detergents dodecyl maltoside and decyl maltoside (DM) was well established[1,2]. However, EmrE had not been previously studied in isotropic bicelles. The two main methods for reconstitution of membrane proteins into isotropic bicelles are i) through organic solvents and ii) via detergent exchange into DHPC and subsequent addition of long-chain lipid. As EmrE is monomeric and unfolded in organic solvent, we avoided method (i)[3,4]. We initially reconstituted EmrE into isotropic bicelles via detergent exchange. We tried exchanging EmrE from DM into DHPC when EmrE with an N-terminal 6× histidine tag was bound to Ni-NTA affinity resin. However, we generally had a low recovery of EmrE using this method. EmrE in DHPC appears to be unstable on Ni-NTA resin. We also tried exchanging EmrE from DM into DHPC using a gel filtration column (S200). However, as shown below, in contrast to predicted detergent removal using the critical micellar concentration and column volume, this method results in destabilizing residual detergent in the final sample.

Samples prepared using these two detergent exchange methods displayed peak shifts between sample preparations, which is not acceptable in NMR studies. In addition, they had variable sample stability, with samples showing precipitation after a few days at the elevated temperatures required for solution NMR experiments. Our modified protocol involved reconstituting EmrE into liposomes first and then adding short-chain lipid to break up the vesicles to form isotropic bicelles. This method ensured complete detergent removal, and led to reproducible samples with long-term stability.

Experiments were designed by E. Morrison and K. Henzler-Wildman and performed by E. Morrison.

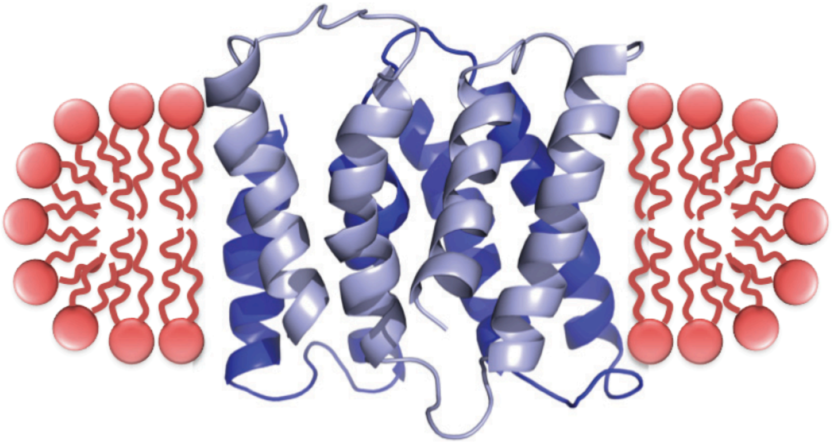

Supplementary Figure 1. Cartoon depiction of the cross-section of EmrE reconstituted into isotropic bicelles (Graphical Abstract figure from[5], PDB 3B5D).

References:

1. Muth, T. R. & Schuldiner, S. A membrane-embedded glutamate is required for ligand binding to the multidrug transporter EmrE. *EMBO J* **19,** 234–240 (2000).
2. Curnow, P., Lorch, M., Charalambous, K. & Booth, P. J. The reconstitution and activity of the small multidrug transporter EmrE is modulated by non-bilayer lipid composition. *J Mol Biol* **343,** 213–222 (2004).
3. Winstone, T. L. *et al.* Organic solvent extracted EmrE solubilized in dodecyl maltoside is monomeric and binds drug ligand. *Biochem Biophys Res Commun* **327,** 437–445 (2005).
4. Schwaiger, M. *et al.* NMR investigation of the multidrug transporter EmrE, an integral membrane protein. *Eur J Biochem* **254,** 610–619 (1998).
5. Morrison, E. A. & Henzler-Wildman, K. A. Reconstitution of integral membrane proteins into isotropic bicelles with improved sample stability and expanded lipid composition profile. *Biochimica et Biophysica Acta (BBA) - Biomembranes* **1818,** 814–820 (2012).

Biochimica et Biophysica Acta 1818 (2012) 814–820

Contents lists available at SciVerse ScienceDirect

Biochimica et Biophysica Acta

journal homepage: www.elsevier.com/locate/bbamem

Reconstitution of integral membrane proteins into isotropic bicelles with improved sample stability and expanded lipid composition profile

Emma A. Morrison, Katherine A. Henzler-Wildman *

Department of Biochemistry and Molecular Biophysics, Washington University School of Medicine, 660 S. Euclid Ave., Box 8231, St. Louis, MO 63110, USA

ARTICLE INFO

Article history:
Received 14 October 2011
Received in revised form 16 December 2011
Accepted 20 December 2011
Available online 29 December 2011

Keywords:
Isotropic bicelles
Membrane mimetic
Membrane protein reconstitution
EmrE
NMR

ABSTRACT

Reconstitution of integral membrane proteins into membrane mimetic environments suitable for biophysical and structural studies has long been a challenge. Isotropic bicelles promise the best of both worlds—keeping a membrane protein surrounded by a small patch of bilayer-forming lipids while remaining small enough to tumble isotropically and yield good solution NMR spectra. However, traditional methods for the reconstitution of membrane proteins into isotropic bicelles expose the proteins to potentially destabilizing environments. Reconstituting the protein into liposomes and then adding short-chain lipid to this mixture produces bicelle samples while minimizing protein exposure to unfavorable environments. The result is higher yield of protein reconstituted into bicelles and improved long-term stability, homogeneity, and sample-to-sample reproducibility. This suggests better preservation of protein structure during the reconstitution procedure and leads to decreased cost per sample, production of fewer samples, and reduction of the NMR time needed to collect a high quality spectrum. Furthermore, this approach enabled reconstitution of protein into isotropic bicelles with a wider range of lipid compositions. These results are demonstrated with the small multidrug resistance transporter EmrE, a protein known to be highly sensitive to its environment.

1. Introduction

Structural and biophysical studies of membrane proteins have traditionally lagged behind those of soluble proteins. One of the major challenges of working with membrane proteins is finding a membrane mimetic environment that is conducive to biophysical studies while still maintaining native structure and function [1]. Techniques such as solution NMR have fast-tumbling requirements that are not fulfilled by conventional lipid vesicles. Detergent micelles, isotropic bicelles, and nanodiscs are some of the media available for the solubilization of integral membrane proteins (IMPs). The high curvature and altered lateral pressure of detergent micelles make them a less than ideal membrane mimetic [1–4]. Detergents must be extensively screened to find a suitable match that preserves native structure and function, and gentler detergents such as alkylglycosides, which may better preserve function, are often not conducive to multidimensional NMR studies [5].

Both isotropic bicelles and nanodiscs provide bilayer environments, and each media has its own merits. Nanodiscs are stable particles that can be separated by physical means such as gel filtration chromatography, unlike isotropic bicelles in which the detergent is in constant equilibrium between monomer and bicelle. This same property of isotropic bicelles allows them to reconstitute at any size by varying the long- to short-chain lipid ratio, whereas nanodiscs can only make discretely sized particles. A new membrane scaffold protein must be expressed and purified for each nanodisc size, and they must be carefully tested to determine the proper ratio of scaffold-to-lipid for each preparation [6]. In addition, NMR spectra of IMPs reconstituted into nanodiscs tend to be broadened [1,2,7].

Use of isotropic bicelles has been limited by their stability and spectral qualities [1,2]. Traditional methods for making bicelle samples require harsh conditions that may not preserve proper protein structure and function. Improved bicelle stability would allow for more widespread use. Previous attempts at increasing bicelle stability and sample lifetime have included using ether-linked lipids and/or adding up to 10% of long- and short-chain lipids with charged headgroups such as PS and PE-DTPA [4,8,9]. However, recent studies have indicated that non-native ether-linked lipids alter the structure and dynamics of antimicrobial peptides [10], making this a less desirable substitution.

Abbreviations: NMR, nuclear magnetic resonance; DM, decylmaltoside; DHPC, 1,2-dihexanoyl-sn-glycero-3-phosphocholine; DLPC, 1,2-dilauroyl-sn-glycero-3-phosphocholine; DMPC, 1,2-dimyristoyl-sn-glycero-3-phosphocholine; DPPC, 1,2-dipalmitoyl-sn-glycero-3-phosphocholine; POPC, 1-palmitoyl-2-oleoyl-sn-glycero-3-phosphocholine; DOPC, 1,2-dioleoyl-sn-glycero-3-phosphocholine; POPE, 1-palmitoyl-2-oleoyl-sn-glycero-3-phosphoethanolamine; POPG, 1-palmitoyl-2-oleoyl-sn-glycero-3-phospho-(1'-rac-glycerol); TPP$^+$, tetraphenylphosphonium$^+$; PS, phosphatidylserine; PE-DTPA, phosphatidylethanolamine-N-diethylenetriaminepentaacetic acid; IMP, integral membrane protein; DLS, dynamic light scattering; TLC, thin layer chromatography.

* Corresponding author. Tel.: +1 314 362 1674; fax: +1 314 362 7183.
E-mail addresses: eamorris@wustl.edu (E.A. Morrison), khenzler@biochem.wustl.edu (K.A. Henzler-Wildman).

0005-2736/$ – see front matter © 2011 Elsevier B.V. All rights reserved.
doi:10.1016/j.bbamem.2011.12.020

Another challenge with isotropic bicelles is the relatively limited lipid compositions currently in use. More varied lipid compositions have been explored with magnetically aligned large bicelles for solid-state NMR [1]. An expanded lipid composition profile would allow for more physiologically relevant isotropic bicelles, similar to nanodiscs, which can be formed with a range of lipids and lipid extracts [2,6].

Here, we present an improved reconstitution of integral membrane proteins into small isotropic bicelles that allows reconstitution into bicelles with a much wider range of lipid compositions. This protocol is easily adaptable to any IMP of interest, with no requirement for organic solvent or specific detergents. It also ensures complete detergent removal, eliminating potential instabilities and inhomogeneities caused by residual detergent and providing an optimal sample for biophysical studies. We have recently demonstrated the utility of these bicelles for solution NMR dynamics measurements of EmrE [11]. These cutting edge NMR measurements would not have been possible without the improved sample stability and homogeneity provided by this method.

2. Materials and methods

2.1. EmrE expression and purification

EmrE was expressed in a pET15b plasmid with an N-terminal 6xHis tag (Geoffrey Chang, Scripps Research Institute) and expressed and purified as previously described [11]. Briefly, isotopically labeled EmrE was grown in ^{15}N- or ^{2}H/^{15}N-labeled M9 minimal media. To purify EmrE, cells were lysed by sonication. The membranes were solubilized in 40 mM DM (Affymetrix Anatrace), purified using Ni-NTA resin (Novagen), and cleaved with thrombin (Sigma-Aldrich). Final purification was performed by gel filtration chromatography on a Superdex 200 column (GE Healthcare) equilibrated with 10 mM DM. The purified EmrE was then reconstituted into isotropic bicelles in deoxygenated buffers.

2.2. Sample preparation

2.2.1. Reconstitution into isotropic bicelles by detergent exchange

Purified EmrE was concentrated to 0.5 mL and DM reduced to less than 30 mM, assuming monomeric detergent passed through the filter while micelles were concentrated along with the protein. The resulting sample was run over a Superdex 200 column equilibrated with 25 mM DHPC (Avanti Polar Lipids). EmrE in DHPC was concentrated to 250 μL and long-chain lipid added to a final ratio of 3:1 short- to long-chain lipid (at least 75 mM long-chain lipid and 130-fold excess of long-chain lipid:EmrE). Four freeze–thaw cycles were carried out to ensure homogeneous bicelles.

2.2.2. Reconstitution into isotropic bicelles via liposomes

Long-chain lipid (DLPC, DMPC, DPPC, POPC, DOPC, POPE, POPG, and *Escherichia coli* polar lipid extract, Avanti Polar Lipids) was hydrated in buffer above the phase transition temperature for 1–2 hours at 20 mg/mL and then sonicated in a high-power bath sonicator (Laboratory Supplies Company, Inc, Hicksville, NY). The lipid vesicles were then incubated with 0.51% octylglucoside (Affymetrix Anatrace) for 15–30 minutes. Purified EmrE in DM was added at a molar ratio of 1:130, EmrE:long-chain lipid. After incubation for an additional 30–60 minutes, Amberlite (Supelco) was added to remove the detergent. Three aliquots of 30 mg Amberlite per mg detergent were added with incubation at room temperature for 1–2 hours, overnight, and another 1–2 hours. The proteoliposomes were collected via ultracentrifugation (50,000 × g, 1 hour, 20 °C) and resuspended in DHPC buffer at a molar ratio of 3:1 short- to long-chain lipid, assuming a 90% recovery of long-chain lipid. The final lipid ratio in the bicelles was confirmed by ^{1}H-NMR using the lipid terminal methyl peaks. The final buffer conditions for all NMR samples were 20 mM potassium phosphate, 30 mM sodium cacodylate, 20 mM NaCl, 0.05% sodium azide, 2 mM TCEP, pH 7, with 2 mM TPP^{+} and EmrE concentrations in the range of 0.5–1.1 mM.

2.3. Transport assay

H^{+}-driven uptake of the substrate dequalinium^{2+} was monitored using fluorescence spectroscopy, following the fluorescence signal of the substrate. EmrE was reconstituted into *E. coli* polar lipid extract as described above with a lipid:EmrE dimer ratio of 640:1. The buffer was 190 mM NH$_4$Cl, 15 mM Tris pH 7 as in ref. [12]. The sample was extruded through a 200 nm filter to create homogeneous vesicles. The proteoliposomes were diluted ten-fold into either the same buffer (no H^{+} gradient) or a buffer of 140 mM KCl, 10 mM Tricine, 5 mM MgCl$_2$, 10 mM Tris pH 8 (H^{+} gradient). The final protein concentration was 1 μM. Transport was initiated upon the addition of concentrated dequalinium^{2+} to the bulk solution. The experiments were carried out in a Varian Cary Eclipse fluorescence spectrometer, at an excitation wavelength of 350 nm and emission wavelength of 460 nm.

2.4. Dynamic light scattering

DLS experiments were carried out on a DynaPro (model 99-E-50, Protein solutions) with the Dynamics V6 software. The instrument was calibrated with an albumin standard (Thermo Scientific) at varying temperatures and concentrations. The NMR samples were diluted four-fold to decrease secondary scattering effects, while still maintaining sufficient lipid concentration to keep the same effective *q*-value, or ratio of long- to short-chain lipids in the bicelle [13]. Data were collected at 10 °C and 25 °C, for five acquisitions of 5 minutes each.

2.5. Thin layer chromatography

TLC was carried out using Whatman K6 silica gel 60A plates and a 65:24:4 chloroform:methanol:water solvent system. Isotropic bicelle samples were diluted 10-fold in 2:1 chloroform:methanol for spotting onto the plates. After running the plates, they were dried and developed in an iodine vapor chamber overnight.

2.6. Refractive index measurements

A Reichert-Jung Abbe Mark II digital refractometer with water-bath temperature control was used to measure the refractive indices of isotropic bicelles at the pertinent concentrations and temperatures.

2.7. Viscosity measurements

A calibrated Cannon-Ubbelohde semi-micro viscometer, size 50, was used to determine the viscosity of isotropic bicelles. Both refractive index and viscosity were measured under the same conditions (lipid concentrations and temperatures) as the diffusion measurements and used to calculate the hydrodynamic radius.

2.8. NMR spectroscopy

All experiments were carried out on a 700 MHz Varian Inova spectrometer at 45 °C. Lipid ratios were confirmed by integrating the terminal methyl resonances of the short- and long-chain lipids in a ^{1}H spectrum. Standard (^{1}H, ^{15}N)-TROSY HSQC spectra with gradient coherence selection were acquired with 120 and 24 scans per increment, respectively, for non-^{2}H and ^{2}H samples. (^{1}H, ^{15}N)-TRACT [14] was used to measure rotational correlation times. The hydrodynamic radius (r_h) is related to the rotational correlation time (τ_c) by

$$\tau_c = \frac{4\pi\eta r_h^3}{3kT}. \tag{1}$$

Data were processed and analyzed using NMRPipe [15] and NMRView [16]. IgorPro (Wavemetrics) was used to fit the diffusion data.

3. Results and discussion

3.1. Reconstitution of an integral membrane protein into isotropic bicelles via liposomes improves bicelle stability and spectral quality

Integral membrane proteins (IMPs) are traditionally reconstituted into isotropic bicelles [3] by two methods: i) direct reconstitution from organic solvent or lyophilized powder; or ii) exchange into DHPC micelles followed by addition of long-chain lipid. Highly stable IMPs can be reconstituted through any method. However, multi-pass α-helical IMPs are generally more sensitive to their environment and handling during purification [17–19]. Organic solvents and lyophilization must be avoided with these proteins, and many are not stable in DHPC micelles. We reconstitute EmrE into vesicles of long-chain lipid and then add DHPC to form bicelles (method iii). This protocol is similar to a strategy used previously to reconstitute the GPCR CXCR1 into large bicelles [20] for solid-state NMR.

EmrE, a 4-transmembrane helix homodimer, is highly sensitive to detergent and lipid environment [18,21] and serves as a representative system. EmrE is monomeric [22] and unfolded [23] in organic solvent. However, it is a "functional" dimer in the detergent dodecyl maltoside [24,25] based on ligand-binding, which provides the best proxy for transporter function in a solubilized state. Thus we eliminated organic solvent reconstitution protocols and focused on methods with the potential to preserve EmrE structure and function.

Initially, we reconstituted EmrE into isotropic bicelles via detergent exchange (method ii) (Fig. 1A, B), but there are several disadvantages to this method. Running long gel filtration columns above the critical micellar concentration of DHPC becomes prohibitively expensive, and EmrE has diminished stability upon exchange into DHPC micelles. In addition, residual DM remains in the samples (Fig. 2). The yield, spectral quality, and stability of the samples were variable, with protein precipitating in 2–14 days at 45 °C. In addition, minor chemical shift changes were sometimes observed between independently prepared samples. Due to the conformational dynamics of EmrE, NMR spectra are exquisitely sensitive to changes in the bicelle environment, making sample reproducibility essential.

Reconstitution via liposomes (method iii) has two advantages. First, it ensures complete detergent removal before the addition of the short-chain lipid to break up the vesicles (Fig. 1A). This protocol creates isotropic bicelles of well-defined composition and removes the requirement for exchange into DHPC, thus making it suitable for proteins not stable in this particular detergent-like lipid. Second, reconstitution into a liposome allows transport assays to be performed, ensuring that EmrE is fully functional immediately before the final step of bicelle formation. We measured proton-driven uptake of substrate by EmrE reconstituted into *E. coli* polar lipid liposomes

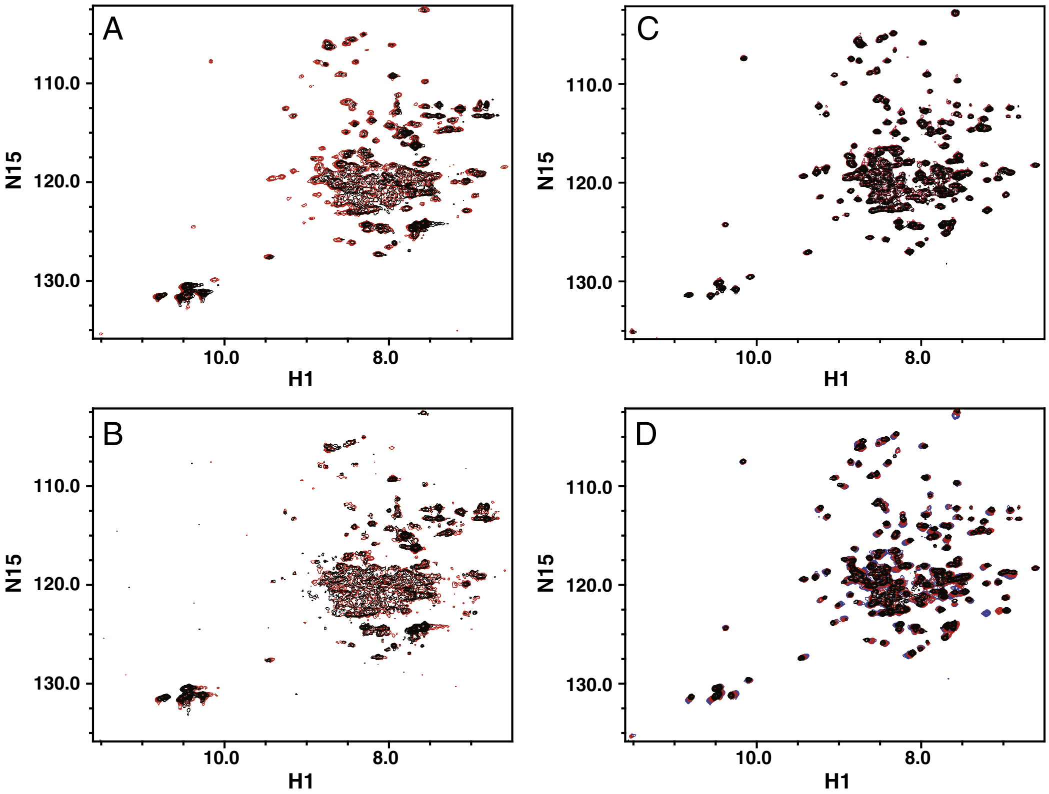

Fig. 1. Overlay of (^{1}H, ^{15}N)-TROSY HSQC spectra of TPP$^+$-bound EmrE in isotropic bicelles reconstituted by different methods. A) ^{15}N-EmrE in DMPC/DHPC bicelles is better resolved and has better signal/noise when reconstituted through liposomes (red) than when reconstituted through detergent exchange (black). B) The spectral quality of ^{15}N-EmrE in DMPC/DHPC bicelles degrades with time for EmrE reconstituted via detergent. After nearly 2 weeks at 45 °C, the spectrum (black) has less signal than the initial spectrum (red). C) The spectrum of ^{2}H/^{15}N/^{13}C-EmrE reconstituted into DLPC/DHPC bicelles via liposomes (red) is virtually unchanged after more than 6 months (black). D) ^{2}H/^{15}N-EmrE can be stably reconstituted into isotropic bicelles made with different chain lengths (DLPC, blue; DMPC, red; DPPC, black), all capped by DHPC. The minor peak shifts indicate only small changes in EmrE structure with change in bicelle thickness. All spectra were collected at 45 °C, in 20 mM KPi, 20 mM NaCl, 30 mM sodium cacodylate, pH 7.

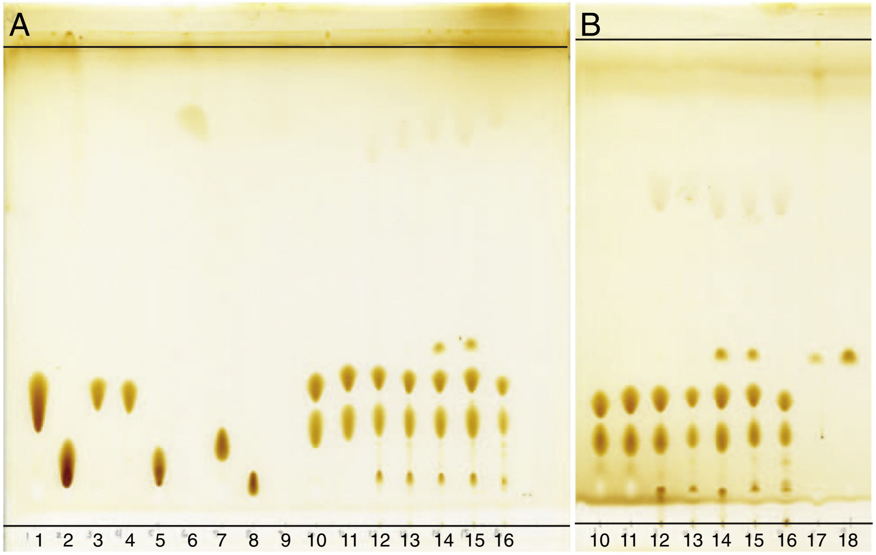

Fig. 2. Thin layer chromatography to qualitatively assess lipid composition and hydrolysis of isotropic bicelle samples used for NMR spectroscopy. The standards include lipids as well as the corresponding breakdown products—lysolipid and fatty acid. A) From left to right: 1) DPPC; 2) 16:0 lyso PC; 3) DMPC; 4) DLPC; 5) 12:0 lyso PC; 6) lauric acid; 7) DHPC; 8) 6:0 lyso PC; 9) hexanoic acid; 10) DLPC/DHPC $q = 0.33$ bicelles; 11) DMPC/DHPC $q = 0.33$ bicelles; 12) initial sample of ^{15}N-EmrE in DMPC/DHPC isotropic bicelles reconstituted through liposomes and 13) after 12 days at 45 °C; 14) initial sample of ^{15}N-EmrE in DMPC/DHPC isotropic bicelles reconstituted through detergent exchange and 15) after 12 days at 45 °C; and 16) ^{2}H/^{15}N/^{13}C-EmrE after roughly 7 months. B) From left to right, repeat of lanes 10–16; 17) EmrE in 10 mM DM after S200 column during sample purification; and 18) 100 mM DM. Iodine vapor does not appear to be sufficient to visualize hexanoic acid.

using Amberlite for detergent removal (Fig. 3). These assays use the naturally fluorescent substrate dequalinium, which shows a concentration-dependent increase in fluorescence at 460 nm. No uptake is observed in the absence of a pH gradient. When a pH gradient is introduced, the fluorescence change indicates dequalinium uptake and concentration inside the liposomes, confirming that purification and reconstitution into liposomes yields functional EmrE. Formation of bicelles from the liposomes requires only the addition of DHPC and several freeze–thaw cycles. A spectrum of TPP^{+}-bound EmrE in *E. coli* polar lipid bicelles (Fig. 4D), the lipid composition used for the transport assays, indicates that the overall structure of EmrE is the same in a variety of lipid environments. It is not possible to measure transport in the final bicelle, but substrate binding affinity and stoichiometry[11] indicate that EmrE is still properly folded and “functional” in bicelles.

2D TROSY spectra of ^{15}N-EmrE reconstituted into DMPC/DHPC isotropic bicelles by either method show that the liposome method produces significantly better spectra (Fig. 1A). These spectra have improved signal to noise for the same protein concentration and sharper lines, consistent with a more homogeneous sample. In addition, spectra from independently prepared samples overlay exactly, a requirement for specific-labeling-based assignment protocols.

Elevated temperatures are commonly used in NMR to improve linewidth. To test stability under these conditions, the samples were incubated in a water bath at 45 °C for nearly 2 weeks and then a second spectrum was acquired to assess spectral changes. No significant changes were observed for EmrE reconstituted via liposomes and there was no precipitate. For EmrE reconstituted via detergent exchange, precipitate was observed and the spectral quality declined (Fig. 1B).

The long-term stability of the isotropic bicelles reconstituted via liposomes is demonstrated in Fig. 1C. After 6 months of storage at room temperature and weeks of NMR experiments at elevated temperatures, a sample of ^{2}H/^{15}N/^{13}C-EmrE in DLPC/DHPC bicelles is unchanged. Contrary to previous reports [4,8], these samples are stable for months without requiring expensive ether-linked lipids or special lipid compositions.

We also experimented with the long-chain lipid composition of the bicelles. A series of samples made using different acyl chain lengths reveal only small local peak shifts (Fig. 1D). EmrE is an *E. coli* protein, so we reconstituted EmrE into liposomes made with *E. coli* polar extract. These varied in yield and spectral quality, likely due to variability between batches of lipid extract. For a more defined environment, we used two compositions designed to mimic *E. coli* lipids. EmrE reconstituted well into isotropic bicelle preparations using long-chain mixtures of i) 70% POPC, 20% POPE, 10% POPG, or ii) 70% POPE, 20% POPG, 10% POPC. Overall, there are minimal peak shifts of EmrE with changes in long-chain lipid composition, but the peak-widths vary significantly (Fig. 4). This suggests that

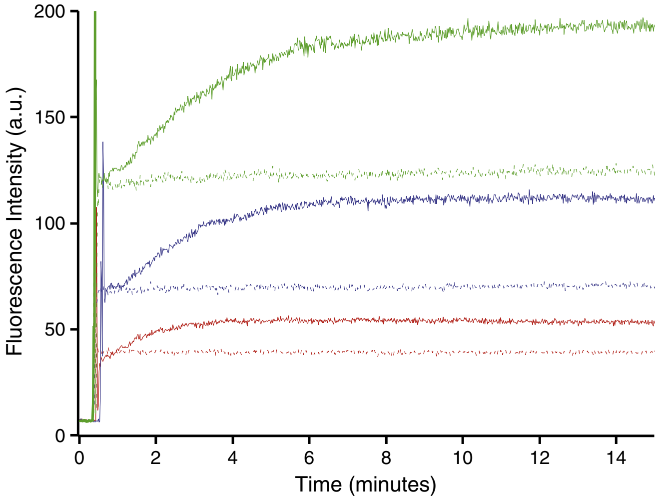

Fig. 3. EmrE is functional when reconstituted into liposomes: H^{+}-driven uptake of the substrate dequalinium^{2+} by EmrE reconstituted into *E. coli* polar liposomes, as observed by monitoring dequalinium^{2+} fluorescence. Kinetics timecourses were acquired with excitation at 350 nm and emission at 460 nm. At time zero, proteoliposomes at pH 7 are diluted into a buffer of pH 7 (no proton gradient) or pH 8 (proton gradient). After roughly 30 sec, substrate is added. Assay was carried out with 1 μM EmrE and 5 μM (red, bottom), 10 μM (blue, middle), and 20 μM (green, top) dequalinium^{2+} and in the presence (solid line) or absence (dashed line) of a H^{+} gradient.

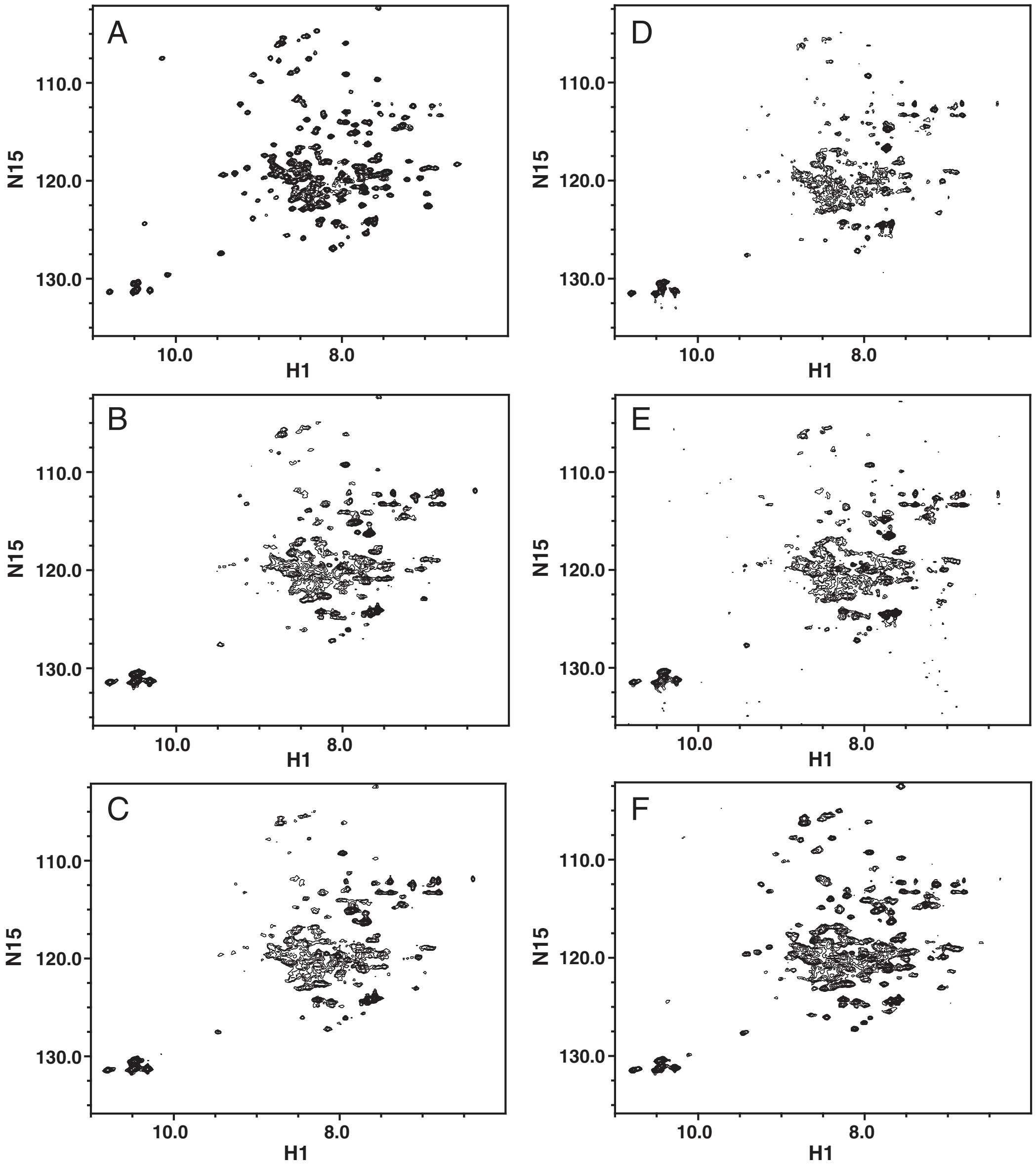

Fig. 4. EmrE was successfully reconstituted with a wide range of long-chain lipid compositions varying in saturation and head-group. (^{1}H, ^{15}N)-TROSY HSQC spectra of TPP$^+$-bound EmrE reconstituted into isotropic bicelles with the following long-chain lipid compositions: A) DPPC, B) POPC, C) DOPC, D) *E. coli* polar lipid extract, E) 70% POPE, 20% POPG, 10% POPC, and F) 70% POPC, 20% POPE, 10% POPG. The DPPC spectrum was collected on ^{2}H/^{15}N-EmrE, while all others were collected on ^{1}H/^{15}N-EmrE. Spectra were collected under the same conditions as above.

we are observing changes in dynamic rate rather than structure. These samples demonstrate the potential for reconstitution of IMPs into isotropic bicelles with a variety of lipid compositions that better mimic native membranes for use in biophysical studies [26,27].

3.2. Analysis of lipid hydrolysis in isotropic bicelles

We used TLC to assess lipid hydrolysis and residual detergent (Fig. 2). The samples consist primarily of the bicelle lipids. Additional minor lysolipid and fatty acid components indicate some lipid

Table 1
Table of hydrodynamic radii of isotropic bicelles determined via DLS and rotational diffusion NMR.

Sample	Hydrodynamic radius (nm)				
	Water Parameters[a]		Bicelle Parameters[b]		
	DLS, 10 °C	DLS, 25 °C	DLS, 10 °C	DLS, 25 °C	NMR, 45 °C [c]
Reconstitution via liposomes, ^{15}N EmrE in DMPC/DHPC bicelles	3.5 ± 0.8	3.0 ± 0.4	2.0 ± 0.3	2.4 ± 0.3	3.2 ± 0.3
Reconsitution via detergent exchange, ^{15}N EmrE in DMPC/DHPC bicelles	3.2 ± 0.8	3.0 ± 0.8	1.9 ± 0.4	2.4 ± 0.6	2.9 ± 0.3
Reconstitution via liposomes, ^{2}H/^{15}N/^{13}C EmrE in DLPC/DHPC bicelles	3.6 ± 0.8	3.3 ± 0.5	2.2 ± 0.5	2.6 ± 0.4	2.7 ± 0.3

[a] R_H values determined from DLS, using the viscosity and refractive index of water.
[b] R_H values determined from DLS, using the viscosity and refractive index of the isotropic bicelle solution at the given temperature (see Materials and methods).
[c] Calculated from rotational correlation time using Eq. (1).

hydrolysis; however, they are still only minor components after 6-months. If hydrolysis is a serious problem, a bicelle with ether-linked lipids, such as DMPC/DIOHPC, can be utilized [9]. However, it is preferable to use ester-linked lipids, as using the non-native ether-lipids may alter the structure and dynamics of peptides in the membrane [10]. An additional component, DM, is visible in the NMR sample reconstituted via detergent exchange (Fig. 2), indicating that the detergent was not fully removed. Precipitation of the NMR samples appears to correlate with small amounts of residual detergent.

3.3. Diffusion of EmrE reconstituted into isotropic bicelles

Disagreement exists in the literature regarding the morphology of isotropic bicelles at small q-values—are they true discs (primarily separated long- and short-chain domains) or mixed micelles? Based on the small apparent hydrodynamic radii (R_H) determined via DLS, small q-value (≤ 0.5) mixtures of long- and short-chain lipids have been differentially diagnosed as mixed micelles [28] or discs[13]. It is difficult to determine shape from DLS data [13] alone and difficult to interpret R_H quantitatively. Electron microscopy [13] and AFM [9], have been used to visually assess the morphology of these mixtures. Discoidal structures were observed with both methods, with larger discs and a few wormlike micelles also being observed via AFM under more physiological conditions. Small angle neutron scattering data also supports a disk-like model [29].

NMR spectroscopy has additionally been used to assess bicelle morphology. ^{31}P chemical shifts are different for DMPC and DHPC headgroups, indicating different environments on average and thus supporting significant separation of the lipids into distinct regions [9,13]. Long- and short-chain lipids are differentially affected by paramagnetic shift reagents, supporting separate regions for the two classes of lipids [29]. Translational diffusion measurements also indicate a distinct separation [30]. Thus, the preponderance of data supports significant domain separation of the long- and short-chain lipids, creating a bilayer-like environment around the protein. Even if lipid separation in the bicelles is incomplete, as is likely the case, this provides a much more native-like environment than a detergent micelle. This is further supported by proper ligand-binding affinity for small multidrug resistance transporters [3,4] and other IMPs [1,2] in bicelles.

The hydrodynamic radii of our isotropic bicelles ($q = 0.33$) were determined using DLS and NMR rotational diffusion data. Table 1 compares the hydrodynamic radii for EmrE samples reconstituted through detergent exchange and via liposomes. There is no significant change in hydrodynamic radius with reconstitution method, and the radii are significantly smaller than those of nanodiscs [6]. Thus, spectral differences between the two bicelle reconstitution methods are not due to differences in overall particle size. Hydrodynamic radii in Table 1 were calculated from the DLS data using both water and isotropic bicelle solution viscosity and refractive index. These parameters have a significant effect on the hydrodynamic radius calculated from DLS. Previous reports in the literature use values for water in these calculations. However, as the bicelles are not at infinite dilution, we also included hydrodynamic radii calculated using the solution parameters measured directly on our bicelle solutions. Using the solution parameters for water, our data match that of bicelles shown to have a discoidal morphology [13]. Additionally, (i) EmrE is unstable in pure DHPC but very stable in bicelles and (ii) the NMR spectra change significantly with long chain lipid composition (Fig. 4), despite the fact that DHPC is the major component in our bicelles (3:1 DHPC:long-chain lipid). This argues against the mixed micelle model.

4. Conclusions

Conventional methods for reconstitution of integral membrane proteins into isotropic bicelles require exposure of the protein to organic solvent or DHPC micelles. These intermediate environments can be destabilizing to sensitive IMPs. We have found that by first reconstituting EmrE into liposomes and then breaking up the proteoliposomes with DHPC, we can achieve samples of higher spectral quality and greater long-term stability. This method is broadly applicable since the IMP may be reconstituted into liposomes using any method suitable for the protein of interest. Addition of DHPC to form isotropic bicelles from liposomes makes this protocol easy to use and optimize relative to nanodiscs.

The environment-sensitive small multidrug resistance transporter EmrE has been successfully reconstituted into isotropic bicelles of a range of compositions using this protocol. Reconstituting EmrE via liposomes has allowed us to assign the majority of backbone residues and quantitatively measure slow timescale dynamics [11]. The increased sample stability and homogeneity provided by this reconstitution method was critical for the success of these novel NMR experiments on an active transporter. Furthermore, the (^{1}H, ^{15}N)-TROSY HSQC spectra in different lipid environments presented here suggest that EmrE dynamics are significantly affected by lipid composition. Experiments are in progress to further investigate the effect of lipid environment on EmrE structure, dynamics, and function.

Acknowledgments

We thank Dr. Gregory DeKoster for modifying the (^{1}H, ^{15}N)-TRACT pulse sequence and Dr. Geoffrey Chang for providing us with the EmrE expression plasmid. We thank the Lohman and Schlesinger labs for use of their fluorimeter, DLS and refractometer. This work was supported by an NSF Graduate Research Fellowship (DGE-1143954) to EAM and the Searle Scholars Program (KAHW).

References

[1] D.E. Warschawski, A.A. Arnold, M. Beaugrand, A. Gravel, É. Chartrand, I. Marcotte, Choosing membrane mimetics for NMR structural studies of transmembrane proteins, BBA - Biomembranes 1808 (2011) 1957–1974.
[2] T. Raschle, S. Hiller, M. Etzkorn, G. Wagner, Nonmicellar systems for solution NMR spectroscopy of membrane proteins, Curr. Opin. Struct. Biol. 20 (2010) 471–479.
[3] S.F. Poget, M.E. Girvin, Solution NMR of membrane proteins in bilayer mimics: small is beautiful, but sometimes bigger is better, Biochim. Biophys. Acta 1768 (2007) 3098–3106.
[4] S.F. Poget, S.M. Cahill, M.E. Girvin, Isotropic bicelles stabilize the functional form of a small multidrug-resistance pump for NMR structural studies, J. Am. Chem. Soc. 129 (2007) 2432–2433.
[5] C.R. Sanders, F. Sönnichsen, Solution NMR of membrane proteins: practice and challenges, Magn. Reson. Chem. 44 (2006) S24–S40 Spec No.
[6] T.H. Bayburt, S.G. Sligar, Membrane protein assembly into Nanodiscs, FEBS Lett. 584 (2010) 1721–1727.
[7] T. Raschle, S. Hiller, T.-Y. Yu, A.J. Rice, T. Walz, G. Wagner, Structural and functional characterization of the integral membrane protein VDAC-1 in lipid bilayer nanodiscs, J. Am. Chem. Soc. 131 (2009) 17777–17779.
[8] S.F. Poget, R. Harris, S.M. Cahill, M.E. Girvin, 1H, 13C, 15N backbone NMR assignments of the Staphylococcus aureus small multidrug-resistance pump (Smr) in a functionally active conformation, Biomol. NMR Assign. 4 (2010) 139–142.
[9] H. Wu, K. Su, X. Guan, M.E. Sublette, R.E. Stark, Assessing the size, stability, and utility of isotropically tumbling bicelle systems for structural biology, Biochim. Biophys. Acta 1798 (2010) 482–488.
[10] K. Bertelsen, B. Vad, E.H. Nielsen, S.K. Hansen, T. Skrydstrup, D.E. Otzen, T. Vosegaard, N.C. Nielsen, Long-term-stable ether-lipid vs conventional ester-lipid bicelles in oriented solid-state NMR: altered structural information in studies of antimicrobial peptides, J. Phys. Chem. B 115 (2011) 1767–1774.
[11] E.A. Morrison, G.T. DeKoster, S. Dutta, R. Vafabakhsh, M.W. Clarkson, A. Bahl, D. Kern, T. Ha, K.A. Henzler-Wildman, Antiparallel EmrE exports drugs by exchanging between asymmetric structures, Nature 481 (2012) 45–50.
[12] D. Rotem, S. Schuldiner, EmrE, a multidrug transporter from *Escherichia coli*, transports monovalent and divalent substrates with the same stoichiometry, J. Biol. Chem. 279 (2004) 48787–48793.
[13] K.J. Glover, J.A. Whiles, G. Wu, N. Yu, R. Deems, J.O. Struppe, R.E. Stark, E.A. Komives, R.R. Vold, Structural evaluation of phospholipid bicelles for solution-state studies of membrane-associated biomolecules, Biophys. J. 81 (2001) 2163–2171.
[14] D. Lee, C. Hilty, G. Wider, K. Wüthrich, Effective rotational correlation times of proteins from NMR relaxation interference, J. Magn. Reson. 178 (2006) 72–76.

[15] F. Delaglio, S. Grzesiek, G.W. Vuister, G. Zhu, J. Pfeifer, A. Bax, NMRPipe: a multidimensional spectral processing system based on UNIX pipes, J. Biomol. NMR 6 (1995) 277–293.

[16] B. Johnson, R. Blevins, NMR view - A computer-program for the visualization and analysis of NMR data, J. Biomol. NMR 4 (1994) 603–614.

[17] J.P. Rosenbusch, Stability of membrane proteins: relevance for the selection of appropriate methods for high-resolution structure determinations, J. Struct. Biol. 136 (2001) 144–157.

[18] C.G. Tate, Practical considerations of membrane protein instability during purification and crystallisation, Methods Mol. Biol. 601 (2010) 187–203.

[19] J.-L. Popot, Amphipols, nanodiscs, and fluorinated surfactants: three nonconventional approaches to studying membrane proteins in aqueous solutions, Annu. Rev. Biochem. 79 (2010) 737–775.

[20] S.H. Park, S. Prytulla, A.A. De Angelis, J.M. Brown, H. Kiefer, S.J. Opella, High-resolution NMR spectroscopy of a GPCR in aligned bicelles, J. Am. Chem. Soc. 128 (2006) 7402–7403.

[21] K. Charalambous, D. Miller, P. Curnow, P.J. Booth, Lipid bilayer composition influences small multidrug transporters, BMC Biochem. 9 (2008) 31.

[22] T.L. Winstone, M. Jidenko, M. le Maire, C. Ebel, K.A. Duncalf, R.J. Turner, Organic solvent extracted EmrE solubilized in dodecyl maltoside is monomeric and binds drug ligand, Biochem. Biophys. Res. Commun. 327 (2005) 437–445.

[23] M. Schwaiger, M. Lebendiker, H. Yerushalmi, M. Coles, A. Gröger, C. Schwarz, S. Schuldiner, H. Kessler, NMR investigation of the multidrug transporter EmrE, an integral membrane protein, Eur. J. Biochem. 254 (1998) 610–619.

[24] P.J.G. Butler, I. Ubarretxena-Belandia, T. Warne, C.G. Tate, The *Escherichia coli* multidrug transporter EmrE is a dimer in the detergent-solubilised state, J. Mol. Biol. 340 (2004) 797–808.

[25] S. Schuldiner, EmrE, a model for studying evolution and mechanism of ion-coupled transporters, Biochim. Biophys. Acta 1794 (2009) 748–762.

[26] H.S. Cho, J.L. Dominick, M.M. Spence, Lipid domains in bicelles containing unsaturated lipids and cholesterol, J. Phys. Chem. B 114 (2010) 9238–9245.

[27] R.E. Minto, P.R. Adhikari, G.A. Lorigan, A 2H solid-state NMR spectroscopic investigation of biomimetic bicelles containing cholesterol and polyunsaturated phosphatidylcholine, Chem. Phys. Lipids 132 (2004) 55–64.

[28] L. van Dam, G. Karlsson, K. Edwards, Direct observation and characterization of DMPC/DHPC aggregates under conditions relevant for biological solution NMR, Biochim. Biophys. Acta 1664 (2004) 241–256.

[29] P.A. Luchette, T.N. Vetman, R.S. Prosser, R.E. Hancock, M.P. Nieh, C.J. Glinka, S. Krueger, J. Katsaras, Morphology of fast-tumbling bicelles: a small angle neutron scattering and NMR study, Biochim. Biophys. Acta 1513 (2001) 83–94.

[30] A. Andersson, L. Mäler, Size and shape of fast-tumbling bicelles as determined by translational diffusion, Langmuir 22 (2006) 2447–2449.

Chapter III. Direct observation of conformational exchange in an asymmetric, antiparallel EmrE homodimer.

This chapter is based on the published paper: EA Morrison[*]*, GT DeKoster*[*]*, S Dutta, R Vafabakhsh, MW Clarkson, A Bahl, D Kern, T Ha, and KA Henzler-Wildman. "Antiparallel EmrE exports drugs by exchanging between asymmetric structures." Nature. (2012)* ***481****: 45-50*[1].

The key step in the single-site alternating-access model of antiport is the interconversion between the inward- and outward-facing states, as this is the step that actually moves substrate across the membrane barrier (**Fig. 1**). According to this model, either two protons or one drug molecule can bind EmrE at a given time. Thus, saturating EmrE with substrate should push EmrE into two-state exchange. Does ligand binding actually push EmrE into two-state exchange, as predicted by single-site alternating-access model? Our objective was to test this hypothesis and directly observe movement between the inward- and outward-facing states. Using solution-state NMR, we were able to quantify the kinetics and thermodynamics of global conformational exchange in the substrate-bound transporter, the key step for transport across the membrane.

Within the single-site alternating-access framework for transport, there are several topological possibilities for the mechanism of exchange in a homodimeric protein (**Fig. 2**). First, the homodimer could function as a parallel, symmetric dimer. In this case, the dimer exchanges between AA and BB conformations such that the two monomers within each conformation are identical. Each conformation has two-fold rotational symmetry around an axis parallel to the bilayer normal. Secondly, the homodimer could function as an antiparallel dimer. The antiparallel homodimer could interconvert between two completely different conformations in which the monomers have different structures in the two conformations. This is effectively an AB-to-CD exchange, with the first monomer exchanging between an A and C structure and the second monomer exchanging between a B and D structure. This case lacks any symmetry relations. However, the antiparallel homodimer could instead function with exchange symmetry. In this case the antiparallel homodimer effectively interconverts with itself in an AB-to-BA exchange. This imparts a pseudo two-fold axis of symmetry around an axis parallel to the plane of the membrane bilayer. Thirdly, the homodimer could exchange between antiparallel (AB) and parallel (CC) conformations, which would be highly unlikely considering that it would require one of the monomers to flip its orientation within the membrane. A combination of solution NMR, fluorescence, and cross-linking experiments allowed us to determine the exchange mechanism for TPP^+-bound EmrE.

EmrE is functional in isotropic bicelles.

Prior to our studies, EmrE had been studied in dodecylmaltoside (DDM) detergent micelles and liposomes of varying lipid composition[2-8]. As elaborated in **Chapter 2**, the native lipid environment combined with the fast tumbling properties of the solubilized isotropic bicelle system make it an attractive system for biophysical studies of EmrE. As transport function cannot be assessed in a solubilized system, we measured transport before solubilizing proteoliposomes to form isotropic bicelles (**Chapter 2**)[1,9] and then used binding as a proxy for function in the final bicellar environment. We measured binding of TPP^+, a commonly studied substrate, to EmrE reconstituted into DMPC/DHPC isotropic bicelles using isothermal titration calorimetry (ITC). Isotropic bicelles are a dynamic system, meaning that the DHPC is in equilibrium between bicelle and monomer. Thus, diluting EmrE in bicelles with titrant would alter this equilibrium and create aberrant heats. To address this issue the ligand was solubilized in a matched bicelle solution. A flat reference titration of TPP^+-bicelle solution into bicelles also indicated that we were not observing the binding or redistribution of TPP^+ in lipid.

For a direct comparison with the literature to show that our purification method produces functional EmrE, we first carried out the titrations with EmrE and TPP^+ in equivalent DDM solutions at 4, 25, and 45°C (**Fig. 3**, **Table 1**). EmrE is accepted to be a properly folded and functional dimer in DDM[2-8,10]. All ITC experiments were performed at pH 7. Since protons are competitive substrates of EmrE, drug binding is linked to pH. The observed binding constant for TPP^+ is tighter at higher pH values and weaker at lower pH values. Thus, care must be taken when comparing to binding constants in the literature. The titrations at 4°C produced curves with few points in the transition region, indicating that the binding was too tight to be accurately measured under the conditions required to produce measurable heats. Published affinities in DDM are roughly 50 nM from $[^3H]TPP^+$-binding assays at pH 7 and 4°C[8,11] and 19 ± 2 nM from ITC at pH 7.5 and an unreported temperature[12], which is consistent with our results. Agreement between our titrations in DDM (120 ± 12 nM) and isotropic bicelles (170 ± 70 nM) at 45°C (**Fig. 3C,D, Table 1**) indicates that our reconstitution method produces functional EmrE in isotropic bicelles. Some difference between detergent and bicelle environments is expected, especially since published dissociation constants for TPP^+ binding to EmrE reconstituted into liposomes with varying ratios of DOPC, DOPE, and DOPG at pH 7.5 and an unreported temperature vary between 19 and 370 nM[12]. In addition, our binding stoichiometries are all close to 0.5 for EmrE reconstituted in both DDM and bicelles (**Table 1**), which is consistent with an EmrE dimer binding a single TPP^+ molecule. Thus, our measured values for TPP^+ binding to EmrE reconstituted into DMPC/DHPC isotropic bicelles at pH 7 are consistent with a fully functional, dimeric protein.

Additional support for a properly folded and functional EmrE is provided by ^{15}N/^{1}H TROSY HSQC spectra of TPP^{+}-bound EmrE reconstituted into both DDM micelles and isotropic bicelles (**Fig. 4**). The spectra are well dispersed, indicating a folded protein. In fact, the chemical shift dispersion is better than expected for an alpha helical membrane protein, which is likely due to the abundance of aromatic residues in the active site. An overlay of these spectra (**Fig. 4**, DDM spectrum from K. Henzler-Wildman) shows that EmrE has the same overall structure in both environments. Peaks shift between the two spectra, consistent with a change in environment, but overall, both spectra have the same chemical shift dispersion, peak pattern, and peak doubling. A comparison of the two spectra also supports the notion that DDM is not optimal for NMR due to longer acquisition times and lower signal-to-noise[13].

EmrE interconverts between two conformations when bound to TPP^{+}.

The ^{15}N/^{1}H TROSY HSQC spectrum of TPP^{+}-bound EmrE in isotropic bicelles (or detergent micelles) reveals a global peak doubling (**Fig. 4**). While EmrE has 105 non-proline residues, there are roughly 210 resolved peaks in its spectrum. This overall peak doubling can be accounted for by an asymmetric dimer or exchange between two states. Structural data from cryoEM and X-ray crystallography indicate that the EmrE dimer is asymmetric[14-16], meaning that two monomers within the dimer have different structures and thus would have unique chemical shifts. However, slow two-state exchange on the NMR timescale could also account for this global peak doubling. The AA-to-BB exchange between two parallel dimers would have two sets of peaks, one from the identical monomers in the AA conformation and the second from the identical monomers in the BB conformation (**Fig. 2**). Only one of the antiparallel exchange mechanisms previously discussed is consistent with a complete peak doubling. The more general AB-to-CD exchange would result in four complete sets of peaks, one from each of the different monomeric states (A, B, C, and D; **Fig. 2**). However, the unique case of antiparallel exchange with exchange symmetry, or an AB-to-BA exchange, reduces this to only two sets of peaks. This distinct exchange mechanism combines an asymmetric dimer with exchange on the NMR timescale. Similar to antiparallel exchange with no symmetry, the antiparallel-to-parallel, or AB-to-CC, exchange would result in more peaks than were observed in the amide HSQC spectrum. This mechanism would result in three sets of peaks, two from the asymmetric, antiparallel dimer, and one from the symmetric, parallel dimer (**Fig. 2**).

Thus, the models that are consistent with 210 peaks for a 105 non-proline amino acid protein are an asymmetric dimer that does not undergo slow exchange on the NMR timescale, a symmetric, parallel dimer undergoing exchange, or an asymmetric, antiparallel dimer undergoing exchange with exchange symmetry. How can these three possibilities be distinguished? As discussed in **Chapter 1**, solution NMR is ideal for measuring protein dynamics on different timescales. Global domain motions that are slow on the NMR timescale (i.e. $k_{ex} \ll \Delta\upsilon$, see **Chapter 1**) can be detected using ZZ-exchange spectroscopy[17]. A modified version of the TROSY-selected ZZ-exchange experiment by Li and Palmer[18] revealed the formation of cross peaks (**Fig. 5**). As described in **Chapter 1**, the only way to observe cross peaks in a ZZ-exchange experiment is if there is a slow exchange process on the NMR timescale. At the concentrations of protein and ligand in the NMR tube, EmrE is fully saturated with ligand, and ligand association/dissociation will not be observed. Thus, the global peak doubling is a result of a two-state conformational exchange process, presumably exchange between the two low-energy conformations of TPP$^+$-bound EmrE.

The ZZ-exchange experiment also identifies exchange partners. The cross-peaks complete boxes that connect the two states (A and B) of a single residue, as shown in **Figure 5**. The populations of the two states can be determined by integrating the two sets of peaks in a fully relaxed ^{15}N/^{1}H TROSY HSQC spectrum. A histogram made from the relative volumes of the minor participant from each exchange partner with two well-resolved peaks is centered at about 0.5 (**Fig. 6**), indicating equal populations in the two states. To get 50/50 populations with a symmetric dimer, AA and BB would need to be distinct conformations that happen to have equivalent free energies. However, the antiparallel model with a pseudo two-fold axis of symmetry requires equal populations for the two exchanging states.

As described in more detail in **Chapter 1**, the auto-peaks decay and cross-peaks grow in as the delay time increases. The rates of these processes are governed by the forward (open-in to open-out) and reverse (open-out to open-in) rates of conformational exchange, which are equivalent because the populations of the two states of EmrE are equal. Thus, there is only a single exchange rate (*k*) to fit. There is additional decay due to the intrinsic relaxation (R^*) of the magnetization during the delay time. The overall change in magnetization in the two states A and B in the ZZ-exchange experiment as a function of time (*t*) is described by:

$$\frac{d}{dt}\begin{bmatrix} A \\ B \end{bmatrix} = \begin{bmatrix} -R^{*A} - k & k \\ k & -R^{*B} - k \end{bmatrix}\begin{bmatrix} A \\ B \end{bmatrix}. \qquad (1)$$

The full solution to this system of differential equations describes the time-dependence of the intensities of the auto-peaks (I_{AA} and I_{BB}) and cross-peaks (I_{AB} and I_{BA}):

$$I_{AA}(t) = I_A^0\left[(k + R^{*B})\left(\frac{e^{\lambda_1 t} - e^{\lambda_2 t}}{\lambda_1 - \lambda_2}\right) + \left(\frac{\lambda_1 e^{\lambda_1 t} - \lambda_2 e^{\lambda_2 t}}{\lambda_1 - \lambda_2}\right)\right] \qquad (2)$$

$$I_{BB}(t) = I_B^0\left[(k + R^{*A})\left(\frac{e^{\lambda_1 t} - e^{\lambda_2 t}}{\lambda_1 - \lambda_2}\right) + \left(\frac{\lambda_1 e^{\lambda_1 t} - \lambda_2 e^{\lambda_2 t}}{\lambda_1 - \lambda_2}\right)\right]$$

$$I_{AB}(t) = I_A^0 k\left[\left(\frac{e^{\lambda_1 t} - e^{\lambda_2 t}}{\lambda_1 - \lambda_2}\right)\right]$$

$$I_{BA}(t) = I_B^0 k\left[\left(\frac{e^{\lambda_1 t} - e^{\lambda_2 t}}{\lambda_1 - \lambda_2}\right)\right]$$

where

$$\lambda_1 = -\frac{(R^{*A} + R^{*B})}{2} - k + \frac{1}{2}\sqrt{(R^{*A} - R^{*B})^2 + 4k^2}$$

$$\lambda_2 = -\frac{(R^{*A} + R^{*B})}{2} - k - \frac{1}{2}\sqrt{(R^{*A} - R^{*B})^2 + 4k^2}$$

and I_A^0 and I_B^0 are the initial intensities (at $t = 0$) of the peaks belonging to states A and B, respectively. In practice, peak heights rather than peak volumes were used because the large EmrE-isotropic bicelle system has fast relaxation. The resulting low signal-to-noise does not allow for accurate integration of volumes. Peak heights were extracted for the auto- and cross-peaks corresponding to the 13 residues with the best signal-to-noise. A total of eight planes with increasing delay times were collected, and the data were fit to the full solution (**eq. 2**) with the residue-specific parameters I_A^0, I_B^0, R^{*A}, and R^{*B} and the global parameter k (**Fig. 7**). This fit provided a value of 4.9 ± 0.5 s^{-1} for the rate of conformational interconversion.

The correlation matrix of all of the parameters in the full fit (**Fig. 8A, B**) indicates that the global parameter k is not correlated with any of the residue-specific parameters. However, for each residue, there is a strong correlation between I_A^0 and R^{*A} and between I_B^0 and R^{*B}. This is not surprising, since peak intensity is dependent on intrinsic relaxation. As expected, the state with the slower relaxation has a higher peak intensity (**Fig. 8C**).

The residue-specific intrinsic relaxation rates provide interesting insight. It is common to make the simplifying assumption that the intrinsic relaxation rates of the two states are equivalent. However, simple observation of the raw data (**Fig. 7**) shows that this is not the case for EmrE. With equal populations in the two states, the intensities of the two auto- and cross-peaks should overlay with each other. For some residues this is the case, but for others it is clear that the intensities are not the same, which is emphasized by the residue-specific fit parameters (**Fig. 9B**). In spin-state selective experiments (such as this TROSY-selected ZZ-exchange experiment), the intrinsic relaxation rate depends on relaxation properties of the amide proton and nitrogen. As a result, differences in dynamics and proton exchange rates, which change with solvent accessibility, can also cause differences in the intrinsic relaxation rate of the two states. The variability between intrinsic relaxation rates is consistent with an alternating-access mechanism of exchange between inward- and outward-facing states, with each state open to only one side of the membrane at a time. Some residues are in similar environments in both states, but others move from being in a protein-packed, more rigid state (closed face) to a looser, water-accessible state (open face). The residues with significant differences in intrinsic relaxation rate map to regions in loops and at the end of helices (**Fig. 9A**), consistent with this mechanism.

In addition to the full fit, ZZ-exchange data can be analyzed using a simpler composite peak ratio analysis[19]. This analysis has the benefit of eliminating the effects of differences in longitudinal relaxation between the two states during the mixing period, transfer efficiency, and transverse relaxation during detection[19]. The composite peak ratio, $\Xi(t)$, has a simple quadratic relationship with the delay time and is given by:

$$\Xi(t) = \frac{I_{AB}(t)I_{BA}(t)}{I_{AA}(t)I_{BB}(t) - I_{AB}(t)I_{BA}(t)} \cong k_{open-in\ to\ open-out}k_{open-out\ to\ open-in}t^2 = k^2t^2 \qquad (3)$$

Eleven residues have adequate signal-to-noise and all four peaks resolved, which is required for data analysis via this method. A global fit to these 11 residues gives a conformational exchange rate of 4.7 ± 0.5 s^{-1} (**Fig. 10**). The 160 ms plane was not used in this analysis due to the low signal-to-noise at long delay times. For this same reason, several residues have abnormally low composite peak ratio values at 130 ms. A jackknife error analysis indicated that no single residue skewed the fit and provided an estimate of the error.

The agreement between the full fit and composite peak ratio analysis confirm that all residues are reporting on a global exchange process that occurs on a single timescale. The residues used in the two analyses are distributed across the whole protein (**Fig. 9A**). These analyses are also in agreement with tryptophan side chain dynamics (5 ± 2 s^{-1}), which were measured using ^{15}N-separated NOESY and ROESY spectra collected with variable mixing times (**Fig. 11**, K. Henzler-Wildman). Considering the difference in conditions (environment and temperature), the rate of interconversion agrees with the rate of an unexplained slow phase observed in a series of stopped flow experiments carried out on DDM-solubilized EmrE at 25°C[11].

<u>TPP$^+$-bound EmrE interconverts between two asymmetric, antiparallel conformations.</u>

Additional experiments were required to determine EmrE topology and distinguish between the models of exchange between symmetric, parallel dimers and exchange between asymmetric, antiparallel dimers with exchange symmetry. Bulk and single-molecule FRET and cross-linking experiments were used to determine the relative orientation of monomers within the EmrE dimer. Single-cysteine mutants were used for these experiments. The three native cysteines (C39, C41, and C95) were mutated to serine and single cysteines were added into termini or loop positions (N2C, T56C, and Q81C). These mutants have been used in published biochemical experiments and are known to be functional[20-22]. Additionally, an overlay of $^{15}N/^{1}H$ TROSY HSQC spectra from WT and T56C on a cys-less background reveals the same peak pattern (**Fig. 12**, S. Dutta), supporting the same overall fold for the mutants.

Labeling for bulk fluorescence experiments was carried out on T56C-EmrE reconstituted into liposomes using the dye pair Alexa Fluor 488 (donor) and Alexa Fluor 568 (acceptor) (work done in conjunction with G. DeKoster). This provided an environment to selectively label a single surface of the dimer. To test for antiparallel dimers, EmrE was labeled with donor and acceptor fluorophores from opposite sides of the membrane (**Fig. 13A**). First, one fluorophore was added to proteoliposomes. This dye would only react with cysteines exposed to the exterior of the liposomes. Then, the proteoliposomes were disrupted with detergent and the second fluorophore was added. This dye would react with all remaining cysteines, i.e. the cysteines that were initially facing the liposomal interior. The resulting sample was solubilized to form isotropic bicelles in order to isolate individual dimers and prevent interactions between fluorophores on different dimers. In the case of an antiparallel dimer, this labeling scheme would result in one donor and one acceptor per dimer and thus FRET signal upon donor excitation. In the case of a parallel dimer, this labeling scheme would instead result in either two donors or two acceptors per dimer, depending on the initial orientation of the dimer within the liposome, and thus no FRET signal upon donor excitation. These samples showed FRET and thus support an antiparallel dimer (**Fig. 13C**, red line).

On the other hand, to test for parallel dimers, T56C-EmrE in liposomes was simultaneously labeled with donor and acceptor fluorophores from one side of the membrane (**Fig. 13B**). A mixture of the two dyes was added to the exterior of the liposomes, producing dimers with only one monomer labeled with a dye molecule in the case of an antiparallel dimer. In the case of a parallel dimer, however, this method would produce a mixture of dimer populations with two donors, two acceptors, or one donor and one acceptor. With this labeling scheme, the only scenario capable of producing FRET is the case of a parallel dimer with one donor and one acceptor dye. These samples showed very little FRET upon donor excitation (**Fig. 13C**, blue line), which could also be due to dye leakage through the membrane or the formation of higher order oligomers. As an additional control, samples were similarly made by labeling only from the exterior of the liposome, but only adding either donor or acceptor fluorophore. After solubilizing into bicelles, donor-only and acceptor-only samples were mixed. This resulted in no FRET signal (**Fig. 13C**, black line), indicating that there was no monomer-swapping between dimers and no direct excitation of acceptor.

Single-molecule FRET (smFRET) studies were carried out to eliminate any concerns due to dye leakage during the labeling procedure and the formation of higher-order oligomers (work by S. Dutta and R. Vafabakhsh). For these studies, the same single-cysteine mutants of EmrE (N2C, T56C, and Q81C) solubilized in DDM micelles were labeled simultaneously with donor and acceptor (Cy3/Cy5), resulting in statistical populations of EmrE labeled with two donors, two acceptors, or one donor and one acceptor, which is the population of interest. The strength of a single-molecule technique for these topological studies is that it allows for characterization of each particle used in the analysis. By selecting for particles that have single donor and single acceptor photobleaching events, there is complete certainty that any FRET signal is originating from a complex labeled with a single donor and a single acceptor fluorophore. A single, narrow FRET distribution was obtained for each of three single-cysteine EmrE samples (**Fig. 13D, Fig. 14**). In the case of a symmetric, parallel dimer, two populations would be observed in the FRET distribution: one with larger distance separation (lower FRET) corresponding to the open conformation, and a second with smaller distance separation (higher FRET) corresponding to the closed conformation where the loops and termini pack together to seal off access to the binding pocket (**Fig. 2**). However, the case of an antiparallel dimer would result in only a single FRET distribution. Although each fluorophore would be attached to a face of the protein that was alternating between open and closed conformations, the overall distance separation between the two fluorophores would remain the same (**Fig. 2**). Thus, the observed single FRET distribution supports an antiparallel topology and corresponds to a FRET efficiency of 0.6-0.7, depending on the labeling location, which in turn corresponds to an inter-dye distance of 50-55 Å. These distances are consistent with fluorophores that are on opposite sides of the membrane. Based on the dimensions of the cryoEM structure, fluorophores that reacted on the same side of the membrane should be a no more than 35 Å apart, which would correspond to a FRET efficiency of greater than 0.9. The three different single-cysteine mutants confirm that the same distances are observed independent of which site is labeled.

The smFRET data alone does not distinguish between an antiparallel dimer with or without exchange symmetry. However, the model of an asymmetric, antiparallel EmrE dimer with exchange symmetry is the only model that is in agreement with both the NMR and fluorescence data. No conformational exchange was observed in the smFRET time traces, even though the rates measured by solution NMR would be on the observable timescale for the method, providing additional supporting idea of an AB-to-BA interconversion with the same distances in both the inward- and outward-facing states.

Additional support for the model of an asymmetric, antiparallel dimer with exchange symmetry is provided by cross-linking experiments (work by S. Dutta). Cross-linking experiments were carried out on S107C and S107C/K22R EmrE (both in a cys-less background) with the homobifunctional cross-linker o-PDM and the heterobifunctional cross-linker s-GMBS. O-PDM has a short, rigid connector and will only covalently cross-link two cysteines that are within close proximity. Thus, o-PDM can only cross-link a parallel dimer, which has the two cysteines on the same side of the membrane (**Fig. 15B, C**). On the other hand, s-GMBS covalently cross-links a sulfhydryl (cysteine) to a nearby primary amine (lysine sidechain or N-terminus). Under identical conditions, o-PDM partially cross-links S107C EmrE, but s-GMBS nearly completely cross-links this single-cysteine mutant (**Fig. 15A**, left). The double mutant S107C/K22R eliminates cross-linking by s-GMBS (**Fig. 15A**, right), indicating that this compound cross-links S107C to K22 rather than the N-terminus, the only other primary amine in the protein. Since K22 and S107C are on opposite sides of the membrane in the monomer, these two residues can only be cross-linked in an antiparallel homodimer (**Fig. 15B, C**). Cross-linking by both o-PDM and s-GMBS is contradictory until considering the possibility of interactions between dimers. Two dimers coming into close proximity can conceivably bring two C-termini close enough for cross-linking by o-PDM to occur. In this situation, an increase in the relative concentration of EmrE within the membrane should result in an increase in cross-linking by the homobifunctional cross-linker. As predicted, a 1:60 ratio of EmrE:lipid results in relatively equal populations of monomer and dimer, but a 1:20 ratio of EmrE:lipid results in nearly complete cross-linking by o-PDM (**Fig. 15D**). As an additional control, cross-linking was performed in the presence of SDS, which monomerizes EmrE. Neither cross-linker was effective in this case (**Fig. 15A**, left), showing that oligomerization is necessary for any cross-linking to occur.

The NMR, fluorescence, and cross-linking experiments provide convincing evidence for the asymmetric, antiparallel model of EmrE with exchange symmetry, but are the two states we observe really the inward- and outward-facing states that the single-site alternating-access model predicts are the two low-energy states for TPP^+-bound EmrE? The regions that are closed in one conformation but open in the other (i.e. loops and ends of helices) will have different water accessibility. Water accessibility can be assessed using a water-soluble paramagnetic probe, such as chelated gadolinium. Paramagnetic ions increase the relaxation of nuclei in a distance-dependent manner. As a result, amides in close proximity to a paramagnetic ion will display line-broadening in a $^{15}N/^{1}H$ TROSY HSQC. Collecting $^{15}N/^{1}H$ TROSY HSQC spectra at increasing concentrations of the probe provides a feel for the level of water accessibility of a given amide (work by G. DeKoster, **Fig. 16A**). Some amides are equally protected from the gadolinium in both states and map to the transmembrane helices (**Fig. 16B**). Others are equally broadened by the gadolinium in both states, and map to loop regions (**Fig. 16B**). The most interesting residues are the ones that are differentially broadened, indicating a change in water accessibility between the two states. These residues map to the pore region, loops, and ends of helices (**Fig. 16B**), and support the existence of two conformations that are each open to only one side of the membrane at a time, consistent with the alternating-access mechanism for transport.

Mechanistic insight can be gained by looking at chemical shift differences between states A and B. Chemical shift is sensitive to local structural changes, and thus chemical shift differences between the two states highlight local regions that change upon the AB-to-BA conformational interconversion, when the two monomers swap states. As discussed previously, the ZZ-exchange experiment identifies exchange partners. The $^{15}N/^{1}H$ TROSY HSQC can essentially be separated into a spectral fingerprint for each state (**Fig. 17**), allowing for the calculation of chemical shift differences according to:

$$\Delta\omega = \sqrt{(\Delta\omega_H)^2 + (\Delta\omega_H/10)^2} \qquad (4)$$

where $\Delta\omega$ is an average of the difference between states A and B of the amide proton ($\Delta\omega_H$) and amide nitrogen ($\Delta\omega_N$) chemical shifts, weighted by gyromagnetic ratio. There is a large variation in chemical shift difference across the protein sequence (**Fig. 18A**), indicating that some regions have larger structural changes upon exchanging states. Plotting these differences on the crystal structure of TPP^+-bound EmrE shows that the largest changes localize to several regions (**Fig. 18B**). Since the crystal structure has a monomer in each state, rotating the monomer in state B by 180° and placing it onto the monomer in state A orients the two monomers in the same way and makes these changes easier to visualize. By aligning TM1-TM3, it becomes clear that TM1-TM3, the helices that form the binding pocket, have relatively small chemical shift changes and behave largely as a rigid unit that is simply reoriented upon interconversion. The largest chemical shift changes in this region are located in the loops, the C-terminal end of TM1, and the C-terminal half of TM3. The changes in the loops and C-terminal end of TM1 are consistent with the changes that must occur to alternatingly close-off and open-up each side of the membrane in the alternating-access mechanism. The large changes in the C-terminal half of TM3 are consistent with the kink at the GVG motif in state A that straightens in state B. The side of TM4 that faces the TM1-TM3 bundle also has some of the largest chemical shift changes due to the reorientation of TM4 with respect to the rest of the protein. The regions that have the largest chemical shift changes coincide with regions that are important mechanistically for the conformational interconversion.

We have directly observed the two-state exchange between inward- and outward-facing states of TPP$^+$-bound EmrE. Along with solution NMR, fluorescence and cross-linking experiments confirm the unique model where EmrE is both asymmetric and undergoes a conformational exchange. Asymmetric, antiparallel EmrE has a pseudo 2-fold axis of symmetry, such that the inward- and outward-facing states are identical. This model resolves the apparent clash between the asymmetric, antiparallel structural data and the functional symmetry of residues in the active site.

Methods (modified from[1]):

EmrE expression and purification. EmrE was expressed using a pET15b plasmid provided by G. Chang[15]. This vector produces EmrE with an amino (N)-terminal 6×His tag that can be removed by cleavage with thrombin to leave only three extra N-terminal residues (GSH). The final protein sequence after cleavage is: GSH MNPYIYLGGA ILAEVIGTTL MKFSEGFTRL WPSVGTIICY CASFWLLAQT LAYIPTGIAY AIWSGVGIVL ISLLSWGFFG QRLDLPAIIG MMLICAGVLI INLLSRSTPH. BL21(DE3) cells transformed with this vector were grown in M9 minimal media. EmrE was induced with 0.33 mM IPTG at an optical density (OD_{600}) of 0.7–0.8 at 17 °C. Cells were harvested after 14-20 hrs. $^1H/^{15}N$-labeled EmrE was produced in the same way substituting 1 g $^{15}NH_4Cl$. $^2H/^{15}N$-labelled EmrE was produced by growing cells in $^2H/^{15}N$ M9 (1 g $^{15}NH_4Cl$, 2 g glucose, 12.8 g $Na_2HPO_4 \bullet 7H_2O$, 3.0 g KH_2PO_4, 0.5 g NaCl, 2 mL 1 M $MgSO_4$ in D_2O, 100 mL 1 M $CaCl_2$ in D_2O, 100 mg ampicillin, one generic multivitamin, and 0.5 g $^2H/^{15}N$ Isogro (Sigma) per liter).

Cell pellets were re-suspended in lysis buffer (100 mM NaCl, 2.5 mM $MgSO_4$, 20mM tris pH 7.5, 250 mM sucrose, 5 mM β-mercaptoethanol, 1mg/mL lysozyme, DNaseI, 1 mg/mL pepstatin, 10 mM leupeptin and 100 mM PMSF) and lysed by sonication. The membrane fraction was separated by a high-speed spin (30,000 ×g for 1 hr), re-suspended in the same buffer and solubilized with 40 mM decylmaltoside (DM, Anatrace) at room temperature for 2 hrs. After a second high-speed spin, the supernatant was applied to Ni-NTA His•Bind beads (Novagen) prewashed with buffer A (10 mM DM, 10 mM KCl, 90 mM NaCl, 20 mM tris, pH 7.8, 5 mM β-mercaptoethanol) and allowed to bind for 15-30 min at room temperature. The beads were washed with 10 bed volumes of buffer A, followed by 10 bed volumes of buffer B (buffer A + 5 mM imidazole). EmrE was eluted with five bed volumes of elution buffer (buffer A + 400 mM imidazole). The salt concentration was increased to 200-250 mM and thrombin was added to cleave the His-tag overnight at room temperature. Samples were then concentrated and 0.5ml aliquots and loaded onto a Superdex 200 column pre-equilibrated with NMR buffer (20 mM potassium phosphate, 20 mM NaCl, pH 7.0) with 10 mM DM. The protein eluted near 14-15 ml with a symmetric peak. Fractions containing EmrE were combined and reconstituted into bicelles. For samples in dodecylmaltoside (DDM, Anatrace), DDM was substituted for DM throughout the protocol and the FPLC were combined and concentrated to the desired final protein/detergent concentration.

Preparation of isotropic bicelles. First, the amount of EmrE in the combined FPLC fractions was determined as described below. Long-chain lipid (DLPC (1,2-dilauroyl-sn-glycero-3-phosphocholine) or DMPC (1,2-dimyristoyl-sn-glycero-3-phosphocholine), Avanti Polar Lipids) was hydrated in NMR buffer at 20 mg/mL. A molar ratio of at least 200:1 lipid:EmrE dimer was used for all samples. The lipids were bath sonicated for 10 min and 0.51% octyl glucoside (Anatrace) was added. After 20 min, they were mixed with the FPLC fractions containing EmrE and incubated for 30 min. Three aliquots of 30 mg BioBeads (BioRad) per milligram of total detergent were used to remove the detergent. After removal of the BioBeads, the vesicles were collected by ultracentrifugation at 50,000 ×g for 1 hr at 20 °C. The supernatant was removed and the pellet was re-suspended in NMR buffer containing DHPC (1,2-dihexanoyl-sn-glycero-3-phosphocholine, Avanti Polar Lipids) to break the liposomes up into bicelles. The DHPC concentration was calculated to produce a 1:3 ratio of long-chain lipid:DHPC, assuming 85-90% recovery of long-chain lipid. Four freeze–thaw cycles were used to produce uniform bicelles. Samples were stored at -80°C until use.

EmrE concentration determination. EmrE concentration was determined using absorbance at 280 nm. The extinction coefficient (38,370 $M^{-1}cm^{-1}$) was calibrated using amino acid analysis of three samples of EmrE each in DDM and DM, and was found to be the same for EmrE in bicelles.

Isothermal Titration Calorimetry. ITC experiments were performed using a VP-ITC titration microcalorimeter (MicroCal) by titrating TPP^+ (50–80 μM) into EmrE (9–13 μM) in isotropic bicelles ($q_{effective}$ = 0.33[23], DMPC/DHPC) or 5 mM analytical grade DDM. Both the TPP^+ and EmrE solutions were in NMR buffer and had matching detergent or lipid concentrations. Matching bicelle stocks were produced by acquiring proton NMR spectra of all samples (empty bicelle blank, TPP^+ stock, and EmrE stock), integrating the DMPC and DHPC terminal methyl peaks, and ensuring that the lipid ratio and peak volumes matched. Isotropic bicelle samples had a total lipid concentration of 30-50 mM and $q_{effective}$ = 0.33. The TPP^+ concentration in the final stock solution was determined spectrophotometrically (ε = 4,400 $M^{-1}cm^{-1}$ at 269 nm and 3,750 $M^{-1}cm^{-1}$ at 276 nm). Heats of dilution were determined from reference titrations of the same TPP^+ stock into empty micelles or bicelles. Data were fit to a model of the ligand TPP^+ (X) binding to n independent and identical sites on the macromolecule EmrE (M) to determine the association constant (*K*), enthalpy of binding (*ΔH*) and binding stoichiometry (*n*), using equation (5):

$$Q_i^{tot} = V_0 \Delta H \cdot M_i^{tot} \frac{nKx}{1+Kx} \qquad (5)$$

where x is the free ligand concentration, M_i^{tot} is the total macromolecule concentration, Q_i^{tot} is total heat after the i^{th} injection and V_o is the cell volume. The data were fit with a nonlinear least-squares approach using the ITC Data Analysis in Origin software supplied with the calorimeter (OriginLab).

Error was determined from standard deviation between replicate experiments. The *K* values from each replicate were averaged, and then the average value was converted to the dissociation constant, K_d.

Bulk FRET sample preparation and measurement. All FRET and cross-linking experiments used single-cysteine mutants of EmrE: the three native cysteines were mutated to serine and a single cysteine was introduced at the desired location. T56C-EmrE was reduced with DTT and then reconstituted into DMPC liposomes with a molar ratio at least 300:1 lipid:EmrE monomer. After ultracentrifugation to collect the liposomes, they were re-suspended in deoxygenated NMR buffer with 2 mM cysteine and extruded through 400 μm filters to produce unilamellar vesicles loaded with cysteine. The sample was passed over a G25 Sephadex column to remove free cysteine from the exterior of the liposomes. The tight-binding substrate TPP^+ was maintained at saturating concentrations throughout the preparation to stabilize EmrE dimers and prevent monomer swapping.

To test for antiparallel topology, the first dye-maleimide was added to the exterior of the liposomes at a 5-fold molar excess relative to EmrE monomer. The reaction was allowed to proceed for 30 min, and then quenched by addition of 20-fold excess of β-mercaptoethanol. Free dye was removed by collecting the liposomes via ultracentrifugation, re-suspending the liposomes in fresh buffer, and repeating the ultracentrifugation. The second dye-maleimide was added along with octyl glucoside to disrupt the liposomes. The reaction was allowed to proceed for 1 hr and then quenched as before. Free dye and detergent were removed by passing the sample over a G25 Sephadex column. DHPC was then added to the liposome suspension to form bicelles. Alexa Fluor 488 was used as the donor and Alexa Fluor 568 as the acceptor for bulk FRET experiments.

To test for parallel topology, samples were produced in a similar manner, but labeled with mixed donor and acceptor only from the exterior of the liposome. After the labeling reaction, remaining free dye was quenched and removed, and then DHPC was added to form bicelles. This should produce EmrE with only one face labeled by fluorescent dye, and any cysteine that faces the interior of the liposome should remain unlabeled. Two additional control samples were independently labeled with either donor only or acceptor only from the exterior of the liposome and then mixed.

Fluorescence measurements were made using a PTI spectrofluorimeter (Photon Technology International) using FeliX fluorescence analysis software version 1.42b (Photon Technology International). Labeled T56C-EmrE samples were diluted into isotropic bicelles or 5% SDS containing 2 mM TPP^+. The donor, Alexa Fluor 488 was excited at a wavelength of 488 nm and emission spectra were collected scanning from 500 to 750 nm. The acceptor, Alexa Fluor 568, was excited at a wavelength of 568 nm and emission spectra were collected scanning from 580 to 750 nm.

Single-molecule FRET experiments. Three different single-cysteine mutants, N2C, Q81C and T56C, were labeled with Cy3-maleimide and Cy5-maleimide for single-molecule

FRET experiments. Labeling was performed in the same manner as bulk FRET samples or by labeling EmrE in detergent micelles using an equimolar mixture of donor and acceptor before reconstitution into isotropic bicelles as previously described. The final bicelles used for single-molecule FRET experiments contained 0.1% biotinyl-DPPE for immobilizing the samples. Single-molecule experiments were performed on a wide-field total internal reflection fluorescence microscope set up[24]. Biotinylated bicelles containing Cy3 and Cy5 labeled EmrE were specifically immobilized on a polymer-coated quartz surface. Then free bicelles were flushed out of the chamber and molecules were imaged in the imaging buffer consisting of 3 mM Trolox and the oxygen scavenger system (0.8% dextrose, 0.1 mg/mL glucose oxidase, 0.02 mg/mL catalase) in NMR buffer (2 mM TPP^+, 20 mM NaCl, 20 mM potassium phosphate, pH 7.0). A 532 green laser (Coherent) was used for Cy3 excitation and the sample was imaged by a charge-coupled-device camera (iXon DV 887-BI; Andor Technology). Homemade IDL and C++ programs were used to record and analyze the movies. FRET efficiency was calculated from $I_A/(I_A + I_D)$, where I_D and I_A are the donor (Cy3) and acceptor (Cy5) fluorescent intensities, respectively.

For each sample, several minute-long movies were collected (imaging area 70 μm × 35 μm) at 100 ms time resolution. Donor and acceptor intensity time traces were corrected for the background and smoothed using four-point adjacent-averaging. FRET efficiencies from molecules that showed single Cy3 and Cy5 photobleaching steps were chosen to build the histograms.

Cross-linking of EmrE. o-PDM (N,N'-(o-phenylene)dimaleimide) and s-GMBS were used to cross-link S107C EmrE to test for parallel (o-PDM) or antiparallel (s-GMBS) topology. These experiments were performed with 90 μM EmrE, 20 mM potassium phosphate, 20 mM sodium chloride, 1 mM TCEP, pH 7, and cross-linking for 20 min at 37°C followed by quenching with β-mercaptoethanol at 20-fold excess over the cross-linker concentration. Cross-linking in detergent was performed in 10 mM DM; cross-linking in lipid was performed in DLPC liposomes at the specified protein:lipid ratio. Addition of SDS monomerizes EmrE and provides a control. S107/K22R serves as a control to determine whether the lysine side chain or N-terminal amine participates in the s-GMBS cross-linking reaction.

NMR sample preparation and data acquisition. All NMR samples were 0.5 – 1.0 mM ^{2}H/^{15}N-EmrE, and contained excess (2 mM) TPP^{+} to saturate the protein with substrate. The sample in DDM (**Fig. 4A**, green) had 118 mM DDM. All other NMR samples were in isotropic bicelles as described above, with at least 100:1 long-chain lipid:EmrE molar ratio, total lipid concentrations of 300-400 mM and $q \approx 0.33$. The q-value was confirmed for each sample by integrating the DMPC (or DLPC) and DHPC methyl resonances. All NMR samples were prepared in 20 mM potassium phosphate, 20 mM NaCl buffer, pH 7.0, and contained 0.05% NaN_3, 2 mM TCEP and 10% D2O.

Two-dimensional TROSY spectra and the ^{15}N-separated nuclear Overhauser enhancement spectroscopy (NOESY)–HSQC and rotating frame nuclear Overhauser spectroscopy (ROESY)–HSQC spectra were acquired on a 700 MHz Varian spectrometer equipped with a room-temperature probe using standard pulse sequences with gradient coherence selection. The TROSY-selected ZZ-exchange experiment[18] was modified to include a lipid 'flipback' pulse. To accomplish this, a UBURP pulse was added immediately preceding the back-transfer (i.e. directly before the pulse labeled ϕ_5 in **Fig. 6C** of **Chapter 1**). This UBURP pulse was centered at 2.9 ppm, with a bandwidth of 2.6 ppm and power optimized for suppression of lipid signal. These spectra were acquired on a 800 MHz Bruker spectrometer equipped with a cryoprobe. ZZ- exchange spectra were acquired with mixing times of 20, 30, 40, 50, 80, 100, 130, 160 ms with 128 scans per increment and 128 complex points in the indirect dimension.

Eighty percent of the backbone resonances were assigned using a non-standard protocol that combined standard triple resonance experiments with amino-acid-specific labeling and ZZ-exchange data. 3D TROSY-HNCA, TROSY-HNCO, and TROSY-HN(CO)CA spectra were collected to walk the backbone. Low signal-to-noise caused by long experiments on a large, dynamic system in addition to the high degree of overlap in the central region of the spectra meant that there were many places where assignments were ambiguous and the walk along the backbone was broken. Single-tryptophan mutants (W31Y, W45Y, and W76Y) were produced to assign those residues, and the active-site residue W63 was assigned via process of elimination. Specific amino acid labeling was performed to simplify the spectra. Amino acid typing was carried out using samples made with specific ^{13}C'/^{14}N/^{1}H amino acids (Phe, Tyr, Leu, Gly, Ile, Ala, and Val) added to a uniform ^{12}C/^{15}N/^{2}H background[25]. These samples produced ^{15}N/^{1}H TROSY HSQC spectra where the specifically labeled amino acid (*i*) dropped out. In addition, only the $i + 1$ residue was observed in an HNCO plane. The TROSY-selected ZZ-exchange experiment was used to assign exchange partners. However, the central region is highly crowded. Specific ^{15}N amino acids (Ile and Leu) were added to a uniform ^{14}N/^{2}H background for simplified ZZ-exchange experiments. Residue and state assignments were confirmed using a ^{15}N-separated ^{1}H-^{1}H NOESY.

NMR data were processed and analyzed with NMRPipe[26], NMRView[27], Sparky[28], and IgorPro (Wavemetrics). All EmrE structure figures were created in PyMOL using Protein Data Bank 3B5D with the backbone rebuilt to render the cartoons.

Table 1. Isothermal Titration Calorimetry Data: EmrE binding to TPP^+

Sample	**Temperature (°C)**	K_A **(M^{-1})**	n^a	**Average K_D (nM)**	**Average *n***
DDM micelles	4	2.03×10^7 1.36×10^7	0.52 0.48	60 ± 20	0.50 ± 0.05
	25	2.47×10^7 1.81×10^7	0.51 0.52	50 ± 10	0.52 ± 0.05
	45	8.60×10^6 8.02×10^6	0.52 0.50	120 ± 12	0.51 ± 0.05
Isotropic bicelles[b]	45	4.18×10^6 1.04×10^7 4.96×10^6 6.51×10^6 3.94×10^6 5.06×10^6	0.44 0.53 0.41 0.47 0.44 0.46	170 ± 70	0.46 ± 0.05

[a] Binding stoichiometry, ligand/protein.

[b] $q_{eff} = 0.33$ DMPC/DHPC bicelles. Replicates are from 3 independently prepared samples.

References:

1. Morrison, E. A. *et al.* Antiparallel EmrE exports drugs by exchanging between asymmetric structures. *Nature* **481,** 45–50 (2012).
2. Schuldiner, S. EmrE, a model for studying evolution and mechanism of ion-coupled transporters. *BBA - Proteins and Proteomics* 1–15 (2009). doi:10.1016/j.bbapap.2008.12.018
3. Charalambous, K., Miller, D., Curnow, P. & Booth, P. J. Lipid bilayer composition influences small multidrug transporters. *BMC Biochem* **9,** 31 (2008).
4. Tate, C. G., Ubarretxena-Belandia, I. & Baldwin, J. M. Conformational changes in the multidrug transporter EmrE associated with substrate binding. *J Mol Biol* **332,** 229–242 (2003).
5. Rotem, D. & Schuldiner, S. EmrE, a multidrug transporter from Escherichia coli, transports monovalent and divalent substrates with the same stoichiometry. *J Biol Chem* **279,** 48787–48793 (2004).
6. Soskine, M., Adam, Y. & Schuldiner, S. Direct evidence for substrate-induced proton release in detergent-solubilized EmrE, a multidrug transporter. *J Biol Chem* **279,** 9951–9955 (2004).
7. Yerushalmi, H., Mordoch, S. S. & Schuldiner, S. A single carboxyl mutant of the multidrug transporter EmrE is fully functional. *J Biol Chem* **276,** 12744–12748 (2001).
8. Muth, T. R. & Schuldiner, S. A membrane-embedded glutamate is required for ligand binding to the multidrug transporter EmrE. *EMBO J* **19,** 234–240 (2000).
9. Morrison, E. A. & Henzler-Wildman, K. A. Reconstitution of integral membrane proteins into isotropic bicelles with improved sample stability and expanded lipid composition

profile. *Biochimica et Biophysica Acta (BBA) - Biomembranes* **1818,** 814–820 (2012).

10. Ubarretxena-Belandia, I. & Tate, C. G. New insights into the structure and oligomeric state of the bacterial multidrug transporter EmrE: an unusual asymmetric homo-dimer. *FEBS Lett* **564,** 234–238 (2004).
11. Adam, Y., Tayer, N., Rotem, D., Schreiber, G. & Schuldiner, S. The fast release of sticky protons: kinetics of substrate binding and proton release in a multidrug transporter. *Proc Natl Acad Sci USA* **104,** 17989–17994 (2007).
12. Miller, D. *et al.* In vitro Unfolding and Refolding of the Small Multidrug Transporter EmrE. *J Mol Biol* **393,** 815–832 (2009).
13. Sanders, C. R. & Sönnichsen, F. Solution NMR of membrane proteins: practice and challenges. *Magn Reson Chem* **44 Spec No,** S24–40 (2006).
14. Ubarretxena-Belandia, I., Baldwin, J. M., Schuldiner, S. & Tate, C. G. Three-dimensional structure of the bacterial multidrug transporter EmrE shows it is an asymmetric homodimer. *EMBO J* **22,** 6175–6181 (2003).
15. Chen, Y. J. *et al.* X-ray structure of EmrE supports dual topology model. *Proc Natl Acad Sci USA* **104,** 18999–19004 (2007).
16. Fleishman, S. J. *et al.* Quasi-symmetry in the cryo-EM structure of EmrE provides the key to modeling its transmembrane domain. *J Mol Biol* **364,** 54–67 (2006).
17. Farrow, N. A., Zhang, O., Forman-Kay, J. D. & Kay, L. E. A heteronuclear correlation experiment for simultaneous determination of 15N longitudinal decay and chemical exchange rates of systems in slow equilibrium. *J Biomol NMR* **4,** 727–734 (1994).
18. Li, Y. & Palmer, A. G. TROSY-selected ZZ-exchange experiment for characterizing slow chemical exchange in large proteins. *J Biomol NMR* **45,** 357–360 (2009).
19. Miloushev, V. Z. *et al.* Dynamic properties of a type II cadherin adhesive domain: implications for the mechanism of strand-swapping of classical cadherins. *Structure* **16,** 1195–1205 (2008).
20. Amadi, S. T., Koteiche, H. A., Mishra, S. & McHaourab, H. S. Structure, dynamics and substrate-induced conformational changes of the multidrug transporter emre in liposomes. *J Biol Chem* (2010). doi:10.1074/jbc.M110.132621
21. Nara, T. *et al.* Anti-parallel membrane topology of a homo-dimeric multidrug transporter, EmrE. *J Biochem* **142,** 621–625 (2007).
22. Mordoch, S. S., Granot, D., Lebendiker, M. & Schuldiner, S. Scanning cysteine accessibility of EmrE, an H+-coupled multidrug transporter from Escherichia coli, reveals a hydrophobic pathway for solutes. *J Biol Chem* **274,** 19480–19486 (1999).
23. Glover, K. J. *et al.* Structural evaluation of phospholipid bicelles for solution-state studies of membrane-associated biomolecules. *Biophysical Journal* **81,** 2163–2171 (2001).
24. Roy, R., Hohng, S. & Ha, T. A practical guide to single-molecule FRET. *Nat Methods* **5,** 507–516 (2008).
25. Takeuchi, K., Ng, E., Malia, T. J. & Wagner, G. 1-13C amino acid selective labeling in a 2H15N background for NMR studies of large proteins. *J Biomol NMR* **38,** 89–98 (2007).
26. Delaglio, F. *et al.* NMRPipe: a multidimensional spectral processing system based on UNIX pipes. *J Biomol NMR* **6,** 277–293 (1995).
27. JOHNSON, B. & BLEVINS, R. NMR VIEW - A COMPUTER-PROGRAM FOR THE VISUALIZATION AND ANALYSIS OF NMR DATA. *J Biomol NMR* **4,** 603–614 (1994).
28. Goddard, T. D. & Kneller, D. G. Sparky 3.

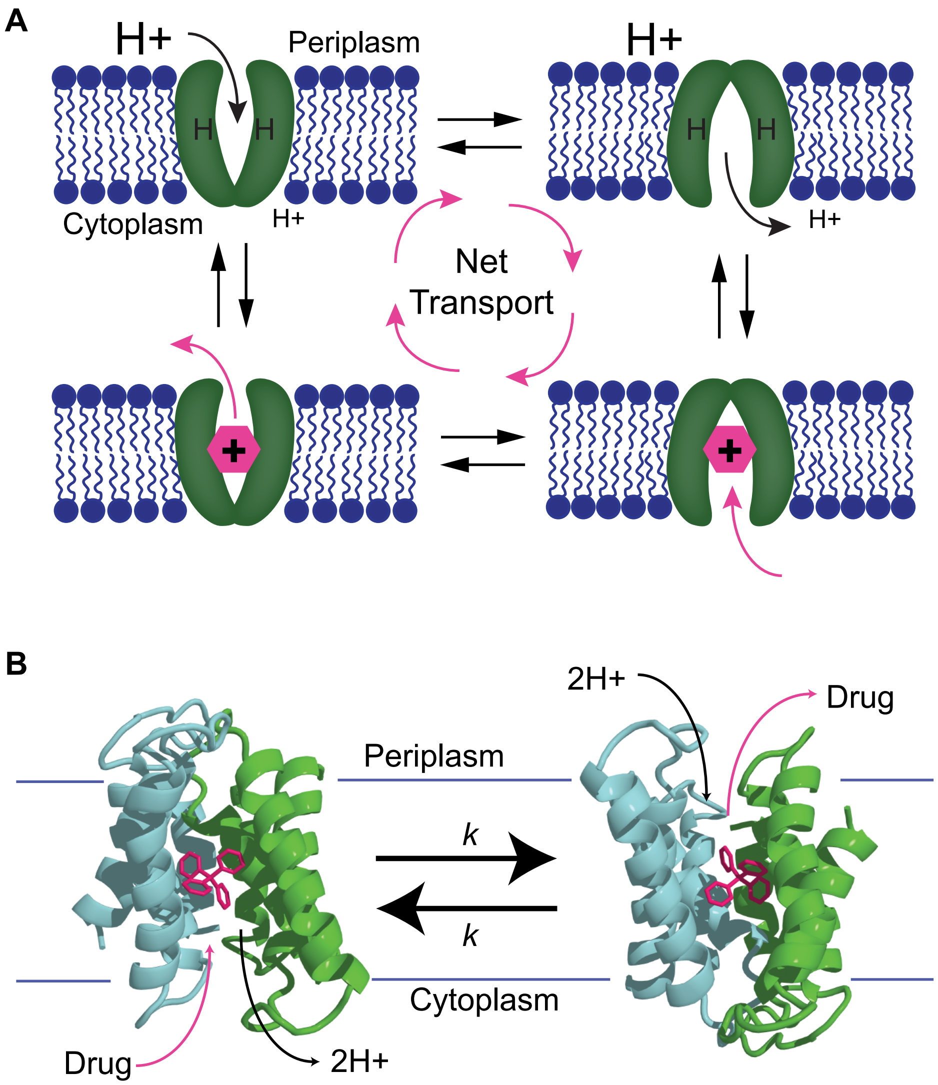

Figure 1. Conformational interconversion in transport mechanism of EmrE. **A.** Cartoon of single-site alternating-access transport by EmrE. In each step of the tranpsort cycle, EmrE is only open to one side of the membrane at a time. EmrE can only alternate access of its binding site between the two sides of the membrane when substrate (either two protons or one drug molecule) is bound. **B.** Proposed interconversion between open-in and open-out conformations of antiparallel, asymmetric EmrE. The two structures are related by a 180° rotation around an axis parallel to the membrane bilayer, going directly into the page. The two monomers are colored differently (blue and green), and TPP^+ is shown in magenta. Figures from Morrison, et al. 2012 (ref. 1).

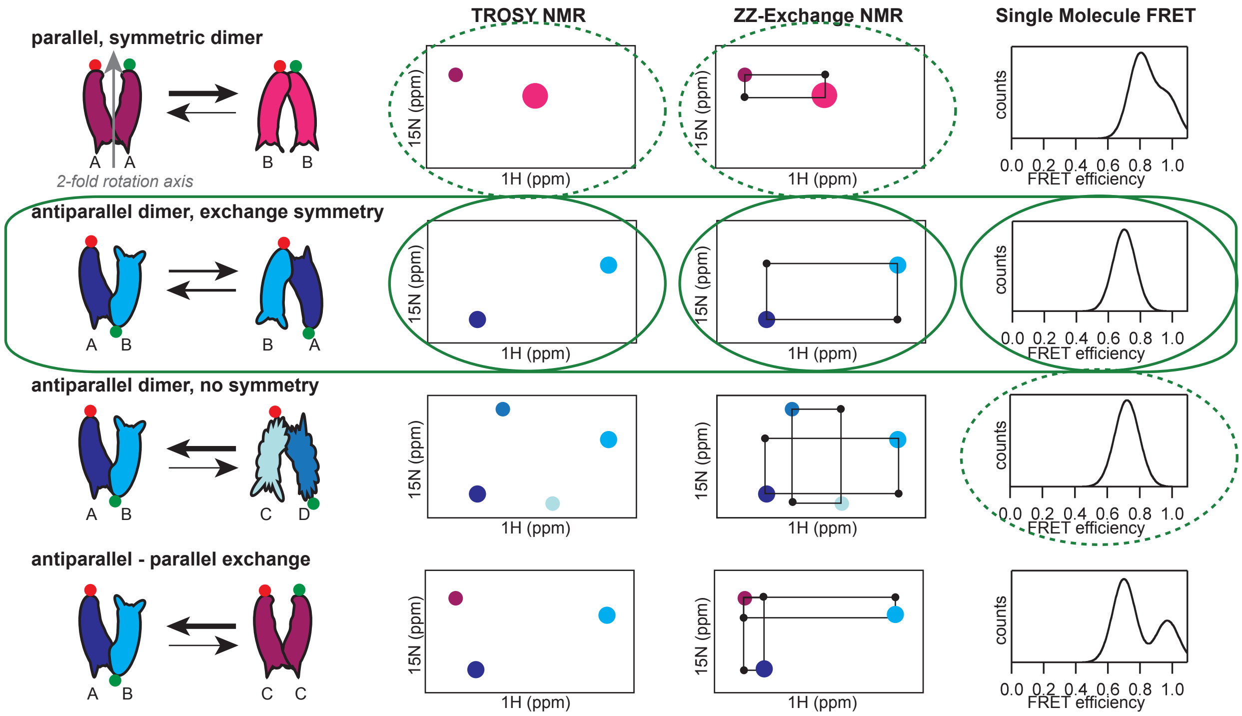

Figure 2. Possible models of conformational interconversion by a homodimeric transporter. Such a transporter can have a parallel or antiparallel topology with varying symmetry relationships, as described in more detail in the text. Qualitative data predictions are shown for each the four models depicted. Within each model, unique monomeric states (with unique chemical shifts) are labeled with a different letter (A, B, C, or D) and color. The coloring connects each monomeric state to a corresponding peak for a single amide in the predicted NMR spectra. Peak size indicates relative populations of the different states. Two peaks within a spectrum are only the same size if the model requires that the corresponding two states have equal populations. The expected smFRET results correspond to a dye pair attached at the positions of the red and green circles, which are at the same residue on all monomers. Dashed green circles highlight outcomes that could be consistent with the experimental results, as described in more detail in the text. Solid green circles indicate the only possibilities that are supported by all the experimental data. Figure from Morrison, et al. 2012 (ref. 1).

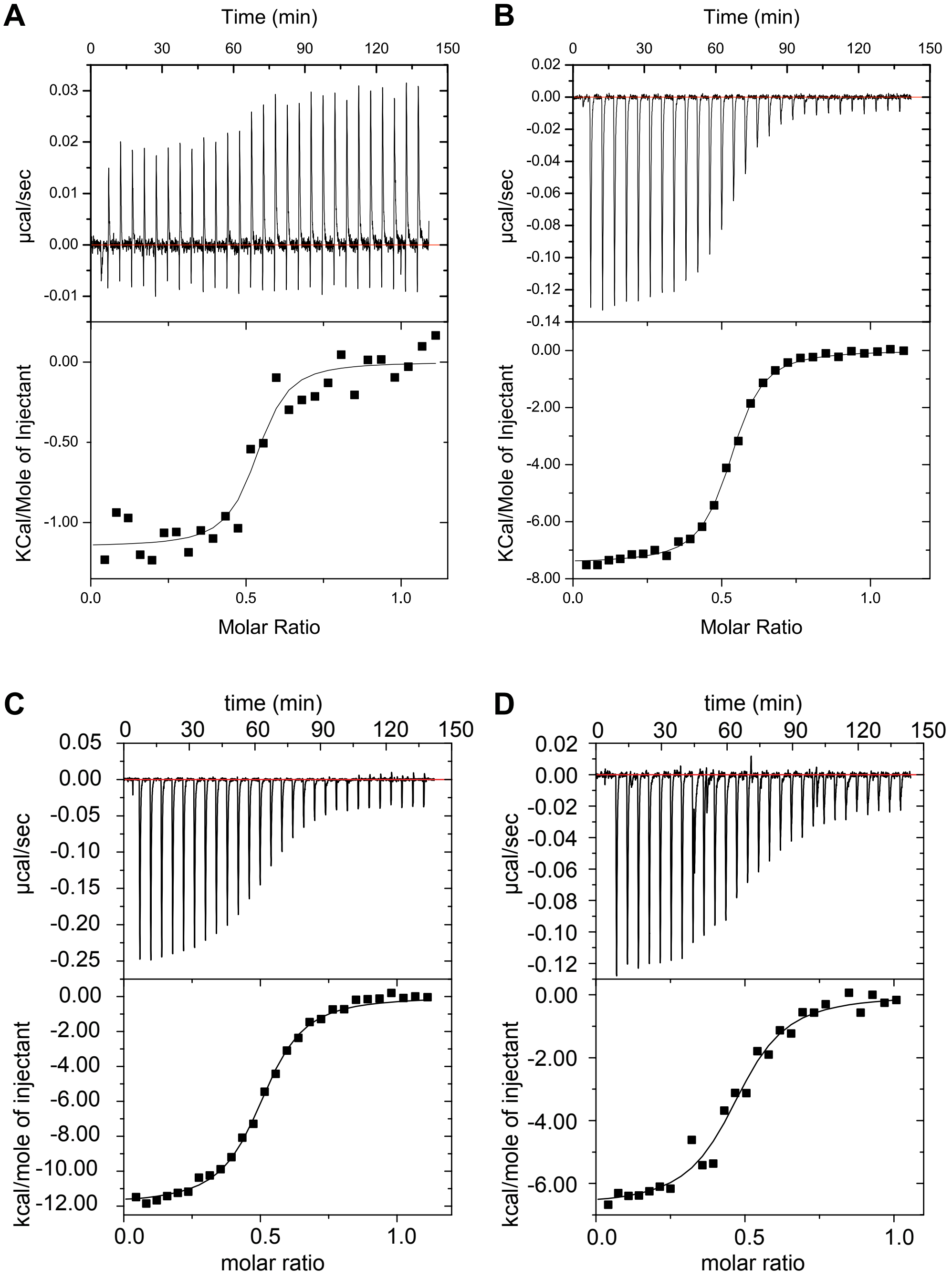

Figure 3. EmrE binds TPP$^+$ comparably in DDM and isotropic bicelles. Representative traces for ITC experiments performed in DDM at 4°C (**A**), 25°C (**B**), and 45°C (**C**) and in isotropic bicelles at 45°C (**D**). All samples were made in 20 mM KPi, 20 mM NaCl, pH 7.0. Fits for all ITC experiments are shown in **Table 1**. Figures from Morrison, et al. 2012 (ref. 1).

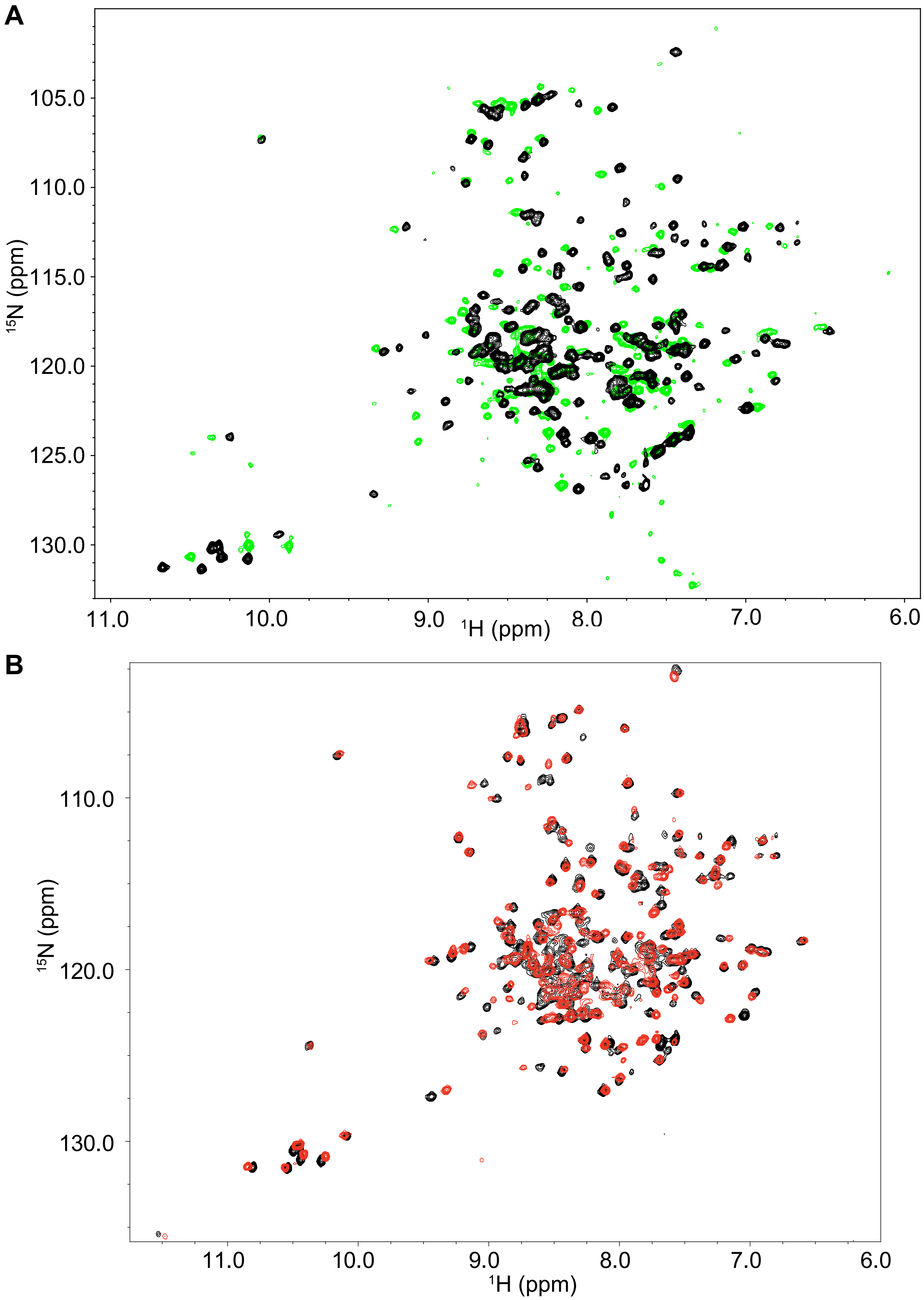

Figure 4. EmrE has the same structure in DDM and isotropic bicelles. ^{15}N/^{1}H TROSY HSQC spectra of TPP^{+}-bound ^{2}H/^{15}N EmrE solubilized in DDM micelles (**A**, green) or reconstituted into DMPC/DHPC (**A** and **B**, black) or DLPC/DHPC (**B**, red) isotropic bicelles. Figures from Morrison, et al. 2012 (ref. 1).

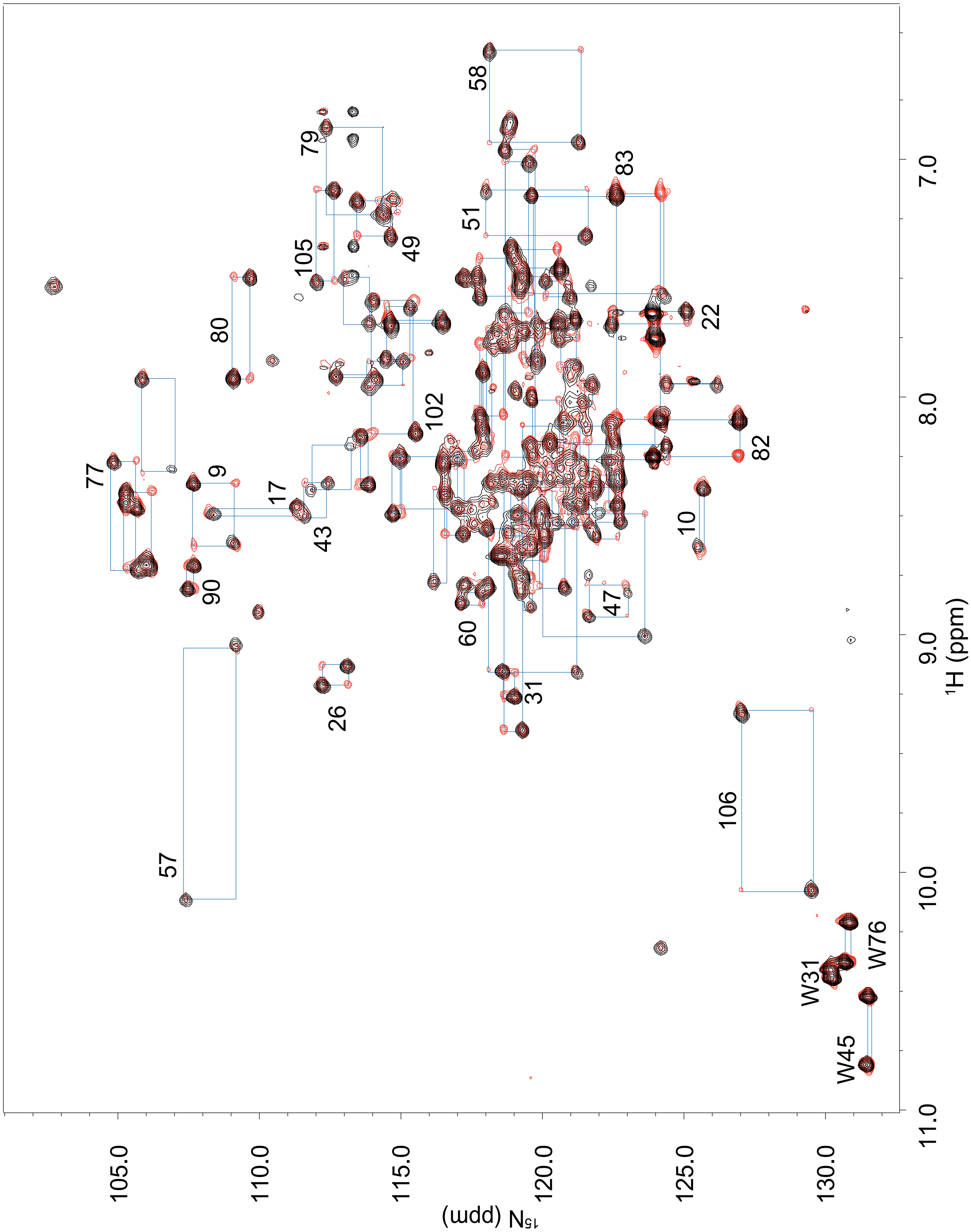

Figure 5. TPP$^+$-bound EmrE is in slow exchange. Overlay of ^{15}N/^{1}H TROSY HSQC spectrum (black) and 100 ms mixing time TROSY-selected ZZ-exchange plane (red) of TPP$^+$-bound ^{2}H/^{15}N EmrE. Blue boxes connect auto- and crosspeaks from amides of individual residues, some of which are labeled with their residue number. Figure from Morrison, et al. 2012 (ref. 1).

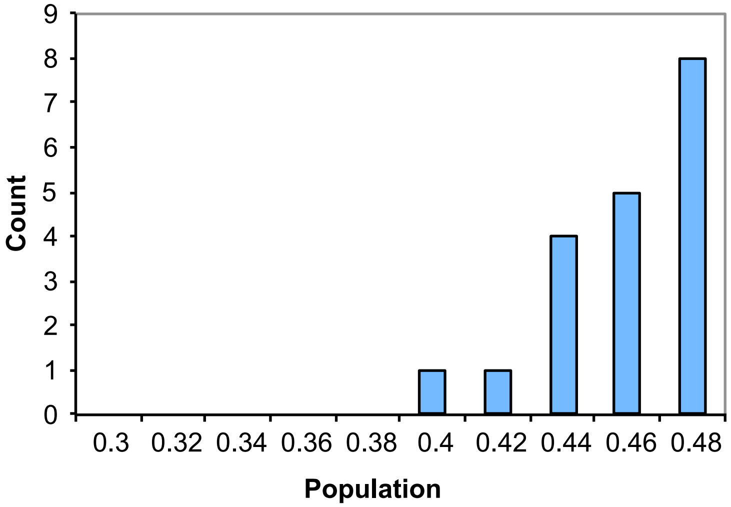

Figure 6. Population histogram of TPP$^+$-bound EmrE. All fully-resolved peak pairs in a fully-relaxed (6 s recycle delay) $^{15}N/^{1}H$ TROSY HSQC spectrum were integrated. Populations were determined from the relative volumes of the two peaks in each pair. The minor population from each pair was plotted in the histogram, which indicates that the populations in the two states are equal. The average population of the minor state is 0.47 ± 0.3. Figure from Morrison, et al. 2012 (ref. 1).

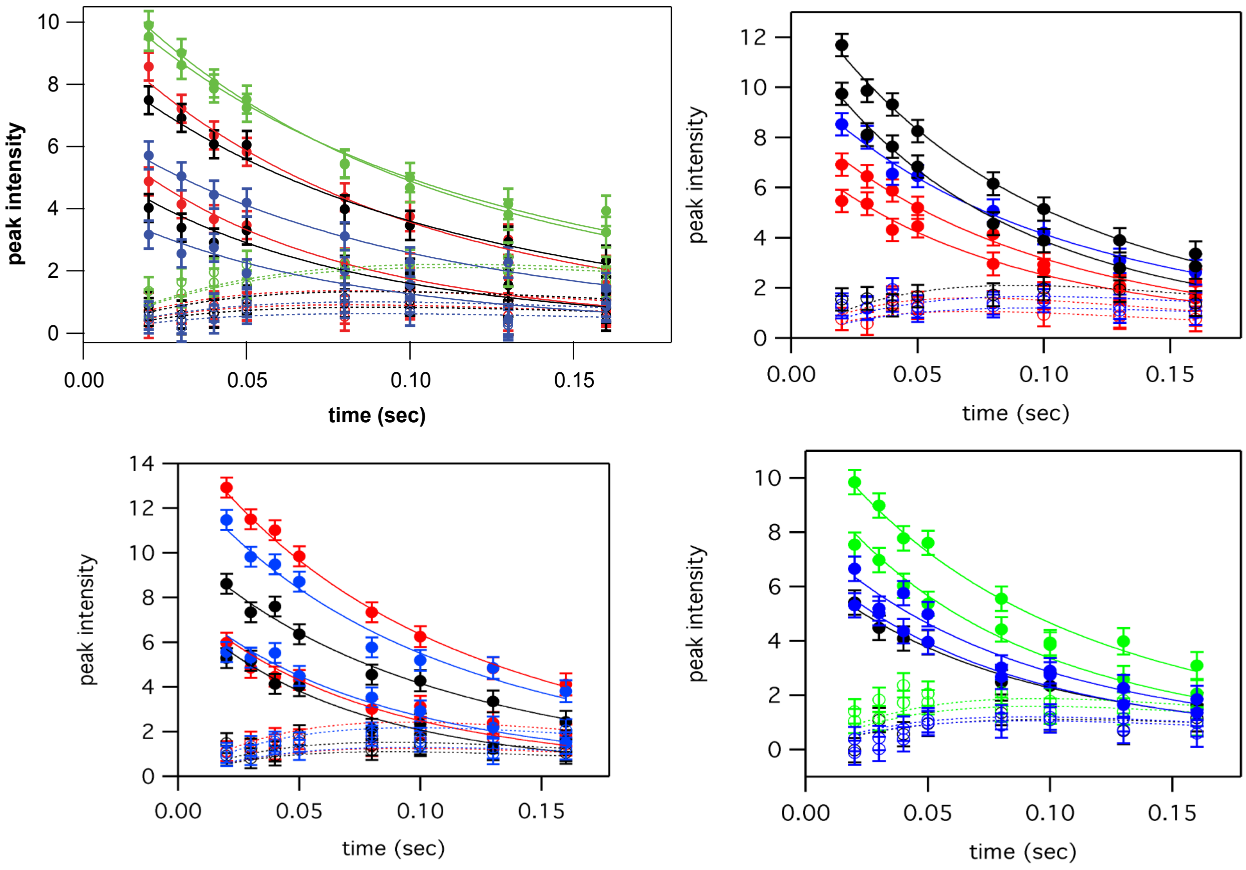

Figure 7. Full fits to ZZ-exchange data. Fits of peak intensity of auto- (data in filled circles, fits in solid lines) and cross- (data in open circles, fits in dashed lines) peaks as a function of mixing time in the TROSY-selected ZZ-exchange experiment. Thirteen residues are plotted between four graphs for easier visualization. Within each graph, auto- and crosspeaks for a single residue are plotted in the same color. Error bars are estimated from the noise of each spectrum. Data from the 13 residues were globally fit to an exchange rate of 4.9 ± 0.5 s^{-1}. Figures from Morrison, et al. 2012 (ref. 1).

A

0	k
1	1Ra
2	1Rb
3	1Ia
4	1Ib
5	2Ra
6	2Rb
7	2Ia
8	2Ib
9	3Ra
10	3Rb
11	3Ia
12	3Ib
13	5Ra
14	5Rb
15	5Ia
16	5Ib
17	6Ra
18	6Rb
19	6Ia
20	6Ib
21	7Ra
22	7Rb
23	7Ia
24	7Ib
25	8Ra
26	8Rb
27	8Ia
28	8Ib
29	10Ra
30	10Rb
31	10Ia
32	10Ib
33	13Ra
34	13Rb
35	13Ia
36	13Ib
37	14Ra
38	14Rb
39	14Ia
40	14Ib
41	15Ra
42	15Rb
43	15Ia
44	16Ra
45	16Rb
46	16Ia
47	16Ib
48	17Ra
49	17Rb
50	17Ia
51	17Ib

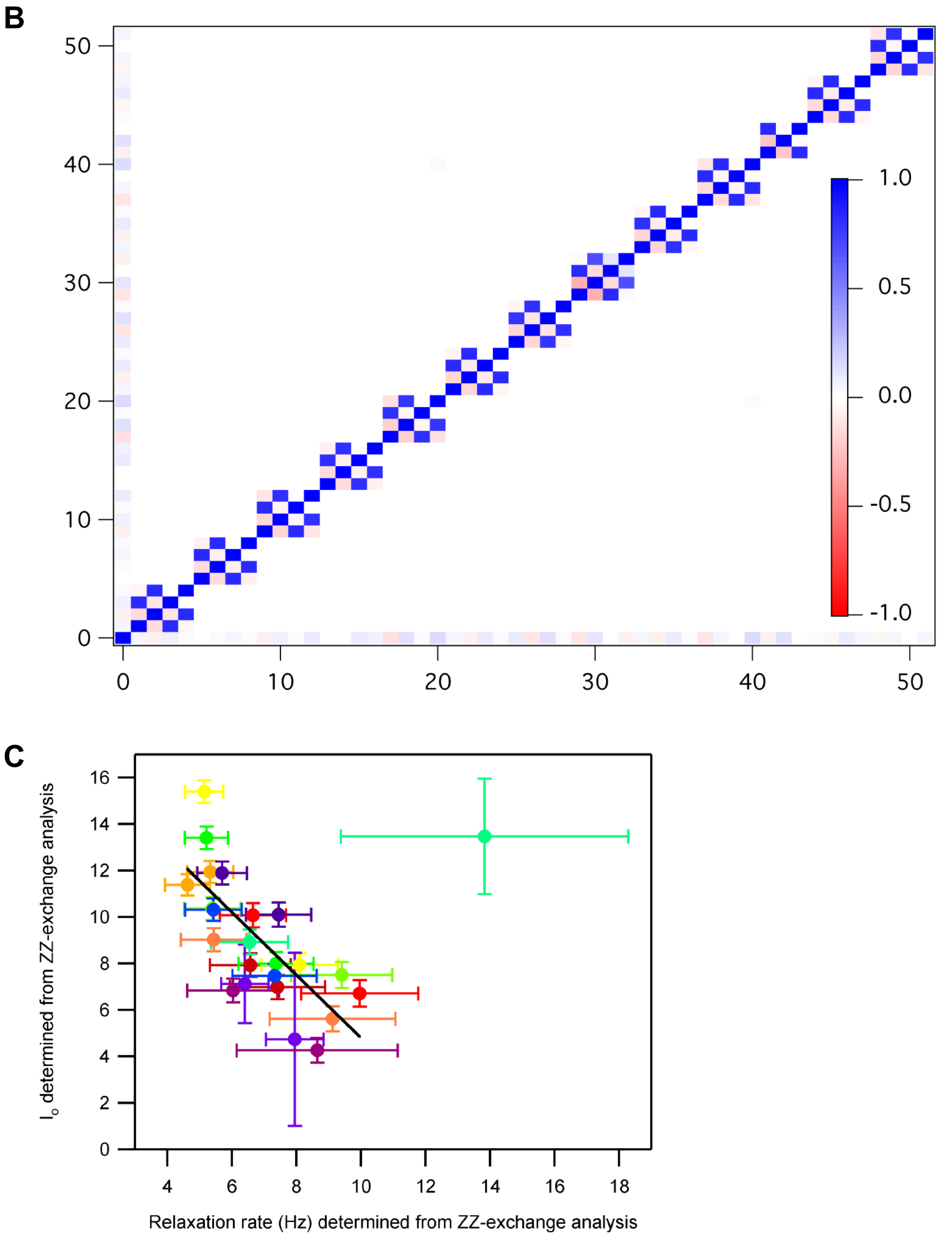

Figure 8. Correlation between variables in the full fit to the ZZ-exchange data (eq. 2) . A correlation matrix is plotted in (**B**) for the single global parameter (k) and four residue-specific parameters (I_A^0, I_B^0, R^{*A}, R^{*B}) for each of the 13 residues included in the global fit (see **Fig. 7**). The numbering key is listed in (**A**). No correlation is evident between k and any residue-specific parameter. There is strong correlation between I^0 and R^* for each state. Plotting I^0 vs. R^* (**C**), with each residue in a different color, shows that the state with faster relaxation has a lower initial intensity, as expected. The one outlier has lower signal-to-noise than most of the other residues analyzed, and one of the cross peaks is not as well resolved. Figures from Morrison, et al. 2012 (ref. 1).

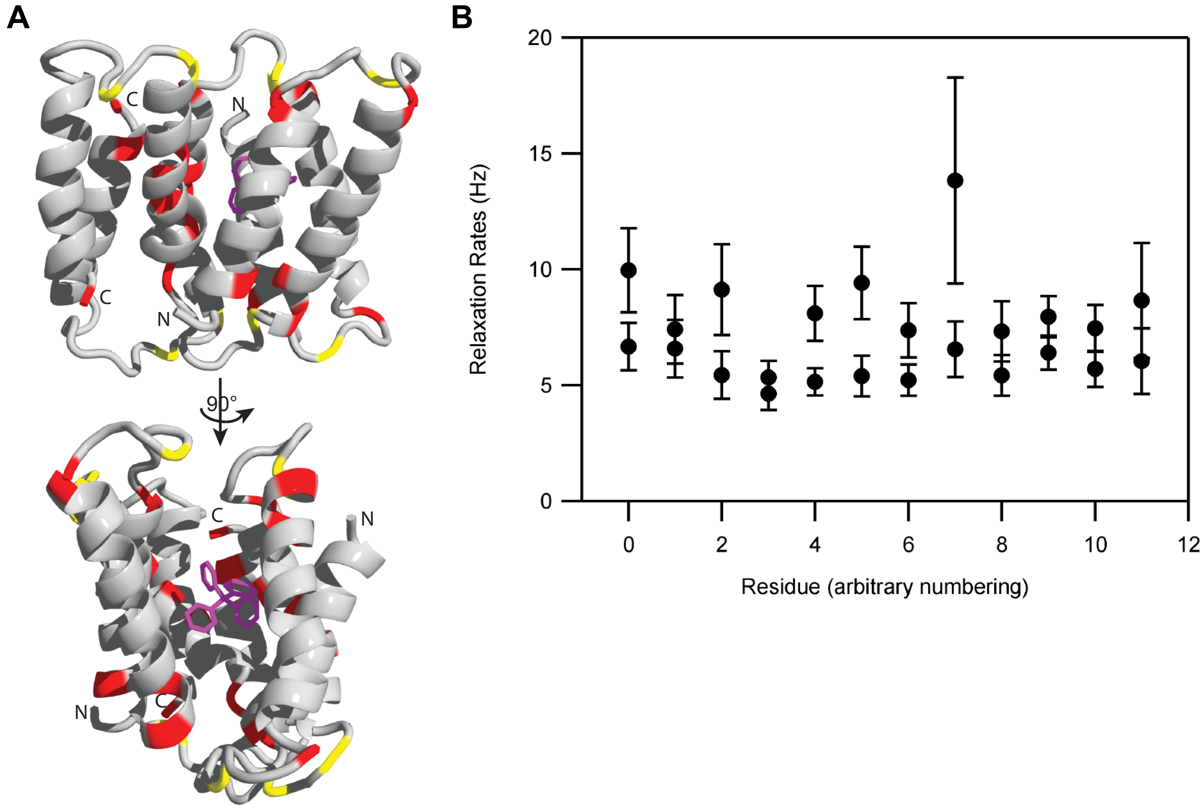

Figure 9. Differential relaxation between states A and B. **A.** The residues used in the quantitative analysis of the ZZ-exchange data are colored on the structure. Residues shown in red have the same intrinsic relaxation rate in both states, while those colored yellow have different relaxation rates between the two states. **B.** The rates used in (**A**) are plotted here. Figures from Morrison, et al. 2012 (ref. 1).

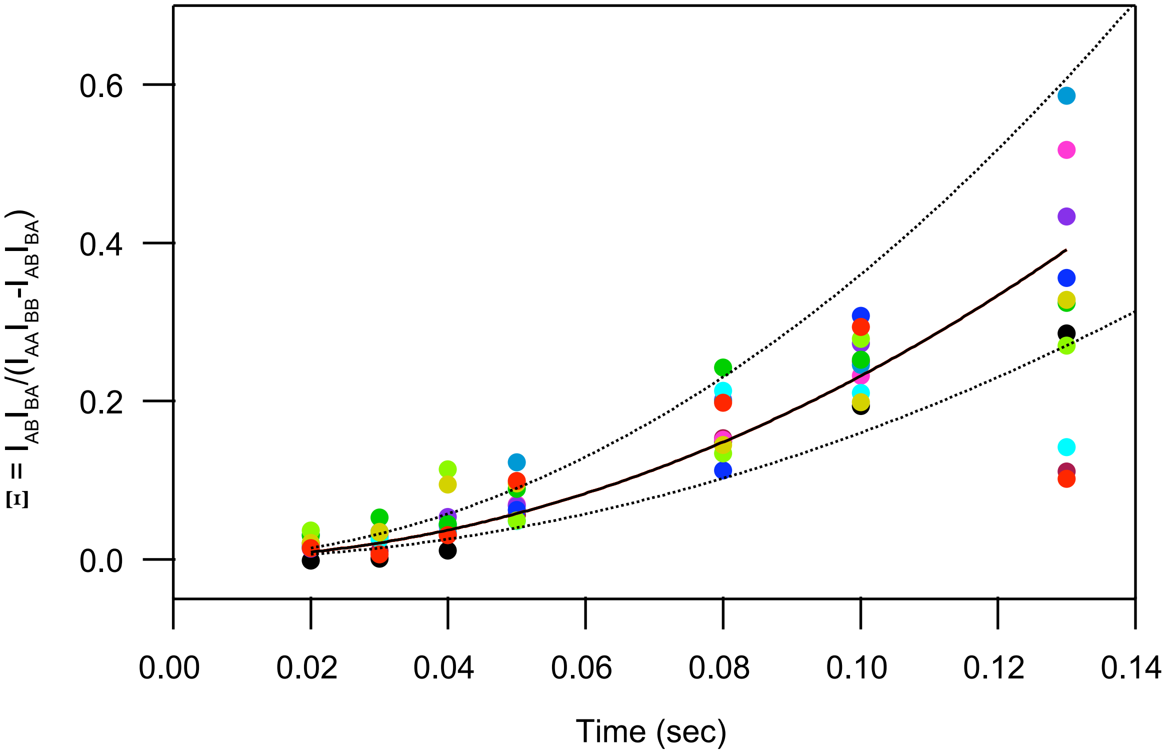

Figure 10. Global exchange process. A global fit to the 11 best-resolved residues using the composite peak ratio analysis (Ξ, eq. 3) gives a conformational exchange rate of $k = 4.7 \pm 0.5\ \mathrm{s}^{-1}$, in agreement with the full fit (eq. 2, **Fig. 7**). Each residue is plotted in a different color, with the global fit plotted as a solid line and dashed lines plotted for $k = 4\ \mathrm{s}^{-1}$ and $6\ \mathrm{s}^{-1}$ for comparison. Low data points at 130 ms are due to the low signal-to-noise of peaks for some residues at this long mixing time. Figure from Morrison, et al. 2012 (ref. 1).

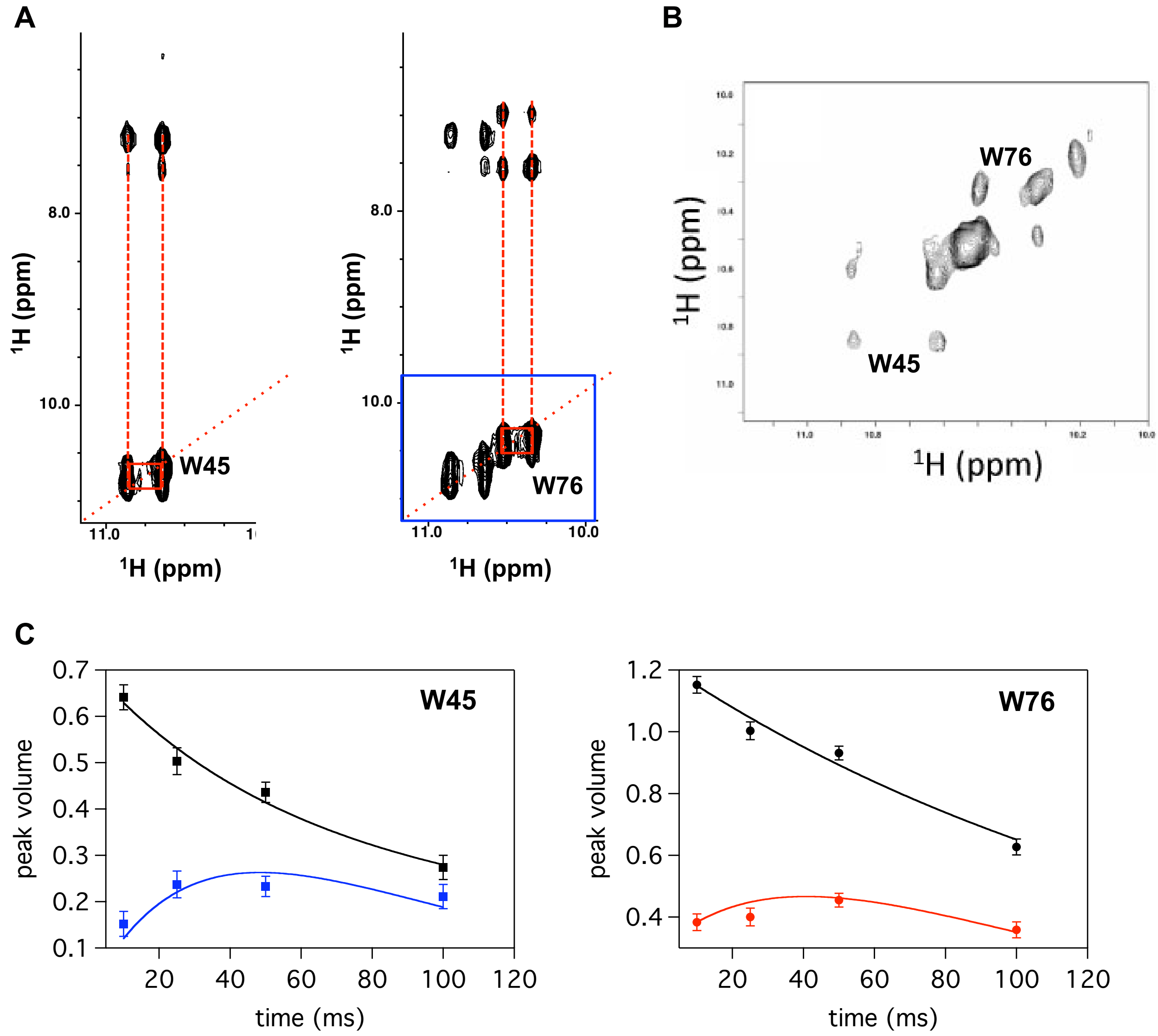

Figure 11. Tryptophan side-chain dynamics. The NOESY/ROESY analysis of tryptophan side-chain dynamics is in agreement with conformational exchange rate determined from ZZ-exchange spectroscopy. **A.** Two planes from a 3D ^{15}N-separated NOESY spectrum of TPP^{+}-bound EmrE in q = 0.33 DMPC/DHPC isotropic bicelles at 45°C, pH 7. Dashed red lines connect the crosspeaks in the ^{1}H NOESY dimension for two of the Trp side-chain amides (W45 and W76). The crosspeaks are nearly identical for each pair, as expected for exchange partners. **B.** The ^{1}H-^{1}H plane from a 3D ^{15}N-separated ROESY spectrum of the same sample showing the region highlighted by the blue square in (**A**). Contours of opposite sign are colored red and black. All the crosspeaks in this region have the same sign as the diagonal, indicating that these crosspeaks are due to exchange and not NOE/ROE. **C.** Diagonal- and crosspeak volumes were extracted from the NOESY spectra as a function of time. The average of the diagonal peak volumes (black) and the average of the crosspeak volumes (colored) are plotted for each of the two resolved Trp. Fitting to a simple equation assuming equal relaxation rates in both states yields the same conformational exchange rate, $k = 5$ s^{-1}, as for the ZZ-exchange analysis. Figures from Morrison, et al. 2012 (ref. 1); data from K. Henzler-Wildman.

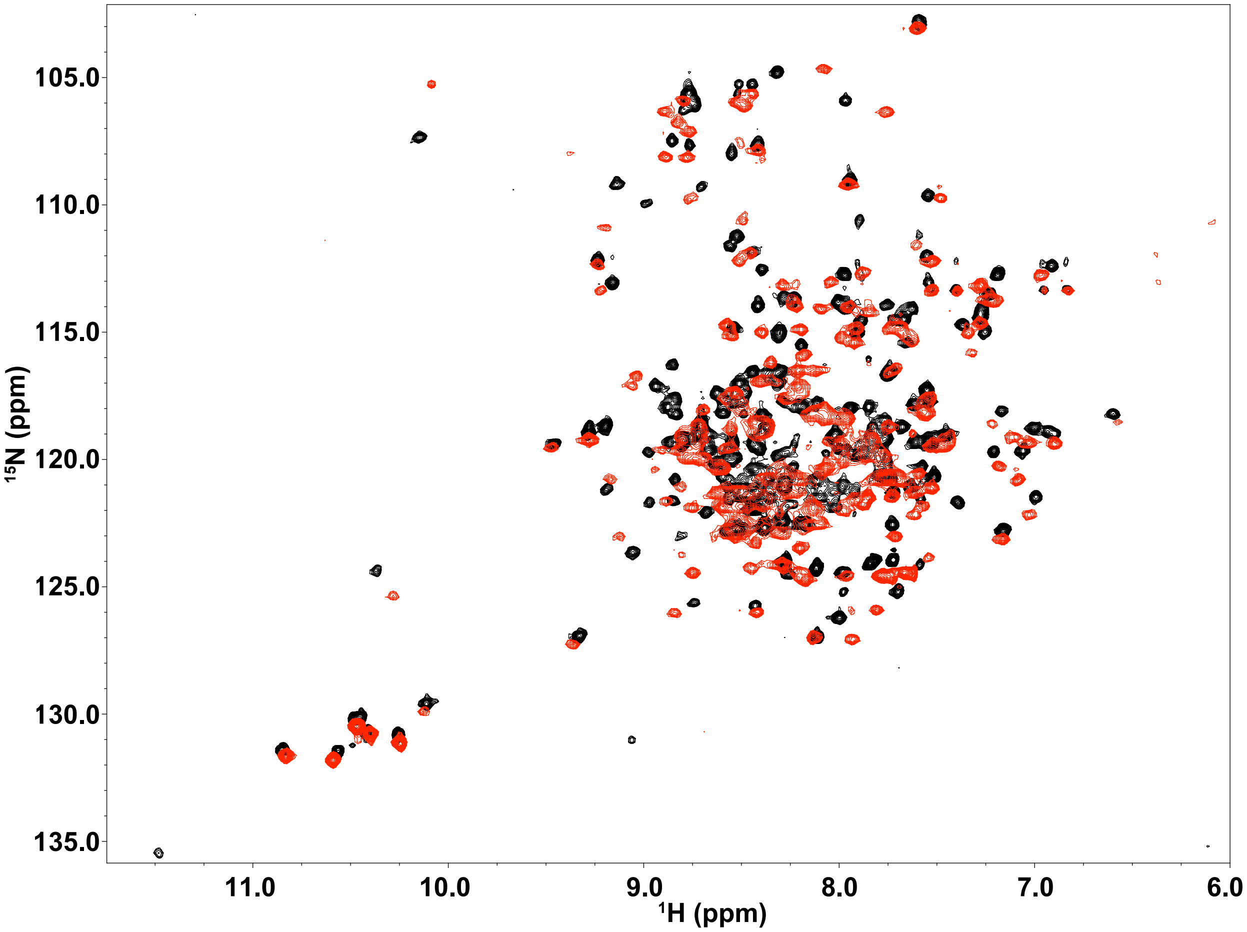

Figure 12. Single-cysteine mutant of EmrE has the same overall fold. An overlay of $^{15}N/^{1}H$ TROSY HSQC spectra of TPP^{+}-bound $^{2}H/^{15}N$-WT (black) and $^{1}H/^{15}N$-T56C (red) EmrE in q = 0.33 DLPC/DHPC isotropic bicelles at 45°C, pH 7. Some small chemical shift differences are observed, as may be expected due to mutation of the three native cysteines to serine in addition to the T56C mutation. The overall spectrum is quite similar, indicating a stable, properly folded structure for this mutant. Figure from Morrison, et al. 2012 (ref. 1); data from S. Dutta.

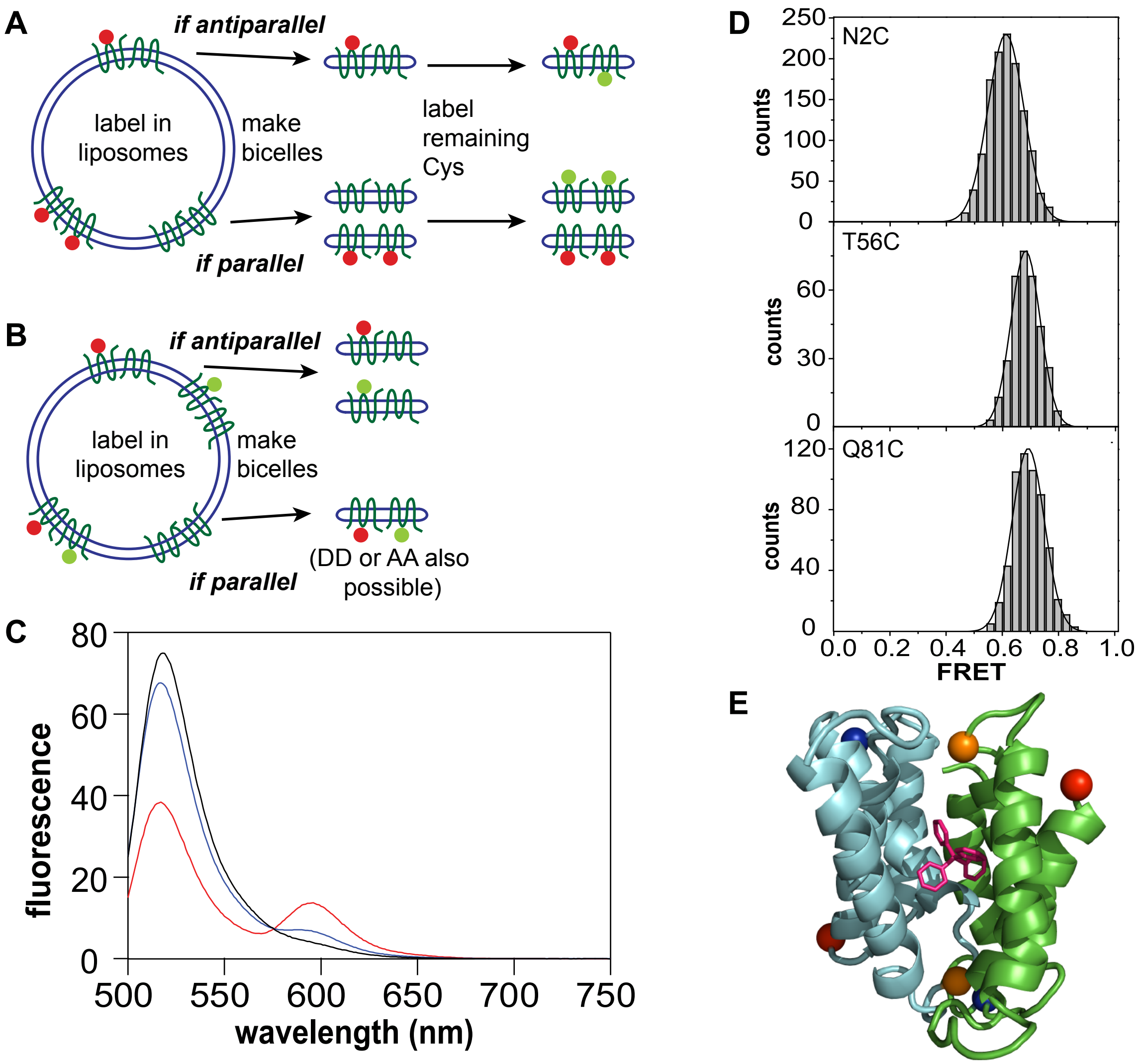

Figure 13. Topological studies of EmrE. T56C-EmrE in liposomes was labeled with fluorescent dyes according to two different schemes. **A.** Labeling with a single dye on each side of the membrane will produce FRET only if EmrE is antiparallel. **B.** Labeling with both donor and acceptor from the same side of the membrane will produce FRET only if EmrE is parallel. **C.** Observation of both donor (Alexa Fluor 488) and acceptor (Alexa Fluor 568) fluorescence upon donor excitation in a sample labeled according to the scheme in (**A**) indicates FRET and an antiparallel topology (red line). In contrast, only minimal FRET was observed in a sample labeled according to the scheme in (**B**) (blue line). The control (black line) excludes monomers swapping between dimers and direct excitation of acceptor. All fluorescence spectra are normalized to total donor fluorescence in SDS, which monomerizes EmrE. **D.** For smFRET experiments, N2C-, T56C-, or Q81C-EmrE was labeled with Cy3/Cy5 in micelles and then reconstituted into bicelles. Particles containing one donor and one acceptor were selected based on photobleaching events (see **Fig. 14**). A single, narrow FRET distribution is observed in each case, with a FRET efficiency consistent with an antiparallel topology. Data from S. Dutta. **E.** Positions of donor/acceptor labeling for fluorescence experiments: T56C (orange), Q81C (blue), or N2C (red; residue 4 or 6 is colored because the N-terminus is missing from the crystal structure). Figure made in PyMOL with PDB 3B5D. Figure from Morrison, et al. 2012 (ref. 1).

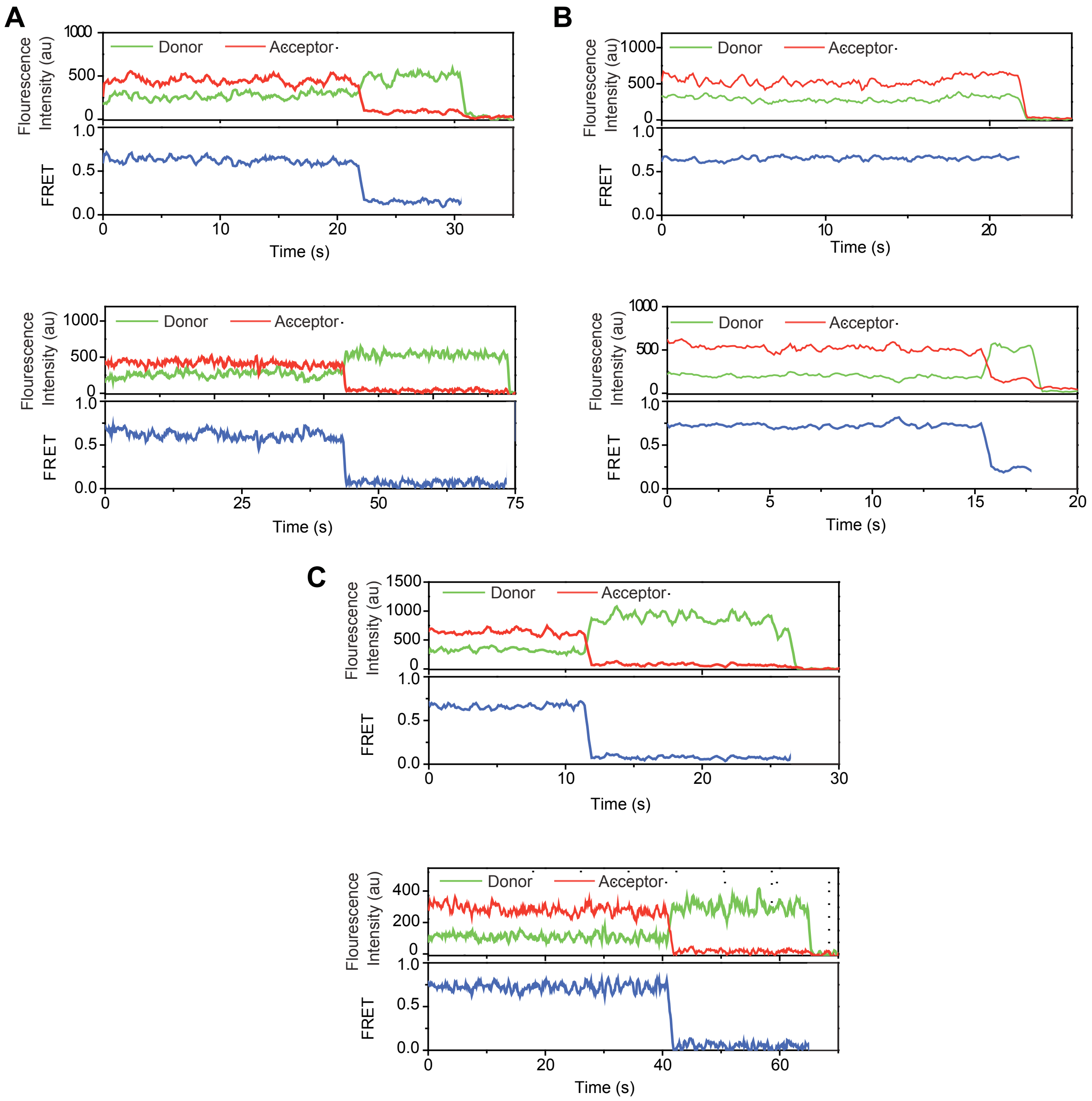

Figure 14. Sample smFRET time traces for single-cysteine labeled EmrE. Donor fluorescence (green), acceptor fluorescence (red), and FRET (blue) for Cy3/Cy5-labeled N2C-EmrE (**A**), T46C-EmrE (**B**), and Q81C-EmrE (**C**). Experiments were performed in DLPC/DHPC isotropic bicelles at pH 7, with saturating concentrations of TPP$^+$ in the imaging buffer. Traces are shown for molecules that had only two photobleaching events, one donor and one acceptor. A large proportion of the single particles observed fall into this class. Data of this type was binned into histograms based on FRET efficiency, as plotted in **Fig. 13D**. Figures from Morrison, et al. 2012 (ref. 1); data from S. Dutta.

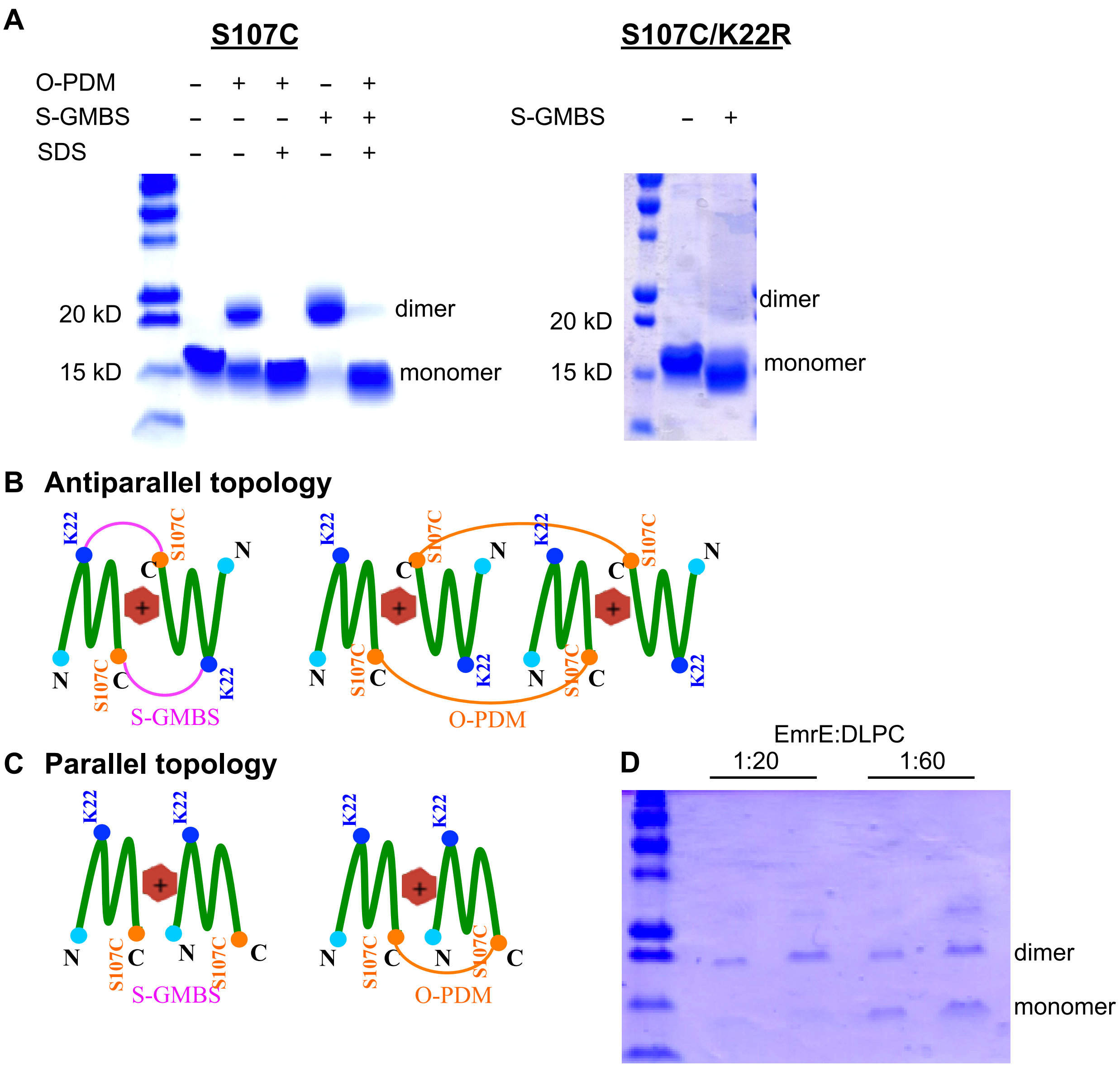

Figure 15. Cross-linking experiments support an antiparallel topology. SDS-PAGE gels show the results of cross-linking experiments using two different bifunctional cross-linking reagents to cross-link EmrE in DDM micelles. O-PDM, a homobifunctional cross-linker, will covalently link two cysteines. S-GMBS, a heterobifunctional cross-linker, will covalently link a cysteine sulfhydryl to a primary amine. **A.** In S107C-EmrE, cross-linking occurs with partial efficiency with o-PDM and nearly 100% efficiency with s-GMBS. SDS monomerizes EmrE and prevents cross-linking. S-GMBS does not cross-link S107C/K22R-EmrE, demonstrating that K22 rather than the N-terminus cross-links with S107C. Cartoons illustrate cross-linking locations for an antiparallel (**B**) and parallel (**C**) EmrE dimer. Cross-linking of an antiparallel dimer by o-PDM can be explained by cross-linking between dimers. In a parallel dimer, s-GMBS cannot cross-link K22 to S107C. **D.** As expected for inter-dimer cross-linking, o-PDM cross-linking efficiency depends on the protein:lipid ratio. At a ratio of 1:60, cross-linking is only about 50% efficient, but this increases to nearly complete cross-linking at a ratio of 1:20. Two identical lanes were run for each sample. Figure from Morrison, et al. 2012 (ref. 1); data from S. Dutta.

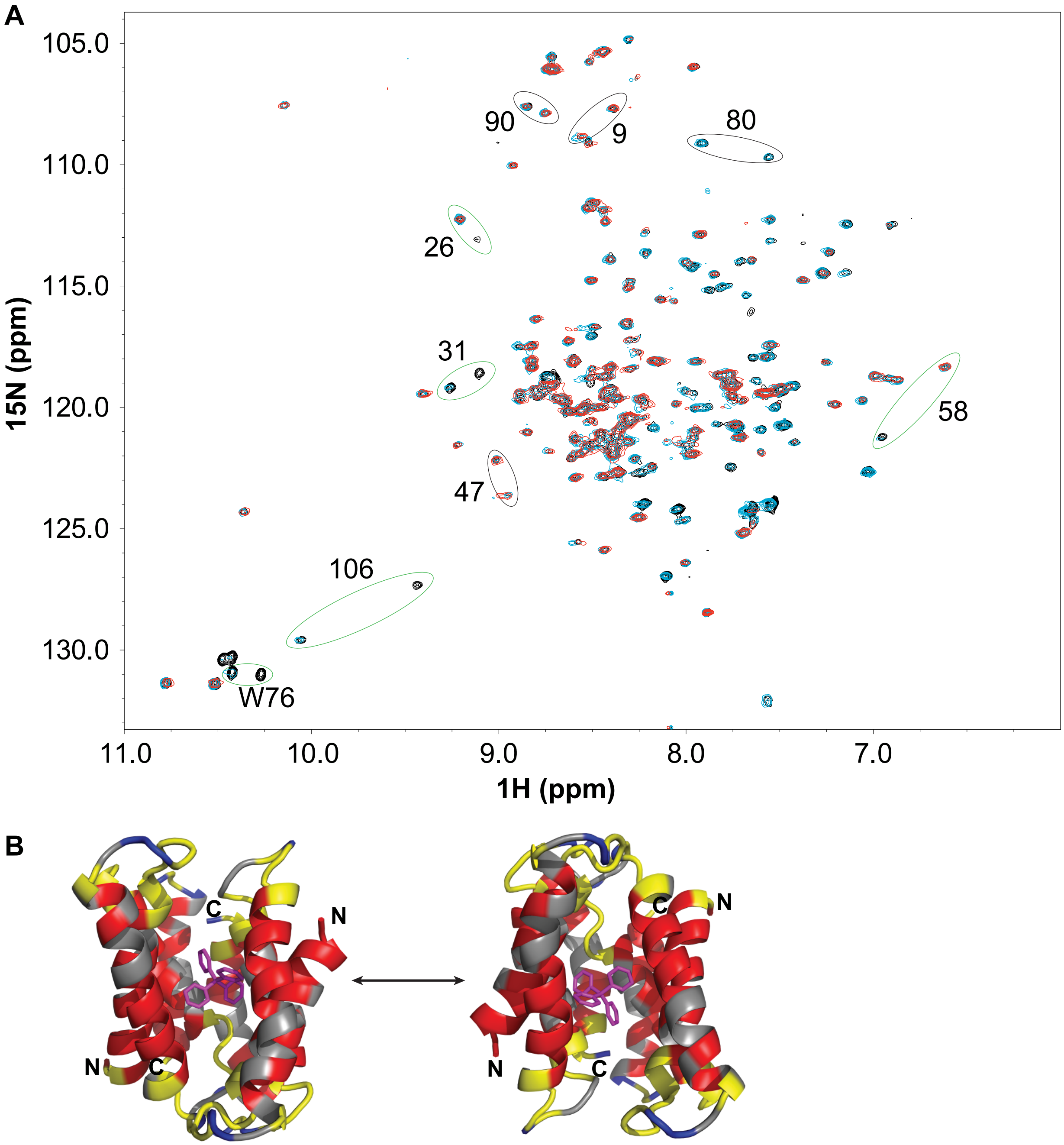

Figure 16. EmrE has asymmetric water accessibility. **A.** Overlay of ^{15}N/^{1}H TROSY HSQC spectra of TPP^{+}-bound EmrE in the absence (black) and presence of 1 mM (blue) and 5 mM (red) of paramagnetic gadobenate dimeglumine. Residues with differential PRE effects (green circles) or the same PRE effect (black circles) in the two states are highlighted. **B.** Residues with equal accessibility (dark blue) or protection (red) from water in both states are plotted on the structure. Grey residues are not assigned in both states. Residues with differential water accessibility (yellow) highlight the pore and loop regions, as expected for exchange between inward- and outward-facing conformations. This is consistent with an antiparallel dimer open to only one side of the membrane at a time, as in the X-ray crystal structure. Figure made using PyMOL, PDB 3B5D. Figures from Morrison, et al. 2012 (ref. 1); data from G. DeKoster.

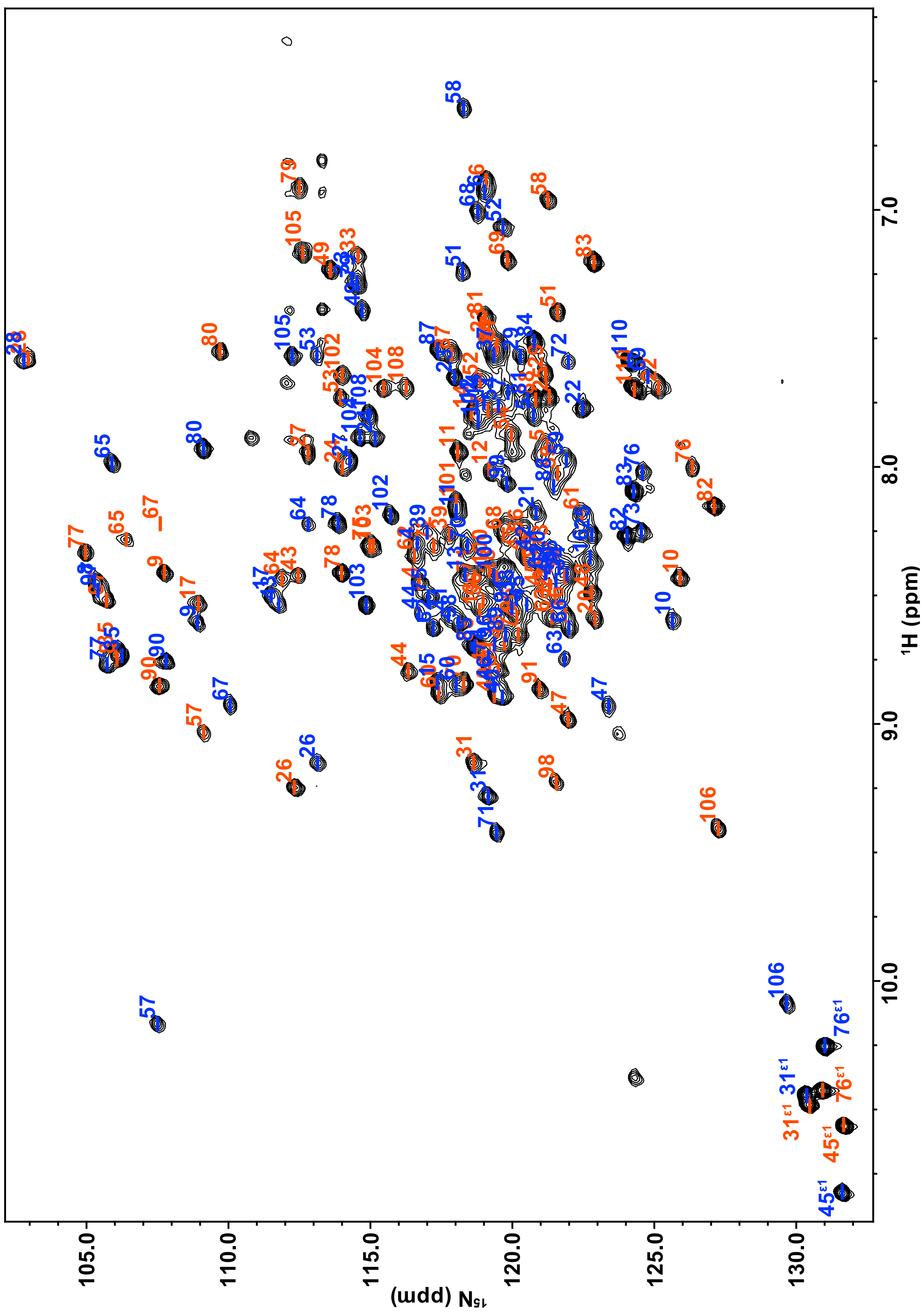

Figure 17. EmrE assignments. $^{15}N/^{1}H$ TROSY HSQC spectrum (black) of TPP^{+}-bound $^{2}H/^{15}N$ EmrE. Residues are labeled with assignments in state A (red) and state B (blue). Due to a lack in connectivity, A vs. B is not known with certainty for residues 17, 31, 67, 98, and 108.

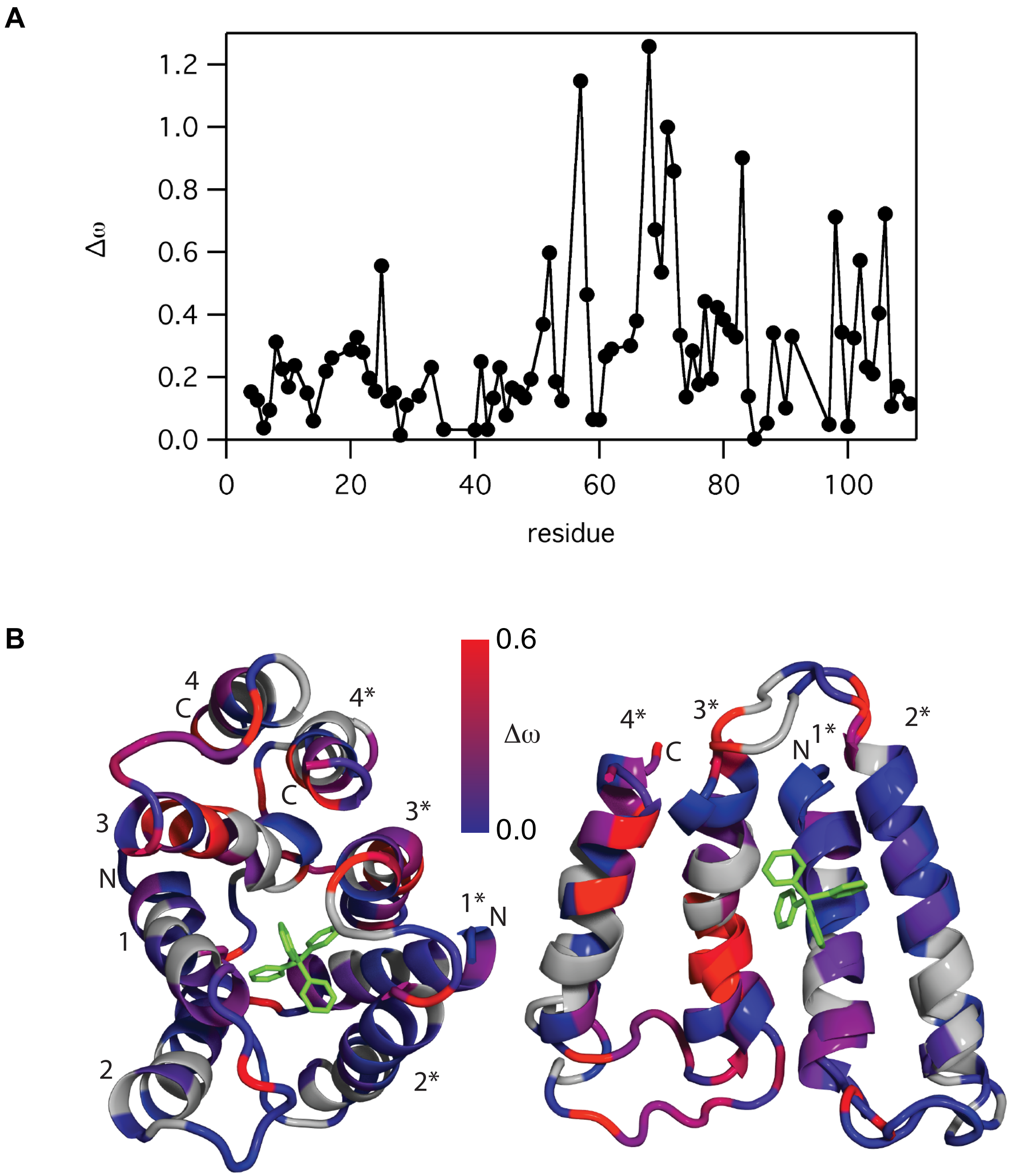

Figure 18. Changes in chemical shifts upon interconversion between inward- and outward-facing states of EmrE. Chemical shift differences between states A and B for all assigned residues were calculated according to eq. 4 (**A**) and plotted on the X-ray crystal structure of asymmetric, antiparallel EmrE (PDB 3B5D, **B**). The monomer in state A was rotated 180° onto the monomer in state B, and TM1-TM3 were aligned in PyMOL. This view highlights the structural differences between the two monomers and the corresponding chemical shift differences. Figures from Morrison, et al. 2012 (ref. 1).

Chapter IV. Transported substrate determines exchange rate in the multidrug resistance transporter EmrE.

In the previous chapter, we demonstrated that we could directly monitor the conformational interconversion between the inward- and outward-facing states of EmrE bound to TPP^+. Using solution NMR we were able to gain valuable insight into this mechanism by characterizing the kinetics and thermodynamics of this exchange along with structural details. The next step was to apply these tools to address the question of broad substrate specificity. As a member of the family of smallest transporters, EmrE must accommodate a wide range of ligands, spanning tetrahedral and planar geometries, a range of sizes, and $^+1$ or $^+2$ charge, into a single small binding pocket and undergo the same global motion to alternate access of its binding pocket between opposing faces of the membrane bilayer.

The manuscript that follows is published in *The Journal of Biological Chemistry*[1] and presented here with additional figures. It describes a series of isothermal titration calorimetry, in-cell efflux assays, and ZZ-exchange spectroscopy to assess differences in EmrE bound to a range of substrates. The results of these experiments indicate that EmrE binds a series of five related monovalent and tetrahedral compounds with affinities varying over three orders of magnitude. Amazingly, the rate of conformational exchange of EmrE bound to these five related compounds also varies to a similar extent. The energetic implications of the binding thermodynamics and exchange kinetics are discussed in detail in the manuscript text, but one of the most remarkable findings is simply the sheer magnitude of these kinetic differences. The conformational interconversion between the inward- and outward-facing states is a large-scale concerted motion, and it can be difficult to conceive that the timescale of this motion can be tuned to such a high degree. A change in ligand structure as small as the addition of a single methyl group is able to affect these dynamics.

In this manuscript, we start to explore the mechanism of this dynamic modulation using chemical shift analysis, however, further experiments will be required to understand the basis for the substrate-dependent effects. A future direction for the lab will be to follow up on Tate's low-resolution cryo-EM studies that suggest a change in helix tilt between when bound to tetrahedral and planar ligands. Using NMR to measure residual dipolar couplings, we will be able to test this and measure the precise tilt angle of each TM helix when EmrE is bound to different ligands. Additional distance restraints between ligand and residues of interest, gathered via paramagnetic NMR and EPR, will also provide additional data on the structural changes induced by the binding of different ligands.

Experiments were designed by E. Morrison and K. Henzler-Wildman, performed by E. Morrison, and analyzed by E. Morrison and K. Henzler-Wildman.

References:

1. Morrison, E. A. & Henzler-Wildman, K. A. Transported Substrate Determines Exchange Rate in the Multidrug Resistance Transporter EmrE. *Journal of Biological Chemistry* **289,** 6825–6836 (2014).

Transported Substrate Determines Exchange Rate in the Multidrug Resistance Transporter EmrE

Emma A. Morrison[1] and Katherine A. Henzler-Wildman[1]

[1]From the Department of Biochemistry and Molecular Biophysics
Washington University in St. Louis School of Medicine, St. Louis, MO 63110

*Running title: *Transported Substrate Determines Exchange Rate in EmrE*

To whom correspondence should be addressed: Katherine A. Henzler-Wildman, Department of Biochemistry and Molecular Biophysics, Washington University in St. Louis School of Medicine, 660 S. Euclid Ave., Box 8231, St. Louis, MO 63110, USA, Tel.: (314) 362-1674; E-mail: khenzler@biochem.wustl.edu

Keywords: multidrug transporters; protein dynamics; NMR; protein drug interactions; membrane transport

---

Background: EmrE transports a broad range of compounds.

Results: EmrE converts between open-in and open-out states with rates that vary over 3 orders of magnitude, depending on substrate.

Conclusions: Substrate affects both ground-state and transition-state energies for conformational exchange, emphasizing the coupling between substrate binding and transport.

Significance: Drug identity determines its own rate of transport by EmrE.

ABSTRACT

EmrE, a small multidrug resistance transporter, serves as an ideal model to study coupling between multidrug recognition and protein function. EmrE has a single small binding pocket that must accommodate the full range of diverse substrates recognized by this transporter. We have studied a series of tetrahedral compounds, as well as several planar substrates, to examine multidrug recognition and transport by EmrE. Here we show that even within this limited series, the rate of interconversion between the inward- and outward-facing states of EmrE varies over three orders of magnitude. Thus, the identity of the bound substrate controls the rate of this critical step in the transport process. The binding affinity also varies over a similar range and is correlated with substrate hydrophobicity within the tetrahedral substrate series. Substrate identity influences both the ground-state and transition-state energies for the conformational exchange process, highlighting the coupling between substrate binding and transport required for alternating-access antiport.

Multidrug transporters are an ideal system for investigating the proposed alternating-access model since their diverse substrates provide a natural toolkit of small molecules to probe the molecular mechanism. At the molecular level, active transport of a substrate against its electrochemical gradient requires two distinct conformations of the transporter, one open to the inner side of the membrane and one open to the outer side of the membrane, and the ability to convert between these two states to move bound substrate across the membrane (1) (**Fig. 1B**). Within this alternating-access framework, stoichiometric antiport can be achieved with two simple conditions: (i) the counter-transported substrates compete for a single binding site such that the transporter cannot bind both substrates simultaneously, and (ii) the transporter is able to interconvert between the inward- and outward-facing states only when a substrate is bound. Energetically, substrate binding must lower the barrier for conformational exchange between the inward- and outward-facing states. This tight coupling between substrate binding and conformational exchange is important for secondary active transporters that use a proton gradient to drive transport, so that the proton motive force needed for ATP synthesis is not dissipated unnecessarily.

But how is substrate binding and conformational exchange coupled in the context of a small *multidrug* resistance transporter such as EmrE, which recognizes and transports many different substrates? EmrE imports two protons across the inner membrane of *E. coli* for each polyaromatic cation substrate exported, conferring resistance to a broad range of drugs that meet this chemical description (2-4). The simple single-site alternating-access model of antiport described above is consistent with the biochemical data available for EmrE (5-8). Recent solid-state NMR studies of tetraphenylphosphonium$^+$ (TPP$^+$) and methyltriphenylphosphonium$^+$ (MeTPP$^+$) binding to EmrE in liposomes have confirmed that TPP$^+$ binds directly to the active site glutamate, E14, and both substrates compete for the same binding site as proposed (9). Polyaromatic cation substrates of EmrE vary in charge (i.e. $^+1$ vs. $^+2$), geometry (i.e. planar vs. tetrahedral), and overall size. Their binding affinities vary widely, reflecting this substrate diversity (2), yet binding of any of these substrates must trigger the same open-in to open-out conformational exchange process in order for transport to occur. Does this important interconversion between open-in and open-out states occur on the same timescale for different substrates? If not, are there substrate properties that determine conformational exchange rate and ultimately the ability of EmrE to confer resistance to a particular substrate?

The very small size of EmrE, which functions as a homodimer with only 110 residues per monomer, raises an additional question: How does such a small protein recognize and actively transport this diverse array of compounds? Multidrug resistance (MDR) proteins are unique in their ability to bind a wide range of ligands and different families of MDR proteins appear to have evolved distinct strategies to recognize diverse compounds. Large MDR transporters from several superfamilies and MDR gene regulators appear to bind different drugs with distinct subgroups of residues within a large, hydrophobic binding pocket, and some can even bind multiple substrates simultaneously (10-12). As a member of the smallest family of MDR transporters, EmrE has a small binding pocket that must accommodate its entire wide range of substrates within a limited space. Multidrug recognition in a single small binding pocket has already been established in one case, the MDR transcription factor BmrR (13). In BmrR, the same set of active site residues interacts with its full array of ligands in a highly rigid binding pocket (13). This is in contrast to the canonical concept of multidrug recognition (11, 12), which postulates a key role for flexibility in accommodating diverse ligands in a single site. However, the requirements for coupling substrate binding to function are fundamentally different in transcription factors and transporters. Indeed, low-resolution cryo-EM data indicates that EmrE alters its structure when bound to planar or tetrahedral substrates (2). Thus, we expect flexibility is important in multidrug recognition by EmrE and that nature has successfully adopted different strategies for multi-substrate recognition in multidrug binding proteins of different sizes and functions. Here we experimentally test how multidrug recognition is achieved by EmrE and coupled to functional transport.

We have previously directly monitored the dynamics of the conformational interconversion between the open-in and open-out states of EmrE bound to the well-studied substrate TPP^+ (14). Now we expand this work to test the hypothesis that the rate of conformational exchange between inward- and outward-facing states, the key step in moving substrate across the membrane, depends on the identity of the transported substrate. By combining NMR dynamics techniques with binding and efflux assays, we directly observe structural details, thermodynamics, and kinetics to link multisubstrate binding with functional motions.

EXPERIMENTAL PROCEDURES

Expression, purification, and reconstitution of EmrE—EmrE was expressed, purified, and reconstituted as previously described (14, 15). Isotopically labeled samples were extensively deuterated by growing in D_2O M9 media supplemented with 1g/L $^{15}NH_4Cl$, 0.5g/L $^2H/^{15}N$ isogro (Sigma-Isotec), and 2g/L $^1H/^{12}C$ D-glucose. Purified EmrE was reconstituted into 1:3 DLPC/DHPC or DMPC/DHPC (mol/mol) isotropic bicelles at a 1:100 molar ratio of protein:long-chain lipid in 20mM potassium phosphate (KPi), 20mM NaCl, pH 7.

Partition coefficients—Partition coefficients were measured via the HPLC method (16). Reference and sample compounds were dissolved in 75% MeOH:25% buffer at roughly 2mg/mL. 5μL samples were injected onto an analytical Waters Sunfire C18 reverse-phase column with isocratic flow of 70% MeOH:30% buffer at 1mL/min. The dead time (t_0) of the column was taken as the retention time of the highly polar thiourea. A capacity factor, c, for each ligand was calculated from retention time (t_R): $c = (t_R - t_0)/(t_0)$. A reference curve of $\log(c)$ vs. well-established experimental values of logP for phenol, p-cresol, 4-chlorophenol, 1-naphthol, 4-phenylphenol, and naphthalene was fit to: $logP = a + b \times \log(c)$ (16). The logP values for the ligands were then calculated from this standard curve.

The propidium^{2+} (PP^{2+}) retention time increases with increasing methanol and decreasing sample concentration, most likely reflecting aggregation of the ligand. The asymptotic value (logP = 4.3) of a dilution series was taken as the true logP, and error bars are larger for this ligand to reflect the greater uncertainty in logP. Repeating the logP determination at 50% methanol does not significantly alter the outcome for any of the tetrahedral ligands or dequalinium^{2+} (DQ^{2+}). However, PP^{2+} does shift to logP = 2.5, as the asymptote of a dilution series.

Extinction coefficient determination for ligands—Extinction coefficients were determined for TPP^+-derivatives for accurate concentration determination. Extinction coefficients for TPP^+ determined in the same manner matched literature values (i.e. 3750 $M^{-1}cm^{-1}$ at 275nm, 4400 $M^{-1}cm^{-1}$ at 268nm, and 3350 $M^{-1}cm^{-1}$ at 262nm), confirming the accuracy of this method. Extinction coefficients were determined in H_2O for $MeTPP^+$ chloride (Sigma-Aldrich), ethyltriphenylphosphonium$^+$ ($EtTPP^+$) chloride (Acros Organics), and 2-methylbenzyltriphenylphosphonium$^+$ ($MBTPP^+$) bromide (Acros Organics). Due to its low solubility, stocks of 2,5-diethoxyphenyltriphenylphosphonium$^+$ ($DPhTPP^+$) iodide (Aldrich Chemicals) were prepared in methanol, and dilutions were made into water for measurements. The molar extinction coefficients were determined from 5 to 6 independently weighed and prepared samples: a) $MeTPP^+$: 2460, 2875, and 2150 $M^{-1}cm^{-1}$ at 274, 267, and 261 nm; b) $EtTPP^+$: 2470, 2980, and 2260 $M^{-1}cm^{-1}$ at 274, 267, and 261 nm; c) $DPhTPP^+$: 4480, 3040, 3390, and 2870 $M^{-1}cm^{-1}$ at 321, 275, 268, and 262 nm; and d) $MBTPP^+$: 3720, 4270, and 3340 $M^{-1}cm^{-1}$ at 276, 268, and 263 nm. The extinction coefficients of the planar ligands are: 5680 $M^{-1}cm^{-1}$ at 478nm for ethidium$^+$ (Eth^+) (17) and 5900 $M^{-1}cm^{-1}$ at 493nm for PP^{2+} (EMD Millipore). The absorbance of DQ^{2+} is 27,500 $M^{-1}cm^{-1}$ at 329nm in aqueous solutions (18) and 28,875 $M^{-1}cm^{-1}$ in decylmaltoside solution (determined by dilution of aqueous stocks).

Isothermal titration calorimetry—All ITC experiments were performed with EmrE reconstituted into $q_{effective}$ = 0.33 (19) DLPC/DHPC isotropic bicelles under NMR conditions (20mM KPi, 20mM NaCl, pH 7, 45°C). Isotropic bicelle solutions were matched between protein and ligand samples, with at least a 100:1 DLPC:protein ratio, never going below 40mM total lipid to preserve bicelle morphology (19). Triplicate titrations were carried out for each of the seven ligands. Injections ranged from 1-2.5 μL, with stirring at 300-350 rpm. Ligand concentrations were determined using extinction coefficients determined as described above. Titrations were performed for each ligand using an average of 900, 600, 40, 35, 30, 650, and 700 μM EmrE and 5, 3, 0.2, 0.14, 0.13, 4, and 4 mM ligand for $MeTPP^+$, $EtTPP^+$, TPP^+, $DPhTPP^+$, $MBTPP^+$, PP^{2+}, and DQ^{2+} titrations, respectively. Due to limitations on sample concentrations, the weakest ($MeTPP^+$, PP^{2+}, and DQ^{2+}) and tightest ($MBTPP^+$) binders have greater error in the determination of K_D.

ITC was performed on a TA Instruments Low Volume Nano calorimeter using ITCRun software and analyzed using ITCAnalysis software (TA Instruments, Lindon, UT). Data were fit to a model of ligand binding to *n* independent and identical sites on EmrE, as in (14). Blank titrations of ligand and bicelles into bicelles always yielded equivalent heats across the titration, but it is difficult to precisely match to each sample. Therefore, the data were fit simultaneously to the binding model and a constant to represent the baseline of bicelle mixing.

In-cell transport assay—In-cell Eth^+ efflux assays based on work from the laboratories of Le Pecq and Schuldiner (20, 21) were carried out in BL21(DE3) and BL21(DE3) Gold strains of *E. coli* transformed with EmrE in pET15b or an empty pET15b control vector in M9 media supplemented with 100 μg/mL ampicillin. At an $OD_{600} = 0.4$, over-expression was induced with 0.33 mM IPTG for 30 min. 40 μM CCCP and 2.5 μM ethidium bromide were added, followed by incubation at 37°C for an additional hour. Individual 2 mL aliquots were spun down and resuspended immediately in 2 mL M9 media with or without 40 μM CCCP and 2.5 μM ligand (Eth^+, $MeTPP^+$, $EtTPP^+$, TPP^+, $MBTPP^+$, or $DPhTPP^+$). Eth^+ fluorescence was measured with excitation at 545 nm and emission at 610 nm. Normalized fluorescence (F_N) was plotted as $F_N(t) = (F(t) - F_0)/F_0$.

NMR spectroscopy and data analysis—Data were collected on 0.8-1.0 mM $^2H/^{15}N$ EmrE reconstituted into q = 0.33 DLPC/DHPC isotropic bicelles in 20 mM KPi (+30 mM cacodylate for PP^{2+} sample), 20 mM NaCl, pH 7, at 45°C. Ligand was added to 10 mM, 5 mM, 16 mM, and 2 mM for $MeTPP^+$, $EtTPP^+$, $MBTPP^+$, and TPP^+, respectively. Due to the low solubility of $DPhTPP^+$, PP^{2+}, and DQ^{2+}, these samples were incubated with excess ligand at 45°C to push the samples to saturation. Most of the NMR data were collected on a 700MHz Varian Inova spectrometer with a room temperature probe. Temperature was calibrated from ethylene glycol peak splitting. The DQ^{2+} data was collected on the Rocky Mountain Regional 900 MHz Varian DD2 spectrometer with room temperature probe. The data for EmrE in DMPC/DHPC isotropic bicelles bound to TPP^+ was collected on the Varian 900 MHz spectrometer with cryo probe at NMRFAM. $^1H/^{15}N$ TROSY HSQCs were collected with 24 scans and 128 complex increments, with recycle delays of 2 s for standard spectra and 6 s for lineshape analysis. The TROSY-selected ZZ-exchange experiment (22) was modified and run as described previously (14). Spectra were collected with 144, 128, 176-256, 128, and 288 scans and 144, 128, 128, 128, and 150 complex increments for $EtTPP^+$, $MBTPP^+$, $DPhTPP^+$, PP^{2+}, and DQ^{2+}, respectively. NMR spectra were processed with NMRPipe (23) and analyzed in NMRViewJ (24), Sparky (25), and

CcpNmr Analysis (26). ZZ-exchange and lineshape data analysis was carried out in Igor Pro (Wavemetrics).

Assignments were transferred from TPP$^+$-bound EmrE (14) to EmrE bound to the other four TPP$^+$-derivatives using data from the HSQC and ZZ-exchange spectra. The ZZ-exchange data significantly reduces the ambiguity of transferred assignments. Only assignments that could be transferred with certainty were used in the analyses.

To extract the conformational interconversion rate, k_{conf}, the ZZ-exchange data for EmrE bound to each ligand were analyzed in the style of Miloushev, et al (27) as described previously for TPP$^+$-bound EmrE (14). With equal populations in the inward- and outward-facing conformations of EmrE (14), the forward (k_{f}) and reverse rates (k_{r}) in this two-state exchange are equal and denoted by $k_{\mathrm{conf}} = k_{\mathrm{f}} = k_{\mathrm{r}}$. The composite peak ratio is a complex ratio of the auto (I_{AA}, I_{BB}) and cross (I_{AB}, I_{BA}) peak intensities as a function of delay time given by:

$$\Xi(t) = \frac{I_{AB}(t) I_{BA}(t)}{I_{AA}(t) I_{BB}(t) - I_{AB}(t) I_{BA}(t)} \cong k_{conf}^2 (t - t_0)^2.$$

The data were fit with an 11.1ms time offset (t_0), which was determined by globally fitting the most intense residues from EmrE complexes with each of EtTPP$^+$, TPP$^+$, and MBTPP$^+$ with a global time offset and individual rates between ligands. This delay time offset matches the calculated back-transfer time in the pulse sequence, confirming that exchange during back transfer must be accounted for with these short ZZ delay times and relatively fast exchange rates(28). This does not affect the determined rate for EmrE-ligand complexes with slow exchange rates, as exemplified by EmrE-DPhTPP$^+$, which fit with $k_{\mathrm{conf}} = 0.4 \pm 0.1$ s^{-1} with or without the time offset. However, exchange during back transfer is significant for faster exchanging complexes when the back-transfer time is comparable to the ZZ delay with fitted rates of 30 ± 6 vs. 25 ± 5 s^{-1} for EtTPP$^+$, 14 ± 3 vs. 13 ± 3 s^{-1} for MBTPP$^+$, and 4.7 ± 0.5 vs. 4.4 ±

0.4 s^{-1} for TPP^+ when determined without or with time offset, respectively. The quality of the fit improved when the time offset was included for these ligands, as judged by reduced residuals. The residues used for the global fits for each ligand-bound EmrE sample were: 9, 26, 58, 77, 80, 82, 83, 106 for $EtTPP^+$; 10, 17, 26, 49, 58, 79, 80, 82, 83, and 106 for $MBTPP^+$; 9, 80, 82, 83, and 90 for $DPhTPP^+$; 58, 80, 82, 106, and 108 for DQ^{2+}; and 17, 26, 58, 80, 82, 83, 106 for PP^{2+}. The standard deviation of the collective individual fits was used to estimate the error of the global fits for each ligand-bound sample.

The relaxation properties of EmrE reconstituted into isotropic bicelles are not conducive to long experiments. As a result, at delay times past 300ms the signal-to-noise was too low to be usable, which limits the accuracy of the rate constant determined for EmrE bound to $DPhTPP^+$, the slowest under exchange conditions, as reported in the text.

The natural abundance ^{15}N of the planar ligands caused significant streaking, which prevented the use of cryo probes. The dynamic properties of EmrE bound to these same ligands made the ZZ-exchange data analysis difficult. Due to these factors, EmrE bound to Eth^+ could not be analyzed quantitatively. Better quality spectra were obtained for EmrE bound to PP^{2+} in DMPC/DHPC rather than DLPC/DHPC bicelles. Therefore, the rate is reported under these conditions since the conformational exchange rate of EmrE bound to TPP^+ does not change between DLPC and DMPC bicelles (**Table 1**, **Fig. 7**).

Spectra for lineshape analysis were processed with exponential line broadening to maintain a Lorentzian lineshape. Analysis was carried out by first extracting integrated 1D slices of TPP^+- and $DPhTPP^+$-bound EmrE from $^1H/^{15}N$ TROSY HSQC spectra using the IDAP Sparky extension (Integrative Data Analysis Platform, IDAP; http://kovrigin.chem.mu.edu/IDAP/) (29). The ^1H lineshapes for all ligand-bound samples were fit to the analytical solution of the two-state Bloch-McConnell equations with equal populations in each state (30). The peak positions (ω_A, ω_B) and intrinsic relaxation rates (R_o^A, R_o^B) were set as adjustable parameters, while the conformational interconversion rate (k_{conf}) was held using the value determined by ZZ-exchange spectroscopy. 1D slices from MeTPP$^+$-bound EmrE spectra were extracted in the same manner and fit with the separation between the chemical shift endpoints ($\Delta\omega$) and intrinsic linewidth values constrained based on the results of the TPP$^+$- and DPhTPP$^+$-bound EmrE fits. Where values varied between ligands, the fitting parameter was allowed to float within constraints that spanned the entire range of values to allow for differences in chemical shift and intrinsic linewidth between ligands. To determine the conformational exchange rate, MeTPP$^+$-bound EmrE lineshapes were globally fit with a single k_{conf} and individual $\Delta\omega$, R_o^A, and R_o^B. The global fits was performed using 12 residues: Y6, G9, G26, W31, S43, L47, Q49, Y53, F78, R82, G90, and L103.

Chemical shift differences ($\Delta\delta_{tot}$) were calculated as a weighted average of the differences in amide proton ($\Delta\delta_H$) and nitrogen ($\Delta\delta_N$) chemical shifts with respect to TPP$^+$-bound EmrE (31):

$$\Delta\delta_{tot} = \sqrt{(\Delta\delta_H)^2+(0.154\Delta\delta_N)^2}.$$

Since MeTPP$^+$-bound EmrE only has a single set of peaks, the chemical shift difference was taken with respect to the average of the two TPP$^+$ peaks for each residue.

The energetic barrier to conformational interconversion was estimated using transition-state theory:

$$\Delta G^{\ddagger}_{conf} = -RTln\left(\frac{hk_{conf}}{k_BT}\right),$$

where R is the universal gas constant, T is the temperature, h is Planck's constant, k_{conf} is the conformational exchange rate determined via NMR methods, and k_B is the Boltzmann constant.

RESULTS

Multidrug recognition and efflux by EmrE—EmrE binds a wide variety of polyaromatic cation substrates. In order to dissect key ligand properties, we began by examining a simple series of five compounds that all share a $^{+}1$ charge and tetrahedral geometry and differ only by substitution of one phenyl ring: TPP^{+}, $MeTPP^{+}$ (also known as $TPMP^{+}$), $EtTPP^{+}$ (also known as $TPEP^{+}$), $DPhTPP^{+}$, and $MBTPP^{+}$ (**Fig. 1A, Table 1**). Since this simple chemical series has not been previously studied, we first confirmed that these compounds are substrates of EmrE based on direct binding experiments via isothermal titration calorimetry (ITC) and in-cell efflux assays.

We used ITC to determine the relative affinity of each of the five tetrahedral substrates for EmrE reconstituted into DLPC/DHPC isotropic bicelles. Surprisingly, the binding affinity varies over three orders of magnitude (**Fig. 2A**, **Fig. 3**). Upon further inspection, within this series of identically charged tetrahedral substrates, binding affinity is roughly correlated with enthalpy (**Fig. 2B**). In addition, the binding enthalpy is correlated with the hydrophobicity of the substrate, as assessed by the measured partition coefficients (**Fig. 2C**). Multiple mutational studies have identified key residues important for substrate binding in EmrE (32-34), and these aromatic and hydrophobic residues line the binding site in the crystal structure (35) (**Fig. 11C**). Thus, the data are consistent with hydrophobicity dominating the binding interaction between the substrate and the active site, provided other ligand properties are similar.

To see whether these trends were generalizable to a wider range of EmrE substrates, we looked at two planar divalent substrates, PP^{2+} and DQ^{2+} (**Table 1**, **Fig. 2A**, **Fig. 3**). The affinity of ethidium^{+} (Eth^{+}) for EmrE was too weak to be measured quantitatively via ITC, but Eth^{+} clearly binds EmrE with a weaker affinity and lower enthalpy than PP^{2+} and DQ^{2+}. Comparison between the planar and tetrahedral substrate series suggests that binding affinity is always correlated with enthalpy (**Fig. 2B**). However, binding enthalpy does not depend simply on substrate hydrophobicity, since ligands with differing charge and geometry do not follow the same trend (**Fig. 2C**). Both charge and geometry may have significant effects on substrate binding for two reasons. First, ligand charge will affect the interaction of the substrates with the critical residue Glu 14 in the binding pocket. Second, the structure of EmrE, and thus its binding pocket architecture, is known to change in order to accommodate different substrate geometries (2). Therefore, multiple ligand properties affect the structure of the transporter-substrate complex and substrate binding affinity.

It is important to investigate how this all comes together in the context of the cell. An *in vivo* assay allows us to monitor the competitive efflux of Eth^+ and the tetrahedral substrates in *E. coli* (**Fig. 4**). Cells overexpressing EmrE efflux Eth^+ considerably faster than control cells (**Fig. 4A**, dashed and solid orange lines, respectively), indicating that a significant portion of the active efflux is due to EmrE. Cells are unable to efflux Eth^+ in the absence of a proton gradient (**Fig. 4A**, orange line, '+CCCP'). The non-EmrE-driven efflux rate is independent of the identity of the competing substrate, with the exception of $DPhTPP^+$ (**Fig. 4A**). On the other hand, cells over-expressing EmrE have a decrease in Eth^+ efflux when one of the TPP^+-derivatives is added (**Fig. 4B**). All five of the tetrahedral substrates compete with Eth^+, indicating that they are transported by EmrE in its native *E. coli* environment. The effect varies with the substrate, demonstrating that the *in vivo* transport rate depends on the identity of the bound substrate (**Table 1**: 'relative transport'). This is not simply blockage by binding of competing substrate to the transport pore, since the effect does not correlate simply with binding affinity (**Table 1**) and $MeTPP^+$ even enhances the final extent of ethidium efflux (**Fig. 4B**, red line).

Differences in the overall transport rate may be a result of changes in several steps in the transport cycle. Both substrate off-rate and conformational exchange rate have been suggested as likely candidates for rate-limiting steps for EmrE transport. Off-rates have been determined previously for several substrates of EmrE (7), but the rate of conformational exchange has only been measured for TPP^+ (14). Therefore, we directly measured the rate of this important step for all the substrates in our ligand series using NMR.

Multidrug conformational exchange—Large-scale global motion, such as exchange between the inward- and outward-facing states of EmrE, can be directly monitored using solution NMR dynamics methods. $^{15}N/^{1}H$ TROSY HSQC spectra of EmrE bound to $EtTPP^+$, $MBTPP^+$, and $DPhTPP^+$ indicate that EmrE bound to these compounds has the same two sets of peaks previously described for TPP^+-bound EmrE (**Fig. 5**) (14). This corresponds to the two monomers in an asymmetric dimer, with inward- to outward-facing transitions occurring via AB-to-BA exchange as predicted by Fleishman, et al. (5) (**Fig. 1B**). The overall pattern of the peaks is similar in each case, indicating the same overall fold. However, local chemical shift changes do occur and are discussed below. Qualitatively, the different extent of line-broadening in each spectrum results from differences in the conformational exchange timescale. This rate is quantified using TROSY-selected ZZ-exchange experiments (22), as demonstrated previously for TPP^+-bound EmrE (14) (**Fig. 6**). The data are presented in the style of Miloushev, et al. (27), which allows easy comparison of global exchange between different substrate-bound states (**Fig. 7**, **Fig. 10A**, **Table 1**). It is clear that the rate of conformational interconversion varies significantly with the identity of the bound substrate.

Amazingly, when EmrE is bound to the remaining member of the series, $MeTPP^+$, it reveals only a single set of peaks in a $^{15}N/^{1}H$ TROSY HSQC (**Fig. 8A**). Thus, when bound to this substrate, EmrE is pushed into intermediate-fast exchange. Under these conditions, each peak represents the average chemical shift of the exchanging states for each residue, and lineshape analysis is used to extract the conformational exchange rate. This requires prior knowledge of the chemical shift difference between the two states in the absence of exchange and the intrinsic linewidths. We determined these parameters by fitting the lineshapes for EmrE bound to TPP^+ and $DPhTPP^+$ using the known conformational exchange rates determined by ZZ-exchange spectroscopy as described in the methods. Since EmrE in complex with these two substrates has the slowest exchange rates, these will be the closest to exchange-free conditions and thus have the lowest extrapolated error. By fitting data sets for multiple substrates, we were able to determine which parameters are sensitive to substrate identity and adjust the constraints and error bars appropriately. The $MeTPP^+$-bound lineshapes of 12 residues were then fit globally to determine the conformational exchange rate (**Fig. 8B,C**).

The rate of conformational exchange for EmrE bound to the two planar substrates was also quantified (**Table 1**, **Fig. 7**, **Fig. 9**). Interestingly, even though the two planar substrates are structurally dissimilar, they have quite similar conformational exchange rates. This is in contrast to the large variation within the tetrahedral substrate series. Overall, the conformational interconversion rate of substrate-bound EmrE varies over almost three orders of magnitude (**Fig. 10A**, **Table 1**). How can EmrE move between its inward- and outward-facing states with such greatly varying kinetics? Since these are slow dynamics overall, are they an important factor in transport rate?

Previous measurement of several substrate on- and off-rates for detergent-solubilized EmrE suggests that substrate association rate is diffusion-limited and dissociation determines affinity (7). Using a the on-rate at pH 7 (7) corrected for the temperature dependence of diffusion and our measured binding affinities (45°C, pH 7), we calculated off-rates for each substrate. The estimated off-rates are within an order of magnitude of the conformational exchange rate for all but one substrate. Thus, both processes may contribute to the overall turnover rate for EmrE with the rate-limiting step depending on the transported substrate. Future experiments to test this hypothesis will require precise measurements under identical conditions.

The significant differences in conformational exchange rate (k_{conf}) when EmrE is bound to different substrates indicate that substrate binding alters the energy landscape. This is illustrated in **Fig. 10B** by approximating the complex energy landscape as a simple two-state process along a single reaction coordinate. Compared to TPP^+, most of the substrates lead to faster conformational exchange rates in EmrE. A faster exchange rate may be due to higher ground-state (substrate-bound state) energy, lower transition-state energy for the conformational exchange process, or some combination thereof. To distinguish the relative importance of these effects, the apo state of the protein provides a convenient substrate-independent reference state to anchor the energy landscape. This approximation assumes that differences in the free energy of the unbound ligand are small relative to the binding energy. Differences in ground-state energy of EmrE bound to different substrates are determined relative to the apo reference state by the free energy of binding (ΔG_{bind}) as calculated from the experimentally determined binding affinities (**Fig. 10B**, left side). This highlights the significant effect of substrate identity on the free energy of the complex, which is particularly interesting in light of the known changes in EmrE structure when bound to different substrates (2).

We then used transition-state theory and the conformational exchange rate determined by NMR to estimate the height of the transition-state barrier ($\Delta G^{\ddagger}_{conf}$) relative to the ground state for each of the substrates (see methods). It is clear that both the ground and transition states are affected by bound substrate (**Fig. 10B**). This is why there is not a simple correlation between binding affinity and conformational exchange rate across all substrates (**Table 1**), as would be expected if only the ground-state energy (free energy of substrate-bound EmrE) were affected by substrate identity and the transition-state energy was the same for all ligands. Within the tetrahedral series, there is less variation in the transition-state energy than in the ground state energy (note in particular the clustering of the transition-state energy for $MeTPP^+$, $DPhTPP^+$, TPP^+, and $EtTPP^+$ despite their wide variation in bound-state energy), and there is general correlation between binding energy and exchange rate within this subset. This suggests that the protein is an important but not exclusive factor in determining the energy of the conformational exchange transition state. Substrate properties also affect this barrier height, particularly when there are differences in substrate charge and geometry (note the higher barrier for the same ground state for the $^+2$ planar substrates vs. $MeTPP^+$). It is this combination of effects that keeps the energy barrier for conformational exchange from becoming too large and enables EmrE to be a *multidrug* transporter.

DISCUSSION

Structural implications—Structural studies have given some insight into the mechanism of multidrug recognition in EmrE. The first three transmembrane helices from each monomer come together to form a hydrophobic binding pocket, while the two TM4 helices form a dimerization arm (35, 36). The correlation we observe between ligand hydrophobicity and binding affinity within the tetrahedral substrate series confirms the importance of this property for substrate interaction with the hydrophobic binding pocket. However, this correlation does not hold across more diverse substrates (**Fig. 2B,C**), indicating that ligand charge and shape are also important for substrate recognition by EmrE. Low-resolution cryo-EM data indicate that the structure of EmrE changes when bound to tetrahedral TPP^+ and three planar substrates (Eth^+, PP^{2+}, and DQ^{2+}) (2). Thus, multidrug binding by EmrE results from a complex interaction between substrate and protein, with ligand properties affecting the structure of the binding site and the free energy of the complex. Since helix tilt depends on the identity of the substrate, and the helices must reorient for alternating access, structural and dynamic changes are likely to be linked.

Throughout these experiments, we observed how relatively small differences in the substrate cause large changes in binding, dynamics, and functional transport by EmrE. Hints at the structural changes induced in EmrE by the different substrates are provided by chemical shift changes in the $^{15}N/^{1}H$ TROSY HSQC spectra (**Fig. 11A,B**). Residues in TM1 such as A10, G17, and I11 that affect substrate binding and specificity (32, 37) (**Fig. 11C**) show significant shifts between EmrE bound to TPP^+ and the four other related compounds as expected for residues in close proximity to the substrate. I94 and V98 are thought to form a “pivot point” in TM4 of the SMRs with importance not only for dimerization, but also a direct role in the mechanism of multidrug efflux (38). While I94 is not assigned, V98 does shift with substrate. Interestingly, V98 has very large shifts in one state and negligible shifts in the other, indicating an asymmetric role for this residue. In the crystal structure, V98 from one monomer faces into the interface between the two TM4 helices near the TM3 kink, while in the other monomer it is rotated into a more outward-facing position. The kink in TM3, caused by the GVG motif (residues 65-67), is also expected to play a key role in conformational interconversion (5, 14, 39), and this kink changes conformation upon substrate binding, as shown by solid-state NMR PISEMA spectra of V66 and V69 (40). Intriguingly, this region has some of the largest chemical shift changes when different substrates are bound, suggesting an important role for this hinge region in translating substrate identity into distinct rates of exchange for the common conformational interconversion process.

Further inspection of the spectra highlights some unique features of the C-terminal region of EmrE. The C-termini are missing from the crystal structure (35), indicating they do not have a single well-defined conformation under those conditions. However, residues in this region, including 104-108, have unique, well-resolved chemical shifts that do not match random coil chemical shifts, indicating that the C-terminus is not simply a floppy tail. In agreement with EPR studies that show a loss in helical periodicity after residue 103 (39), these chemical shifts are not typical of helical secondary structure, as might be expected if the final helix extended beyond the point where it is resolved in the crystal. Additionally, at least one of each pair of peaks for residues 105, 106, and 108 is highly sensitive to bound substrate (**Fig. 11A**). Arginine 106 (**Fig. 5**) provides a particularly well-resolved example of the behavior of residues in this region. Examination of the crystal structure reveals that on the open face of EmrE, the entrance to the transport pore extends between the TM3 helices (**Fig. 1B**) and there is space for C-terminal residues from monomer A to extend into this region. Using differential water accessibility to identify monomers A and B (14), it is precisely the peaks corresponding to the C-terminal tail of monomer A that are sensitive to substrate identity. Although its exact role is not known, the C-terminus of EmrE is as sensitive to bound substrate identity as other key regions of EmrE and should not be ignored when considering the structure and function of the protein despite its absence in the crystal structure.

Implications for protein dynamics—The importance of protein motions on different timescales for biological function is well-established (41, 42). The large-scale inward- to outward-facing conformational change of EmrE is key to the biological activity of this multidrug resistance transporter. As we have shown, the dynamics of this large-scale structural change are modulated over several orders of magnitude by the identity of the substrate being transported. Global domain motions that are modulated (in a non switch-like fashion) to this extreme have not been extensively reported. Only one similar example of a transporter exists: LeuT interconversion dynamics differ when bound to either alanine or leucine (43). However, the differences in rates do not vary as significantly as reported here, and the extreme differences in rate observed for EmrE may reflect the unique properties required for multidrug recognition and transport. Thus, we propose that large changes in dynamics with substrate identity may occur in many MDR transporters.

The coupled effects of substrate binding on EmrE structure and dynamics provide important insight into the transport mechanism. For EmrE, our results are consistent with large structural differences when bound to diverse substrates (2) leading to significant differences in the free energy of the bound state that are dependent on ligand size, charge, and hydrophobicity. This bound state is the ground state for the conformational transition between open-in and open-out states. The observation that there is less variation in the transition state energy within the tetrahedral series indicates the importance of EmrE itself in influencing the conformational exchange transition. This is reminiscent of the finding that partially active mutants and phosphorylation of NtrC alter the rate of exchange between the active and inactive states of this signaling protein by changing the ground-state energy and have very little effect on the transition state energy. Mutations of NtrC residues participating in the transition pathway do affect the transition state energy (44). However, in EmrE, there is structural overlap between the regions involved in substrate binding and interconversion. The chemical shift differences between EmrE bound to different substrates (**Fig. 11A,B**) reveal significant effects in TM3 and TM4. TM3 forms part of the hydrophobic binding pocket and contains the critical binding residue W63. The TM3 kink structure is sensitive to substrate binding (40), and together with the TM4 hinge is believed to play a critical role in the conformational interconversion (5, 14, 38, 39). Based on this data, changes in helix tilt upon ligand binding alter the ground-state energy for the complex, and can affect the transition-state energy via the effect of altered helix tilt on the TM3-TM4 hinge point or direct ligand interaction with the TM3 hinge. Thus, we propose that TM3 plays a central role in coupling substrate binding to conformational exchange between inward- and outward-facing states in EmrE.

The influence of substrate on the transition-state energy for EmrE converting between inward- and outward-facing states is consistent with the alternating-access model of antiport. Unlike soluble enzymes, which have frequently been found to pre-sample the enzymatically-active conformation in the apo state (45-49), EmrE should not undergo transport-related motions when not bound to substrate in order to achieve coupled antiport. This is more similar to PKA-C, where nucleotide binding is required to achieve a state with both structure and dynamics primed for catalysis (50). For single-site alternating-access antiport, the transition state for conformational exchange cannot be determined solely by the protein and must have a significant influence from the substrate, in agreement with our data for EmrE. This suggests a mechanism for transport inhibition. A very tight-binding substrate may stabilize the ground state sufficiently to create a nearly insurmountable energetic barrier for conformational exchange, thus trapping a single state of EmrE and preventing efflux.

Acknowledgments: We thank Scott Wildman for medicinal chemistry advice, Tim Lohman and Jim Janetka for the use of the fluorimeter and HPLC, and G. Chang for the EmrE expression plasmid. For assistance with NMR acquisition, we thank Greg DeKoster, Marco Tonelli (NMRFAM), and Geoffrey Armstrong (Rocky Mountain NMR Facility). This study made use of the Rocky Mountain NMR Facility and the National Magnetic Resonance Facility at Madison (NMRFAM). NMRFAM is supported by NIH grants P41RR02301 (BRTP/ NCRR) and P41GM66326 (NIGMS), the University of Wisconsin, the NIH (RR02781, RR08438), the NSF (DMB-8415048, OIA-9977486, BIR-9214394), and the USDA. This work was supported by the National Institutes of Health (1R01GM095839), the Searle Scholars Program (K.H.W.), and an NSF graduate research fellowship to E.M. (DGE-1143954).

TABLE 1. Summary of thermodynamics and kinetics of EmrE bound to range of tetrahedral and planar ligands.

Ligand	Binding constant (K_d^{pH7}, μM)[a]	ΔH (kJ/mol)	n	Interconversion rate (k_{conf}, s^{-1})	Relative transport[c]	LogP
MeTPP$^+$	130 ± 20	-12.7 ± 0.2	0.60 ± 0.04	190 ± 80	1	1.8 ± 0.1
EtTPP$^+$	21.8 ± 0.7	-16.6 ± 0.2	0.57 ± 0.04	25 ± 5	2	1.9 ± 0.1
TPP$^+$	0.45 ± 0.01	-22 ± 1	0.49 ± 0.05	4.4 ± 0.4 4.7 ± 0.6 [b]	4	2.2 ± 0.1
DPhTPP$^+$	0.16 ± 0.02	-39.4 ± 0.3	0.53 ± 0.05	0.4 ± 0.1	5	3.0 ± 0.2
MBTPP$^+$	0.04 ± 0.01	-38 ± 2	0.544 ± 0.009	13 ± 3	3	2.5 ± 0.1
DQ^{2+}	100 ± 20	-5.7 ± 0.3	0.58 ± 0.02	11 ± 2	N/A	3.4 ± 0.1
PP^{2+}	90 ± 10	-16.3 ± 0.7	0.58 ± 0.06	13 ± 3 [b]	N/A	4.3 +0.5/-1.0

[a] Observed binding constant from ITC at pH 7, 45°C.
[b] Reconstituted into DMPC/DHPC isotropic bicelles.
[c] Determined via in-cell assay. Ranked 1 through 5, from fastest to slowest EmrE-dependent ethidium efflux in the presence of each competing ligand.

REFERENCES

1. Jardetzky, O. (1966) Simple allosteric model for membrane pumps. *Nature* **211**, 969–970
2. Korkhov, V. M., and Tate, C. G. (2008) Electron crystallography reveals plasticity within the drug binding site of the small multidrug transporter EmrE. *J Mol Biol* **377**, 1094–1103
3. Rotem, D., and Schuldiner, S. (2004) EmrE, a multidrug transporter from Escherichia coli, transports monovalent and divalent substrates with the same stoichiometry. *J Biol Chem* **279**, 48787–48793
4. Schuldiner, S. (2009) EmrE, a model for studying evolution and mechanism of ion-coupled transporters. *BBA - Proteins and Proteomics*, 1–15
5. Fleishman, S. J., Harrington, S. E., Enosh, A., Halperin, D., Tate, C. G., and Ben-Tal, N. (2006) Quasi-symmetry in the cryo-EM structure of EmrE provides the key to modeling its transmembrane domain. *J Mol Biol* **364**, 54–67
6. Yerushalmi, H., and Schuldiner, S. (2000) A model for coupling of H(+) and substrate fluxes based on "time-sharing" of a common binding site. *Biochemistry* **39**, 14711–14719
7. Adam, Y., Tayer, N., Rotem, D., Schreiber, G., and Schuldiner, S. (2007) The fast release of sticky protons: kinetics of substrate binding and proton release in a multidrug transporter. *Proc Natl Acad Sci USA* **104**, 17989–17994
8. Henzler-Wildman, K. (2012) Analyzing conformational changes in the transport cycle of EmrE. *Curr Opin Struct Biol* **22**, 38–43
9. Ong, Y.-S., Lakatos, A., Becker-Baldus, J., Pos, K. M., and Glaubitz, C. (2013) Detecting substrates bound to the secondary multidrug efflux pump EmrE by DNP-enhanced solid-state NMR. *J Am Chem Soc* **135**, 15754–15762
10. Higgins, C. F. (2007) Multiple molecular mechanisms for multidrug resistance transporters. *Nature* **446**, 749–757
11. Wade, H. (2010) MD recognition by MDR gene regulators. *Curr Opin Struct Biol* **20**, 489–496
12. Neyfakh, A. A. (2002) Mystery of multidrug transporters: the answer can be simple. *Mol. Microbiol.* **44**, 1123–1130
13. Bachas, S., Eginton, C., Gunio, D., and Wade, H. (2011) Structural contributions to multidrug recognition in the multidrug resistance (MDR) gene regulator, BmrR. **108**, 11046–11051
14. Morrison, E. A., Dekoster, G. T., Dutta, S., Vafabakhsh, R., Clarkson, M. W., Bahl, A., Kern, D., Ha, T., and Henzler-Wildman, K. A. (2012) Antiparallel EmrE exports drugs by exchanging between asymmetric structures. *Nature* **481**, 45–50
15. Morrison, E. A., and Henzler-Wildman, K. A. (2012) Reconstitution of integral membrane proteins into isotropic bicelles with improved sample stability and expanded lipid composition profile. *Biochimica et Biophysica Acta (BBA) - Biomembranes* **1818**, 814–820
16. Organization for Economic Co-operation and Development (OECD) (2004) OECD guidelines for the testing of chemicals No. 117: "Partition coefficient (n-octanol/water), high performance liquid chromatography (HPLC) method." 1–11
17. Garbett, N. C., Hammond, N. B., and Graves, D. E. (2004) Influence of the amino substituents in the interaction of ethidium bromide with DNA. *Biophysical Journal* **87**, 3974–3981
18. Wright, R. G., Wakelin, L. P. G., Fieldes, A., Acheson, R. M., Waring, M. J., (null),

(null), (null), (null), and (null) (1980) Effects of ring substituents and linker chains on the bifunctional intercalation of diacridines into deoxyribonucleic acid. *Biochemistry* **19**, 5825–5836

19. Glover, K. J., Whiles, J. A., Wu, G., Yu, N., Deems, R., Struppe, J. O., Stark, R. E., Komives, E. A., and Vold, R. R. (2001) Structural evaluation of phospholipid bicelles for solution-state studies of membrane-associated biomolecules. *Biophysical Journal* **81**, 2163–2171
20. Lambert, B., and Le Pecq, J. B. (1984) Effect of mutation, electric membrane potential, and metabolic inhibitors on the accessibility of nucleic acids to ethidium bromide in Escherichia coli cells. *Biochemistry* **23**, 166–176
21. Yerushalmi, H., Lebendiker, M., and Schuldiner, S. (1995) EmrE, an Escherichia coli 12-kDa multidrug transporter, exchanges toxic cations and H+ and is soluble in organic solvents. *J Biol Chem* **270**, 6856–6863
22. Li, Y., and Palmer, A. G. (2009) TROSY-selected ZZ-exchange experiment for characterizing slow chemical exchange in large proteins. *J Biomol NMR* **45**, 357–360
23. Delaglio, F., Grzesiek, S., Vuister, G. W., Zhu, G., Pfeifer, J., and Bax, A. (1995) NMRPipe: a multidimensional spectral processing system based on UNIX pipes. *J Biomol NMR* **6**, 277–293
24. JOHNSON, B., and BLEVINS, R. (1994) NMR VIEW - A COMPUTER-PROGRAM FOR THE VISUALIZATION AND ANALYSIS OF NMR DATA. *J Biomol NMR* **4**, 603–614
25. Goddard, T. D., and Kneller, D. G. Sparky 3.
26. Vranken, W. F., Boucher, W., Stevens, T. J., Fogh, R. H., Pajon, A., Llinas, M., Ulrich, E. L., Markley, J. L., Ionides, J., and Laue, E. D. (2005) The CCPN data model for NMR spectroscopy: development of a software pipeline. *Proteins* **59**, 687–696
27. Miloushev, V. Z., Bahna, F., Ciatto, C., Ahlsen, G., Honig, B., Shapiro, L., and Palmer, A. G. (2008) Dynamic properties of a type II cadherin adhesive domain: implications for the mechanism of strand-swapping of classical cadherins. *Structure* **16**, 1195–1205
28. Tollinger, M., Skrynnikov, N. R., Mulder, F. A., Forman-Kay, J. D., and Kay, L. E. (2001) Slow dynamics in folded and unfolded states of an SH3 domain. *J Am Chem Soc* **123**, 11341–11352
29. Kovrigin, E. L. (2012) NMR line shapes and multi-state binding equilibria. *J Biomol NMR* **53**, 257–270
30. McConnell, H. M. (1958) Reaction Rates by Nuclear Magnetic Resonance. *The Journal of Chemical Physics* **28**, 430–431
31. Tugarinov, V., and Kay, L. E. (2003) Quantitative NMR studies of high molecular weight proteins: application to domain orientation and ligand binding in the 723 residue enzyme malate synthase G. *J Mol Biol* **327**, 1121–1133
32. Gutman, N., Steiner-Mordoch, S., and Schuldiner, S. (2003) An amino acid cluster around the essential Glu-14 is part of the substrate- and proton-binding domain of EmrE, a multidrug transporter from Escherichia coli. *J Biol Chem* **278**, 16082–16087
33. Elbaz, Y., Tayer, N., Steinfels, E., Steiner-Mordoch, S., and Schuldiner, S. (2005) Substrate-induced tryptophan fluorescence changes in EmrE, the smallest ion-coupled multidrug transporter. *Biochemistry* **44**, 7369–7377
34. Rotem, D., Steiner-Mordoch, S., and Schuldiner, S. (2006) Identification of tyrosine residues critical for the function of an ion-coupled multidrug transporter. *J Biol Chem* **281**,

18715–18722
35. Chen, Y. J., Pornillos, O., Lieu, S., Ma, C., Chen, A. P., and Chang, G. (2007) X-ray structure of EmrE supports dual topology model. *Proc Natl Acad Sci USA* **104**, 18999–19004
36. Ubarretxena-Belandia, I., Baldwin, J. M., Schuldiner, S., and Tate, C. G. (2003) Three-dimensional structure of the bacterial multidrug transporter EmrE shows it is an asymmetric homodimer. *EMBO J* **22**, 6175–6181
37. Elbaz, Y., Salomon, T., and Schuldiner, S. (2008) Identification of a glycine motif required for packing in EmrE, a multidrug transporter from Escherichia coli. *J Biol Chem* **283**, 12276–12283
38. Poulsen, B. E., Cunningham, F., Lee, K. K. Y., and Deber, C. M. (2011) Modulation of Substrate Efflux in Bacterial Small Multidrug Resistance Proteins by Mutations at the Dimer Interface. *J Bacteriol* **193**, 5929–5935
39. Amadi, S. T., Koteiche, H. A., Mishra, S., and McHaourab, H. S. (2010) Structure, dynamics and substrate-induced conformational changes of the multidrug transporter emre in liposomes. *J Biol Chem*
40. Gayen, A., Banigan, J. R., and Traaseth, N. J. (2013) Ligand-induced conformational changes of the multidrug resistance transporter EmrE probed by oriented solid-state NMR spectroscopy. *Angew Chem Int Ed Engl* **52**, 10321–10324
41. Henzler-Wildman, K., and Kern, D. (2007) Dynamic personalities of proteins. *Nature* **450**, 964–972
42. Akke, M. (2002) NMR methods for characterizing microsecond to millisecond dynamics in recognition and catalysis. *Curr Opin Struct Biol* **12**, 642–647
43. Zhao, Y., Terry, D. S., Shi, L., Quick, M., Weinstein, H., Blanchard, S. C., and Javitch, J. A. (2011) Substrate-modulated gating dynamics in a Na+-coupled neurotransmitter transporter homologue. *Nature* **474**, 109–113
44. Gardino, A. K., Villali, J., Kivenson, A., Lei, M., Liu, C. F., Steindel, P., Eisenmesser, E. Z., Labeikovsky, W., Wolf-Watz, M., Clarkson, M. W., and Kern, D. (2009) Transient non-native hydrogen bonds promote activation of a signaling protein. *Cell* **139**, 1109–1118
45. Henzler-Wildman, K. A., Thai, V., Lei, M., Ott, M., Wolf-Watz, M., Fenn, T., Pozharski, E., Wilson, M. A., Petsko, G. A., Karplus, M., Hübner, C. G., and Kern, D. (2007) Intrinsic motions along an enzymatic reaction trajectory. *Nature* **450**, 838–844
46. Labeikovsky, W., Eisenmesser, E. Z., Bosco, D. A., and Kern, D. (2007) Structure and dynamics of pin1 during catalysis by NMR. *J Mol Biol* **367**, 1370–1381
47. Villali, J., and Kern, D. (2010) Choreographing an enzyme's dance. *Curr Opin Chem Biol* **14**, 636–643
48. Velyvis, A., Yang, Y. R., Schachman, H. K., and Kay, L. E. (2007) A solution NMR study showing that active site ligands and nucleotides directly perturb the allosteric equilibrium in aspartate transcarbamoylase. *Proc Natl Acad Sci USA* **104**, 8815–8820
49. Vogt, A. D., and Di Cera, E. (2013) Conformational selection is a dominant mechanism of ligand binding. *Biochemistry* **52**, 5723–5729
50. Veglia, G., and Cembran, A. (2013) Role of conformational entropy in the activity and regulation of the catalytic subunit of protein kinase A. *FEBS J.* **280**, 5608–5615

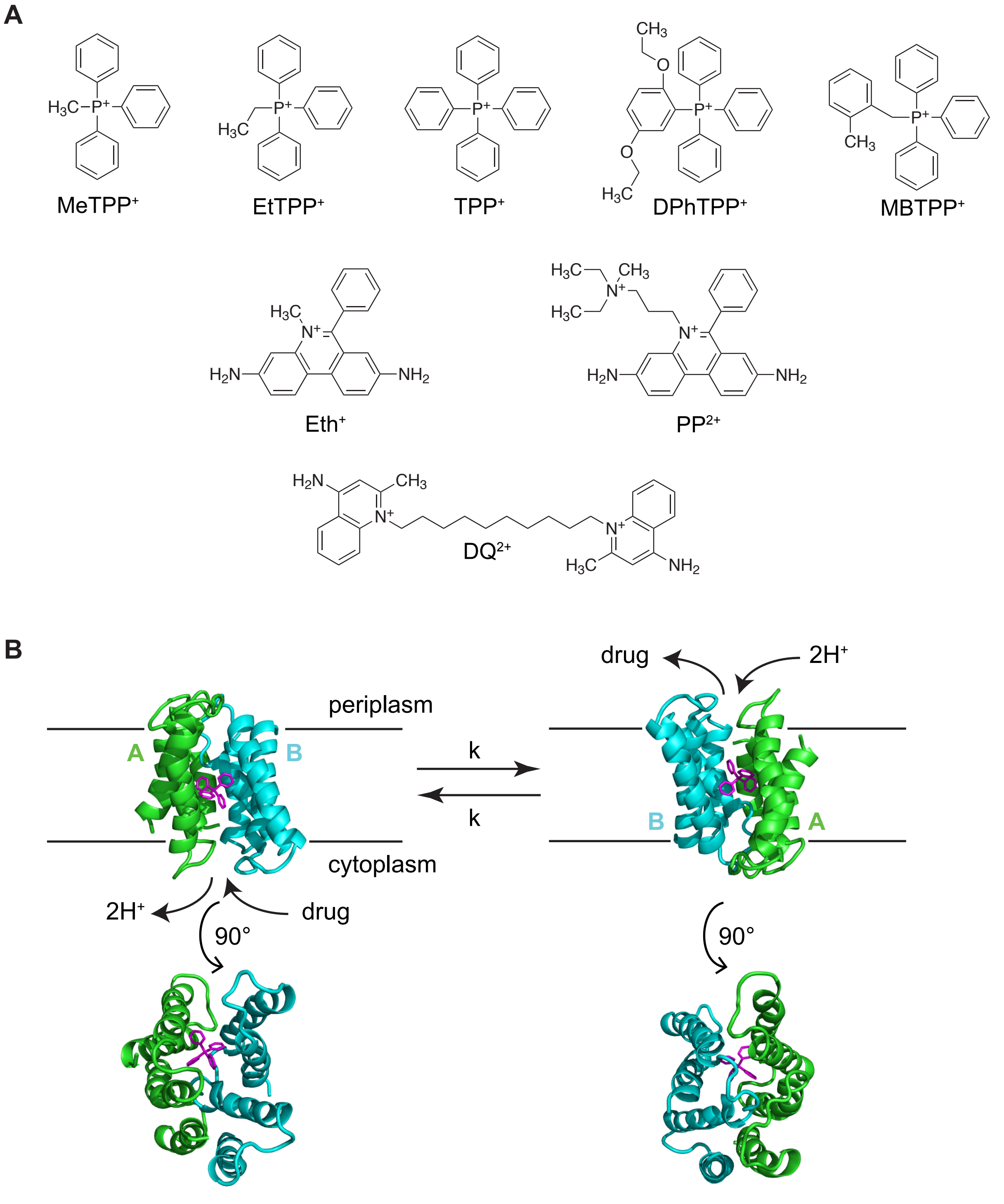

Figure 1. EmrE binds and transports a broad range of ligands. **A.** Chemical structures of the tetrahedral and planar ligand series. **B.** The EmrE dimer exchanges between an AB and BA conformation (state A in green; state B in blue) as it converts between the inward- and outward-facing conformations. A 90° rotation permits a view of the open and closed faces of EmrE (PDB 3B5D, PyMOL). Figure from Morrison and Henzler-Wildman, 2014.

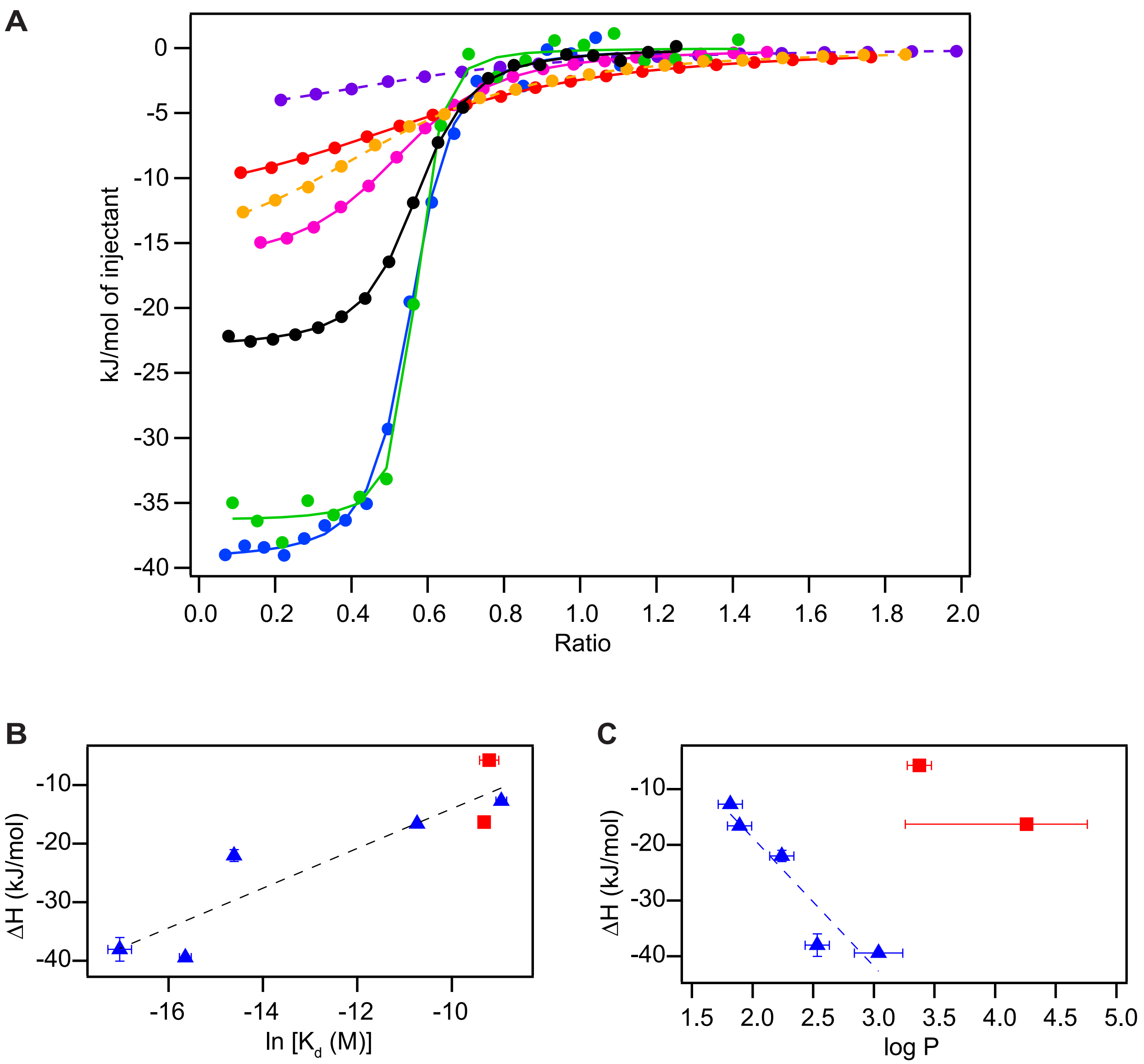

Figure 2. Variation in binding affinity of EmrE substrates. **A.** Overlay of representative ITC binding curves of the five TPP$^+$-derivatives and two planar compounds: MeTPP$^+$ (red), EtTPP$^+$ (magenta), TPP$^+$ (black), MBTPP$^+$ (green), DPhTPP$^+$ (blue), PP^{2+} (orange), and DQ^{2+} (purple) with the fit baseline subtracted. **B.** Binding affinity is correlated with enthalpy, regardless of ligand geometry (tetrahedral in blue triangles, planar in red squares, R^2= 0.84). **C.** Partition coefficients, a measure of ligand hydrophobicity, correlate with enthalpy within the tetrahedral ligand series (blue triangles, R^2 = 0.89) but not between ligand series. Figure from Morrison and Henzler-Wildman, 2014.

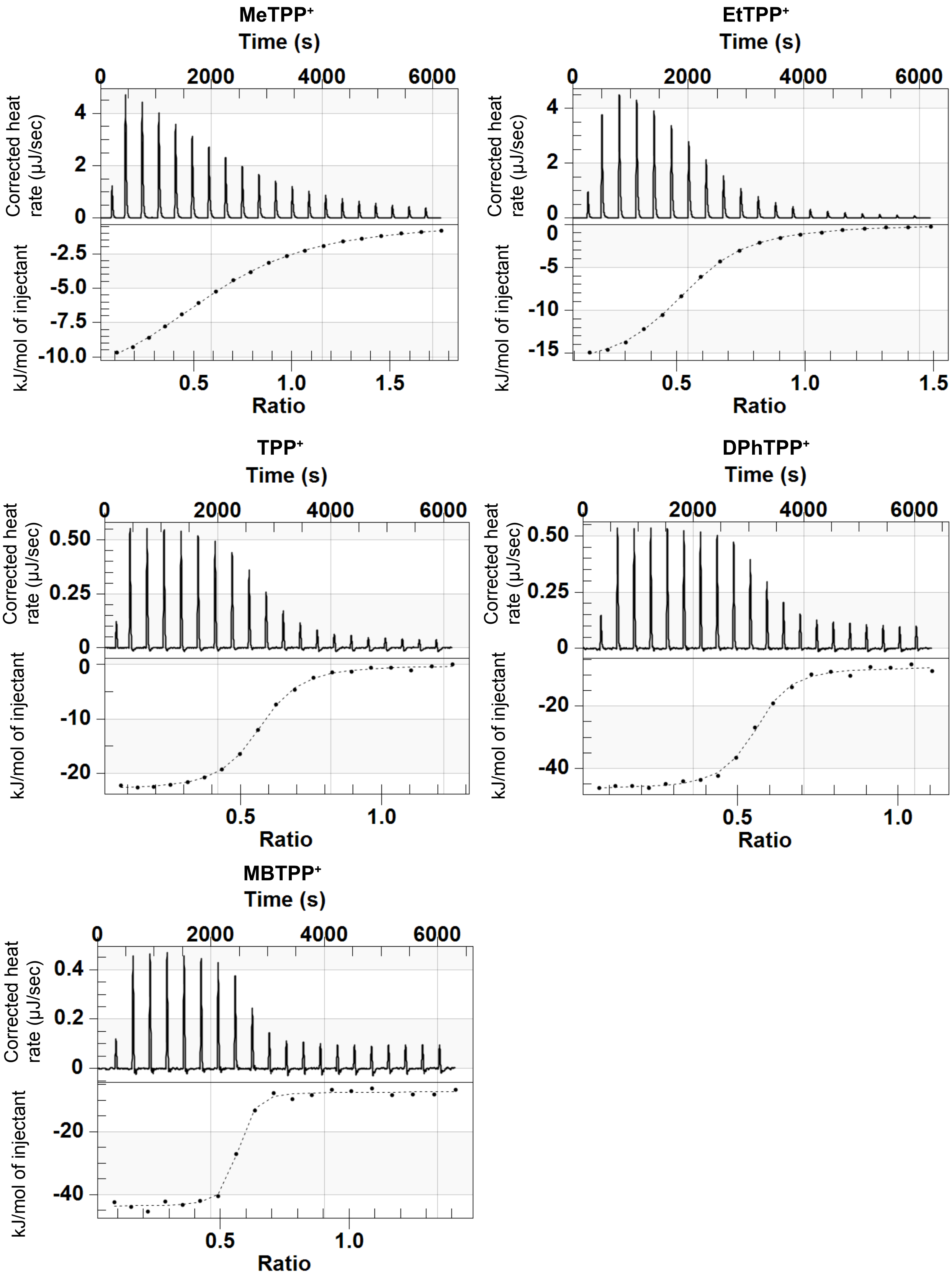

Figure 3. Representative ITC titration for each ligand.

PP^{2+}

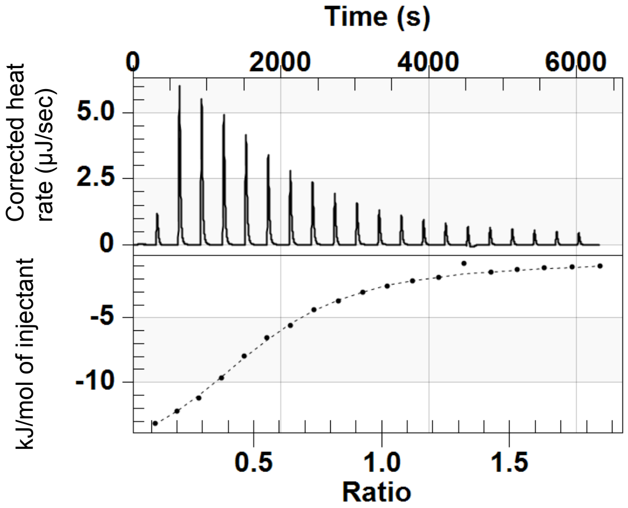
Time (s)
0
2000
4000
6000
Corrected heat rate (µJ/sec)
5.0
2.5
0
kJ/mol of injectant
-5
-10
0.5
1.0
1.5
Ratio

DQ^{2+}

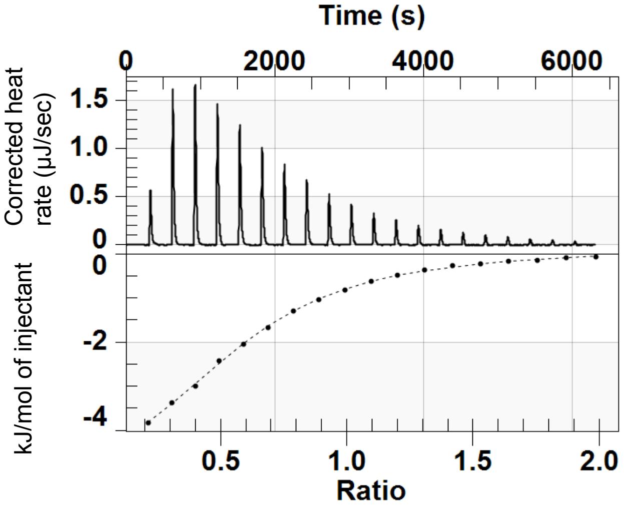
Time (s)
0
2000
4000
6000
Corrected heat rate (µJ/sec)
1.5
1.0
0.5
0
kJ/mol of injectant
0
-2
-4
0.5
1.0
1.5
2.0
Ratio

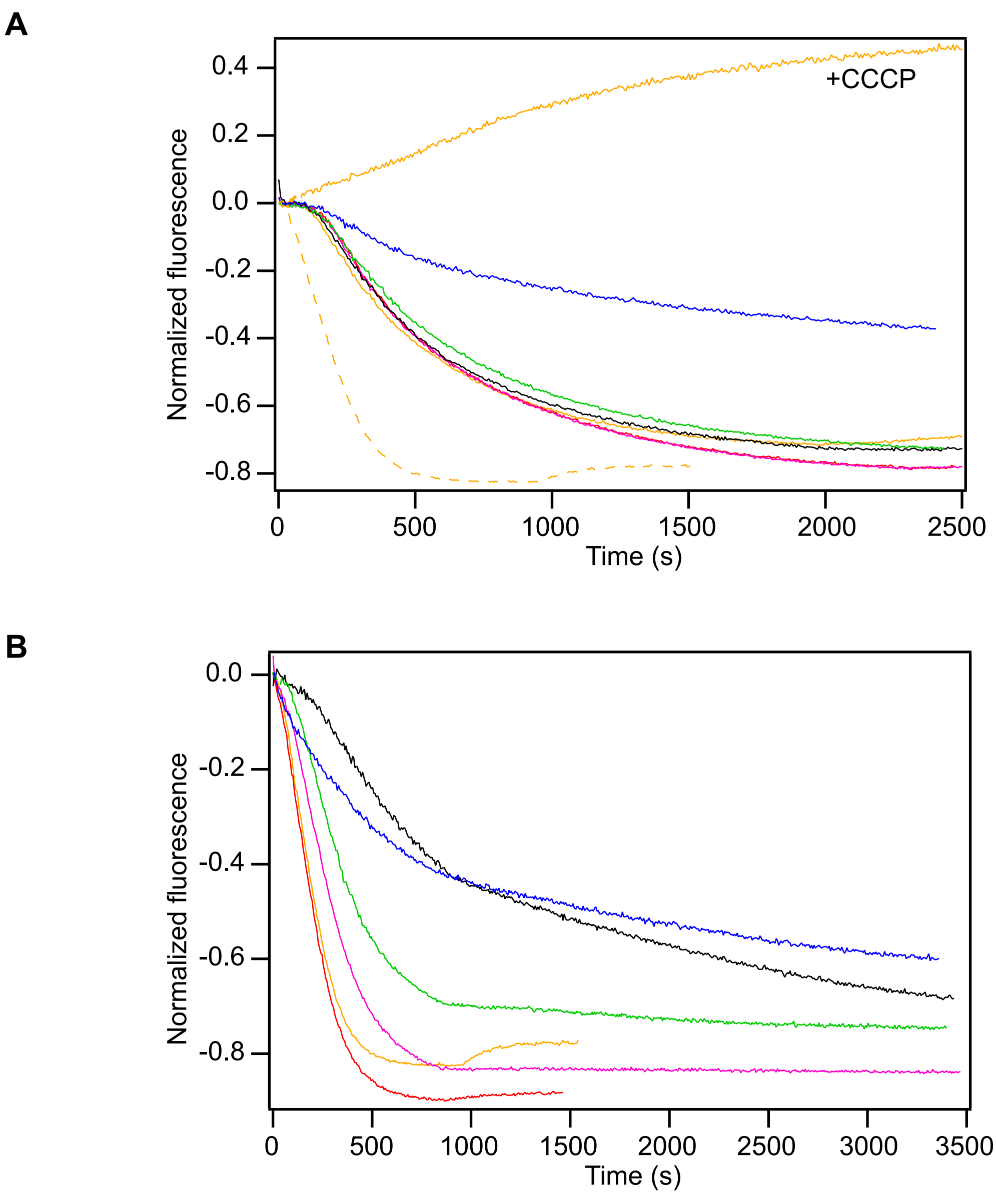

Figure 4. Ligand identity determines transport rate in E. coli. In this competitive transport assay in *E. coli*, Eth^+ efflux is monitored upon induction of (**A**) empty vector or (**B**) EmrE in BL21(DE3) with addition of external Eth^+ (orange) or the competing ligands $MeTPP^+$ (red), $EtTPP^+$ (magenta), TPP^+ (black), $MBTPP^+$ (green), and $DPhTPP^+$ (blue). The data shown is from a single batch of cells, to ensure equal protein expression levels between traces. Results were reproducible between batches of cells and were qualitatively similar between two BL21 cell lines. In (**A**) the Eth^+ trace from cells over-expressing EmrE is re-plotted as a dashed orange line for reference. Addition of CCCP inhibits Eth^+ efflux (**A**, '+CCCP'). Figure from Morrison and Henzler-Wildman, 2014.

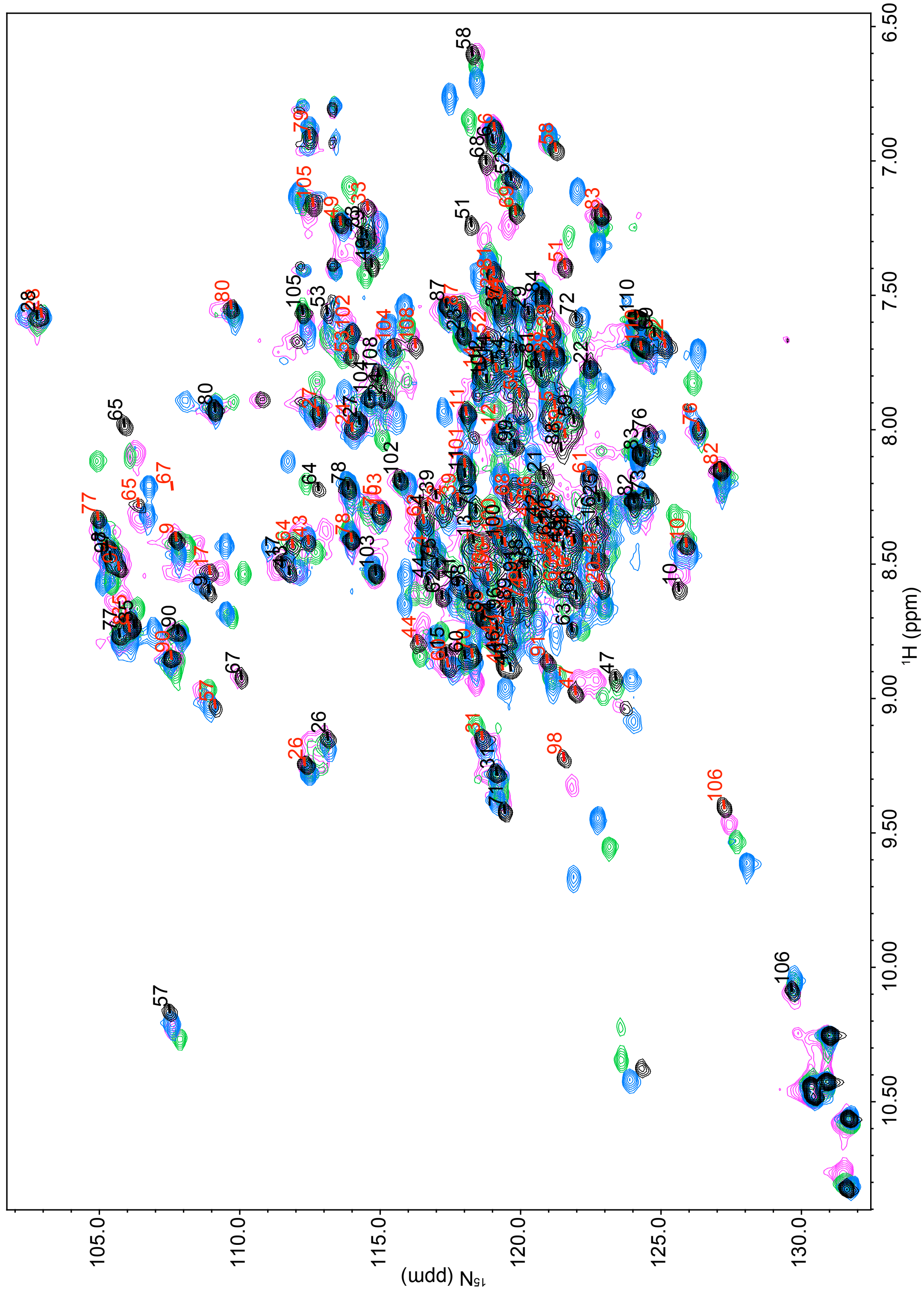

Figure 5. NMR spectra of EmrE bound to the tetrahedral substrates indicate the same overall protein structure but varying dynamics. ^{15}N/^{1}H TROSY HSQC spectra of EmrE bound to EtTPP^{+} (magenta), TPP^{+} (black), DPhTPP^{+} (blue), and MBTPP^{+} (green), are similar, with two peaks per residue corresponding to slow exchange of the asymmetric dimer. The TPP^{+}-bound EmrE assignments are displayed for states A (red) and B (black).

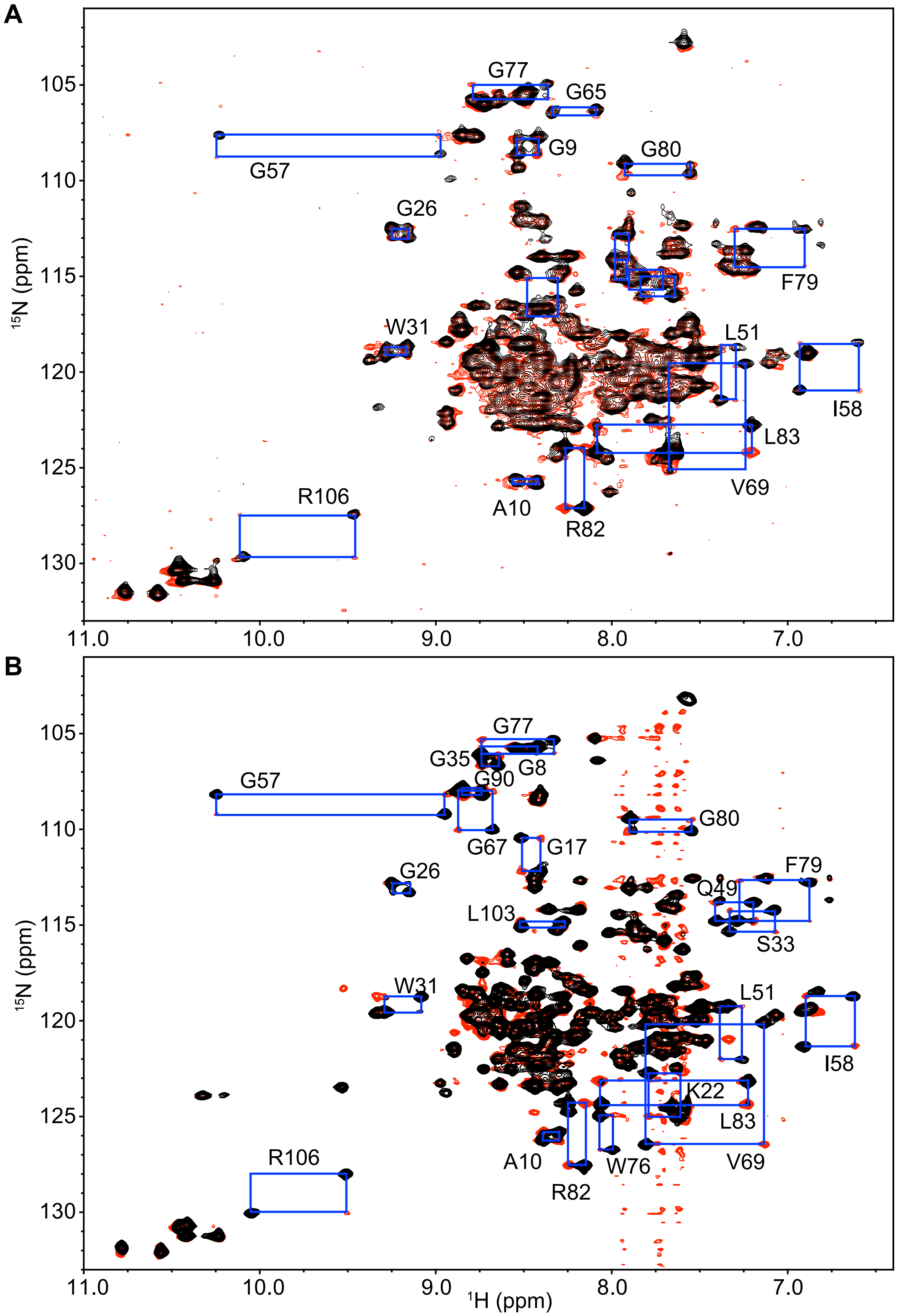

Figure 6. Overlay of a representative ZZ-exchange plane (red) with the $^{15}N/^{1}H$ TROSY HSQC (black) of EmrE bound to each of the tetrahedral ligands: (**A**) $EtTPP^+$, 45ms; (**B**) $MBTPP^+$, 80ms; and (**C**) $DPhTPP^+$, 200ms. For TPP^+-bound EmrE, see Morrison, et al., 2012.

C

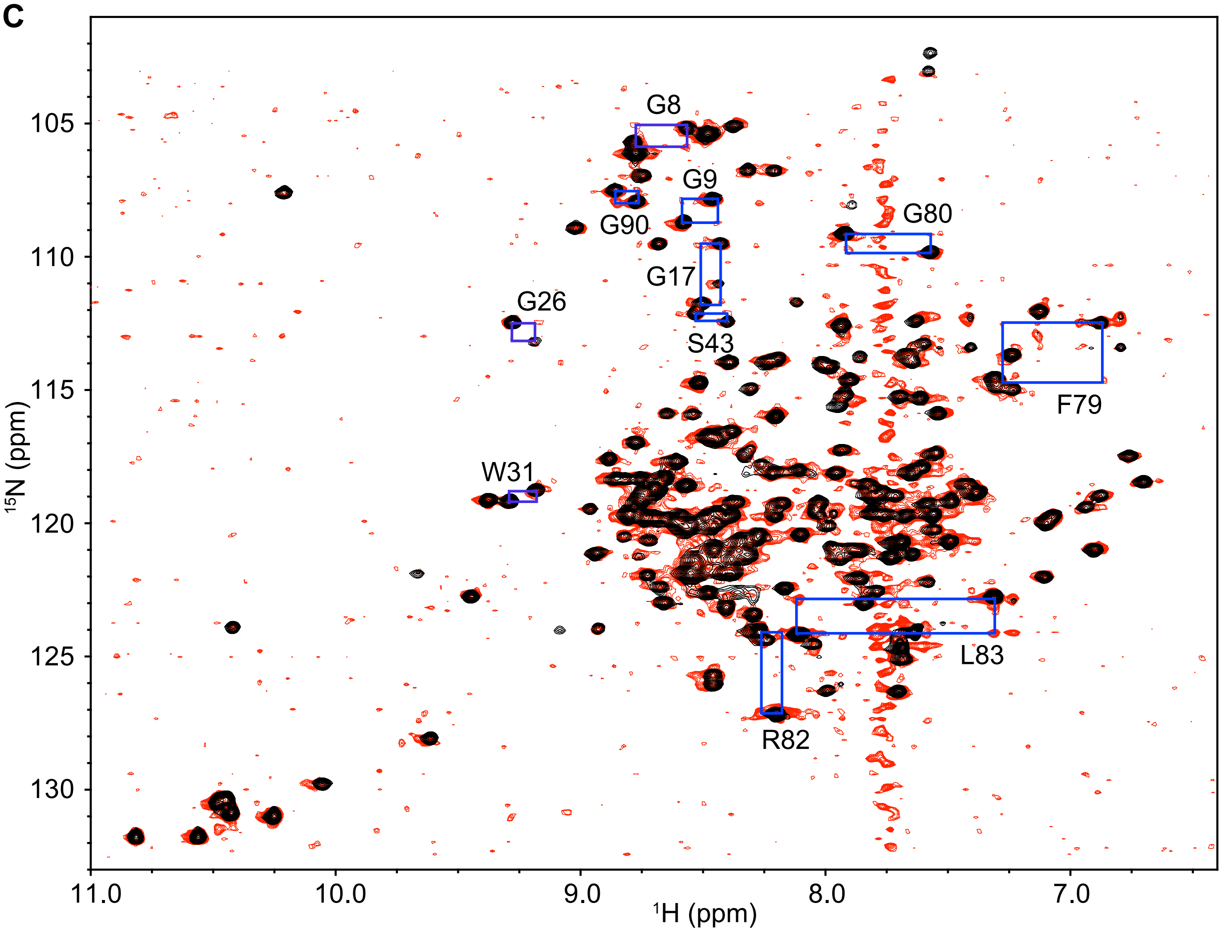

G8
G9
G80
G90
G17
G26
S43
F79
W31
L83
R82
105
110
115
120
125
130
^{15}N (ppm)
11.0
10.0
9.0
8.0
7.0
^{1}H (ppm)

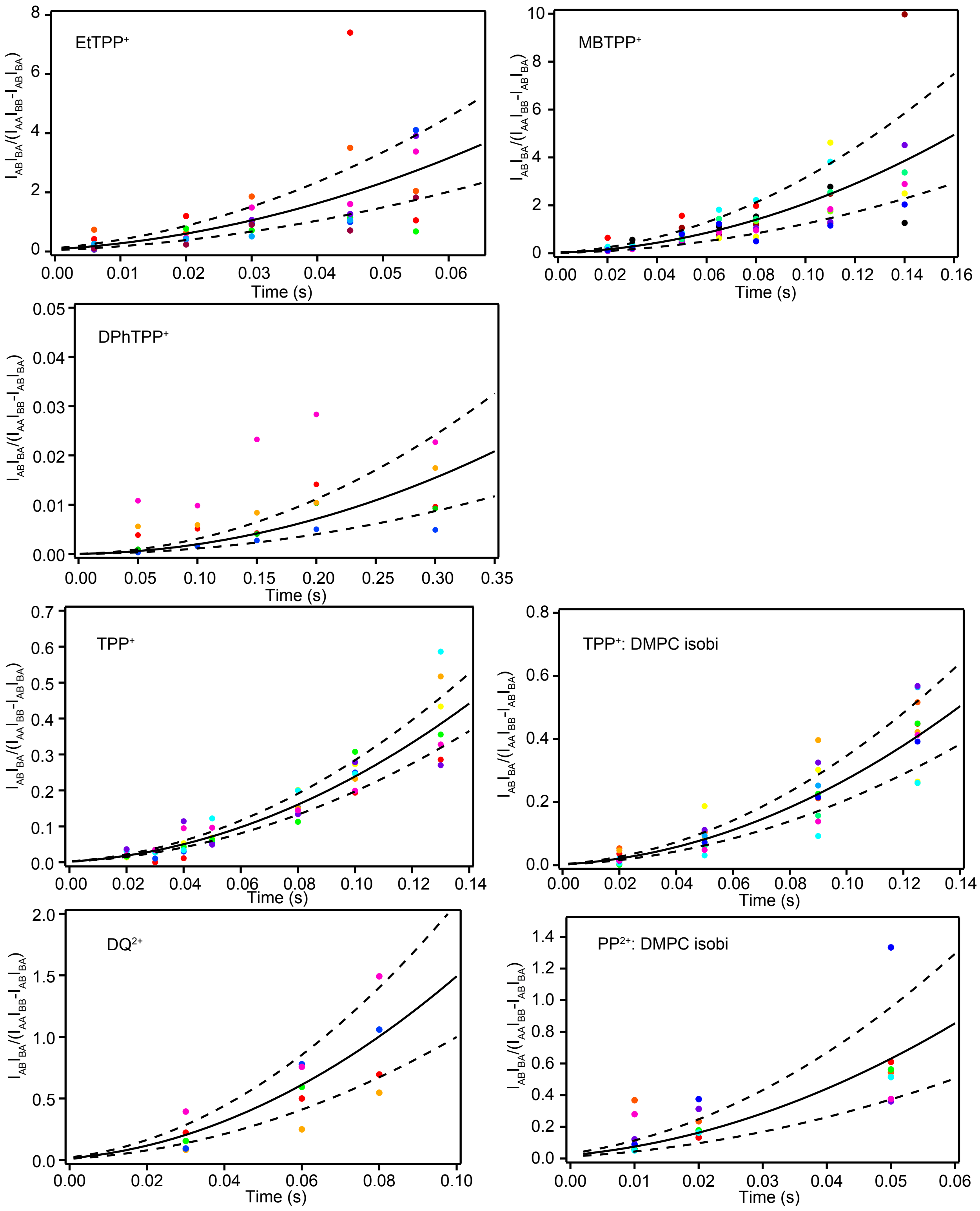

Figure 7. Composite peak ratio analysis plotted for each ligand-bound sample. Each residue used in the global fit is plotted in a different color (color-residue relationship does not hold across samples). The solid black line shows the global fit to each ligand-bound form, as summarized in **Table 1**. The dashed black line shows the error in the fit, which was taken as the standard deviation of the individual fits to each residue.

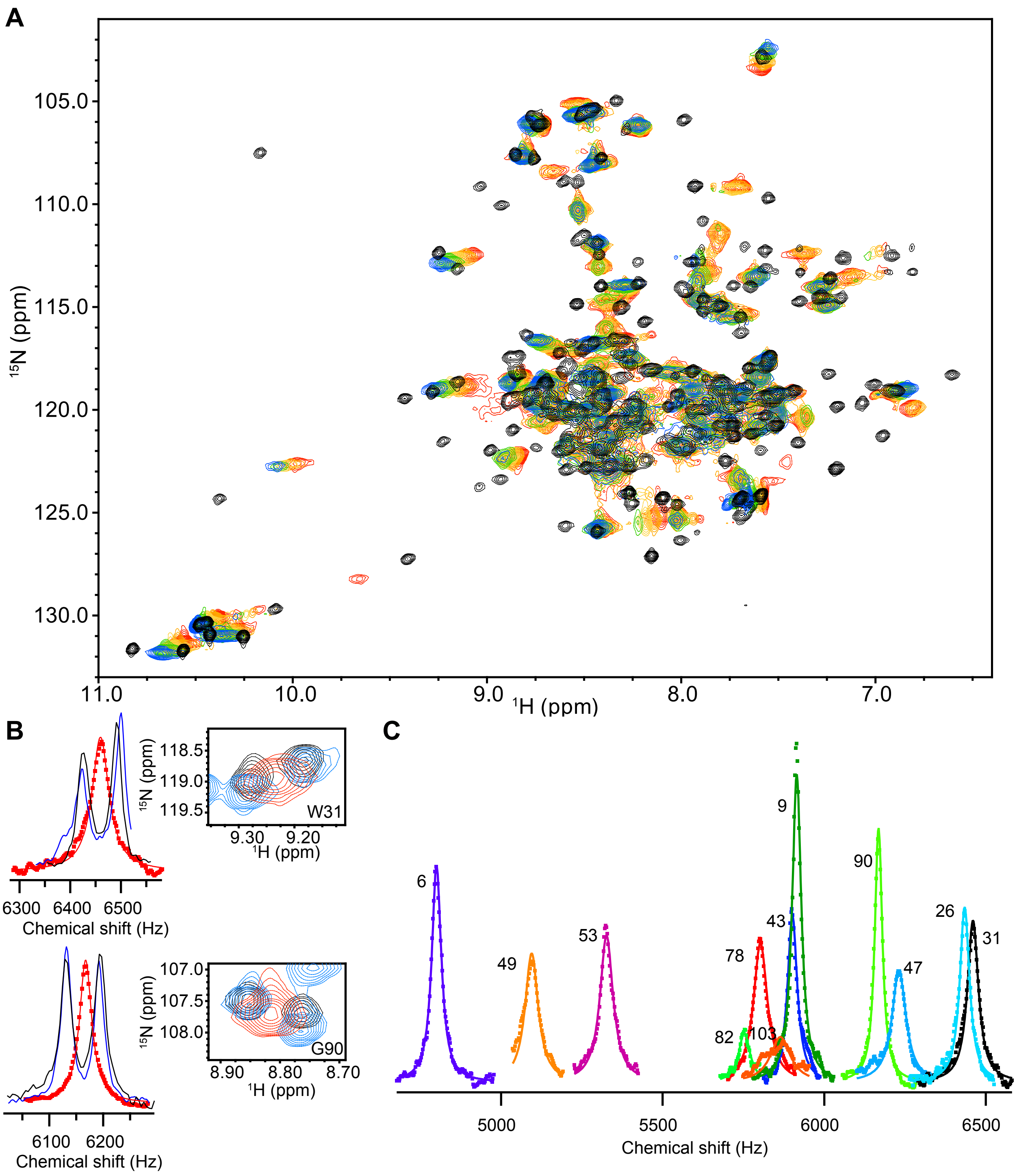

Figure 8. EmrE bound to MeTPP$^+$ is in fast exchange. **A.** Overlay of $^{15}N/^{1}H$ TROSY HSQC spectra of TPP$^+$-bound EmrE (black) with the temperature titration of MeTPP$^+$-bound EmrE: 63°C (red), 56°C (orange), 52°C (yellow), 45°C (green), and 40°C (blue). All MeTPP$^+$-bound spectra were collected with d1 = 6s. **B.** Representative fits from lineshape analysis for residues W31 (top) and G90 (bottom) alongside the $^{15}N/^{1}H$ TROSY HSQC overlay for EmrE bound to TPP$^+$ (black), DPhTPP$^+$ (blue) and MeTPP$^+$ (red). **C.** Global fit to 12 residues in a lineshape analysis of the MeTPP$^+$-bound EmrE data (see methods), giving a fit of $k_{conf} = 190 \pm 80\ s^{-1}$.

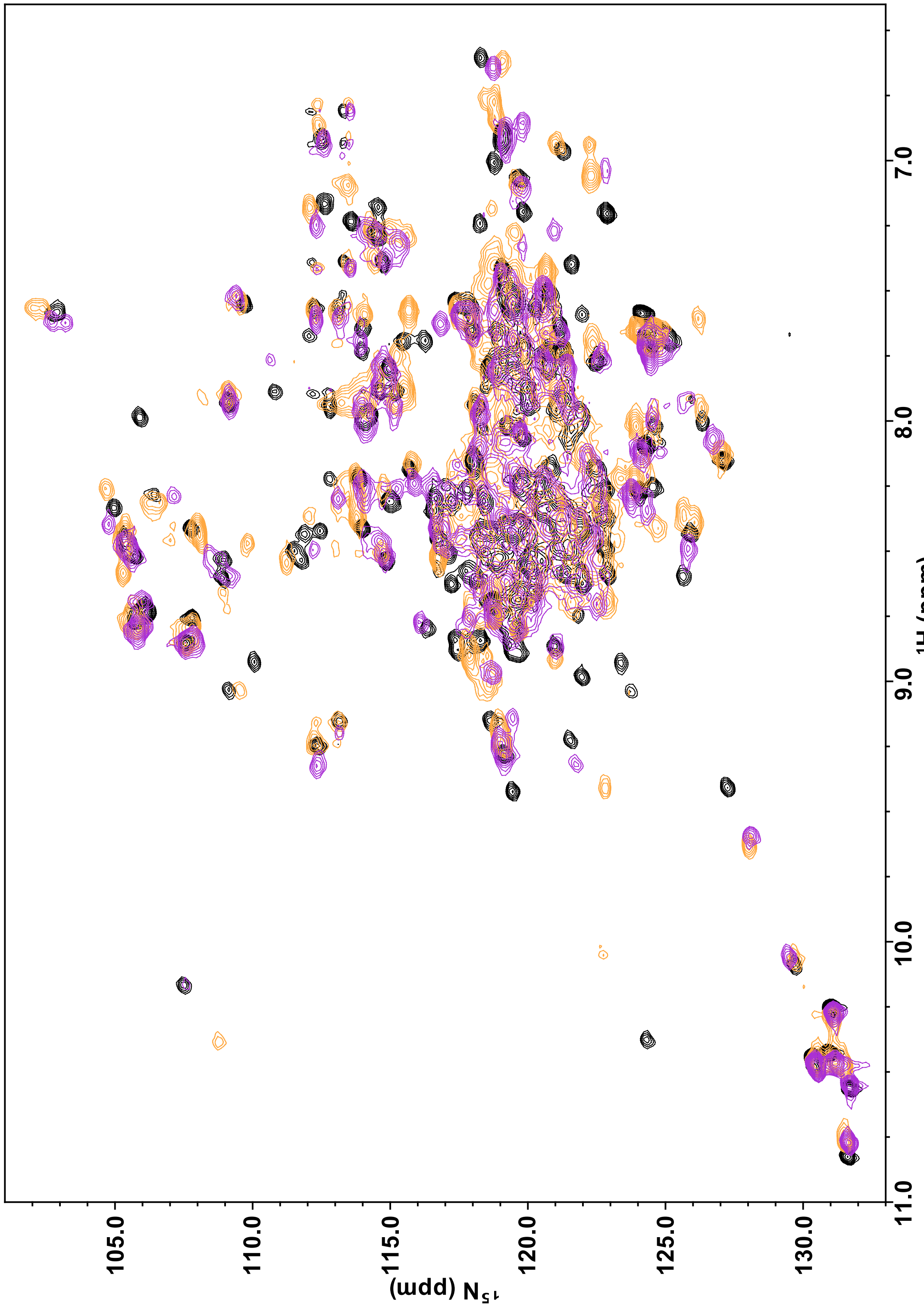

Figure 9. NMR spectra of EmrE bound to the tetrahedral and planar substrates indicate the same overall protein structure but varying dynamics. Overlay of TPP$^+$-bound EmrE (black) with EmrE bound to the two planar ligands, PP^{2+} (DMPC bicelles; orange) and DQ^{2+} (purple). All spectra were collected identically at pH 7 and 45°C.

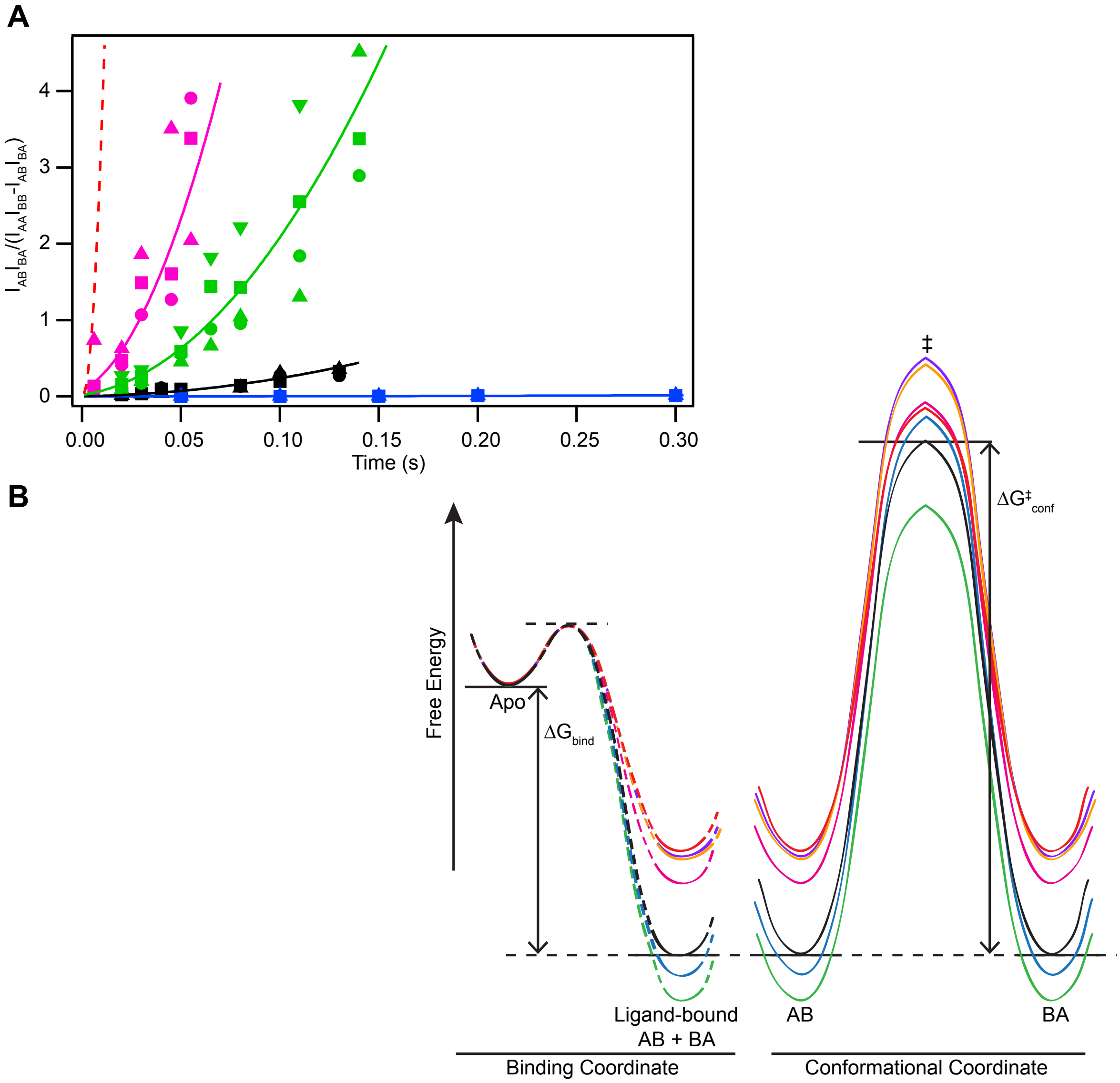

Figure 10. Substrate identity determines rate of EmrE conformational exchange. **A.** Composite peak ratio analysis of ZZ-exchange data shows significantly different exchange rates for EmrE bound to TPP^{+} (black) and the other slow-exchanging derivatives, $EtTPP^{+}$ (magenta), $MBTPP^{+}$ (green), and $DPhTPP^{+}$ (blue). Global fits are depicted with solid lines, along with data points for several representative residues from each ligand. The dashed red line corresponds to a simulation of the composite peak ratio of $MeTPP^{+}$ using the rate of conformational interconversion determined via lineshape analysis (**Fig. 8**). **B.** A simplified energy diagram illustrates the connection between ligand-binding (left) and conformational exchange between the open-in (AB) and open-out (BA) states of ligand-bound EmrE (right). The free energy of binding, ΔG_{bind}, was calculated from measured binding affinities. The dashed lines indicate that nothing is known about the transition state connecting the apo and bound states of EmrE. The two ligand-bound ground states (AB and BA) have equal energy and are separated by the transition state, ‡, with energetic barrier of height $\Delta G^{‡}_{conf}$ calculated from the rates of conformational interconversion and transition state theory. The same ligand color scheme is used as in (**A**) for the tetrahedral ligands, with the addition of the planar substrates DQ^{2+} (purple) and PP^{2+} (orange).

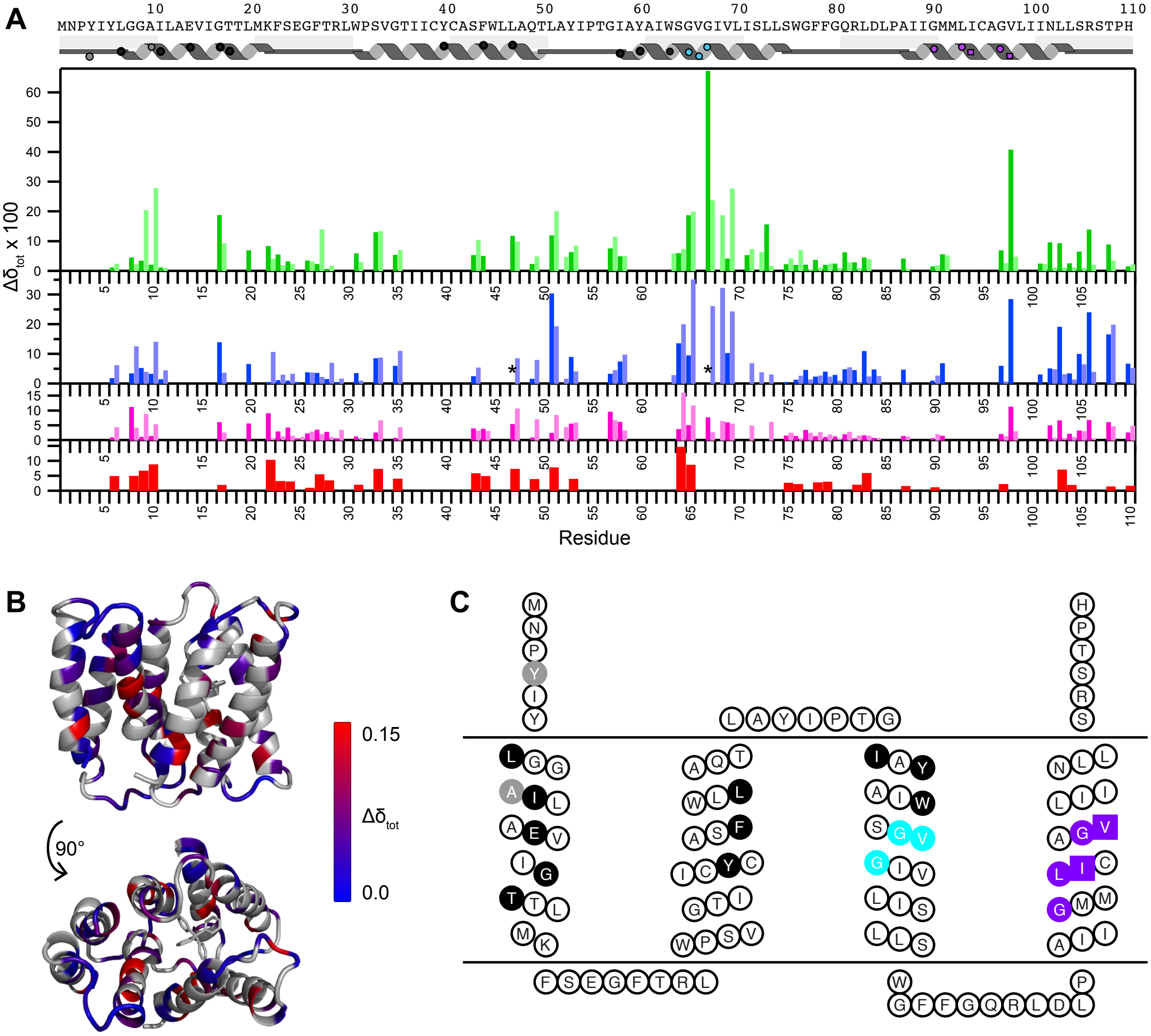

Figure 11. Chemical shift differences highlight important functional residues. **A.** Chemical shift changes between TPP$^+$-bound EmrE and EmrE bound to other TPP$^+$-derivatives (MeTPP$^+$, red; EtTPP$^+$, magenta; DPhTPP$^+$, blue; MBTPP$^+$, green). States A and B are distinguished via the dark and light shades, respectively. Due to a lack in connectivity, state A vs. B is not known for residues 17, 31, 67, 98, and 108. The asterisk (*) indicates that the peak moves significantly, but the exact assignment is uncertain. Residues with no data indicate a lack of transferred assignment. The approximate secondary structure according to the crystal structure is shown at the top and includes symbols to allow easy comparison with (**C**). **B.** Chemical shift differences between MBTPP$^+$- and TPP$^+$-bound EmrE, plotted onto the TPP$^+$-bound structure (PDB 3B5D, PyMOL) reveal regions sensitive to ligand identity. Residues in grey indicate a lack of data. **C.** EmrE topology diagram highlighting specific functional regions of EmrE based on previously published mutagenesis studies: direct substrate binding and substrate specificity (black), TPP$^+$/H$^+$ coupling (grey), GVG helix kink motif (cyan), and GG7 dimerization motif (purple, squares represent "pivot point"). Figure made using TOPO2 (http://www.sacs.ucsf.edu/TOPO2/).

Chapter V. Conclusion and Future Directions.

My thesis studies have focused on the transport mechanism of the small multidrug resistance transporter EmrE. Biophysical investigations required that EmrE be reconstituted into a membrane mimetic environment that produced reproducible, long-lived samples that would be stable at elevated temperatures for extended periods of time. I optimized a protocol for the reconstitution of EmrE into isotropic bicelles, or small bilayer discs that are capped off by short-chain lipid. Isotropic bicelles preserve a native bilayer environment, while meeting the fast-tumbling requirements for solution NMR. In addition, the optical clarity of these bicelles makes them suitable for absorbance and fluorescence measurements. Although I only carried out extensive studies in a limited lipid composition, I found that the protocol allowed for EmrE to be reconstituted into bicelles with a variety of lipid compositions, including mixtures of synthetic lipids and even *E. coli* lipid extract. Interestingly, comparison of $^{15}N/^{1}H$ TROSY HSQC spectra of TPP^{+}-bound EmrE reconstituted in an assortment of these lipid compositions indicated that EmrE has the same overall structure in each of these environments, but with local structural changes and potential changes in dynamics that would be an interesting avenue of exploration for future studies in the lab.

Using this optimized system, we made the first direct observation of conformational exchange between the inward- and outward-facing states of TPP^{+}-bound EmrE. This study is among the first of functional transport motions in the literature, with others including single-molecule FRET work on the sodium-dependent amino acid transporters LeuT and Glt_{Ph}[1-3]. Our investigations provided support for Fleishman's model of exchange between AB and BA conformations in an asymmetric, antiparallel homodimer[4]. We directly quantified this conformational interconversion, and confirmed that the two low-energy conformations being observed were indeed structures that were only open to one side of the membrane at a time, as required by the single-site alternating-access model for transport. In Fleishman's model, the two monomers swap states within the dimer such that, although the dimer is asymmetric, the open-in and open-out structures are related by a two-fold axis of symmetry within the membrane bilayer. Two-fold symmetry and inverted repeats, which is essentially dual topology of two domains within a monomeric protein, are common themes within the transporter field[5,6]. As analyzed in detail for the prolific LeuT fold, inverted repeats inherently have pseudo-two-fold symmetry axes in the bilayer plane[5], and the SMRs are likely to be another family with this global property. Dual repeats and two-fold exchange symmetry within the membrane bilayer is an elegant way to arrive at two low-energy conformations[4], the inward- and outward-facing conformations of the alternating-access mechanism for transport.

How is this elegant mechanism for conformational exchange by a dual topology protein exploited by EmrE to carry out *multidrug* transport? EmrE recognizes a diverse range of polyaromatic cations and binds these substrates with affinities ranging over many orders of magnitude. Even what seems like a small change in ligand structure, such as the substitution of a single position in a tetrahedral compound, has a profound impact on binding, conformational interconversion, and transport function. How can this be? We know that ligand hydrophobicity has a strong effect on binding enthalpies, which in turn is positively correlated with binding affinity. We also know that cryoEM projection maps suggest a difference in conformation/helix tilt between one tetrahedral and three planar ligands[7]. Thus, there are several contributing factors affecting the energetics of the system: direct protein-ligand interactions and structural changes that alter the architecture of the binding site and mechanistic hotspots. Using apo EmrE as the common reference state and assuming relatively small differences between the energies of the unbound substrate, it is clear that substrate binding lowers the ground state energy to different extents (see **Fig. 10B** of **Chapter 4**). However, by using transition-state theory to calculate the barrier height to interconversion for each EmrE-substrate complex, it is clear that substrate identity also differentially affects the transition state. A functional antiporter cannot interconvert in its truly apo form. Thus, ligand binding must lower the transition state significantly. However, the transition state is not the same between different EmrE-substrate complexes. In such a small transporter, the binding site overlaps with structural regions important for interconversion, so the effects of substrate on these two aspects of function (binding and conformational exchange) are convoluted. What initially seems like a small change in ligand structure, such as the substitution of a methyl group for a phenyl group in a tetrahedral phosphonium compound, actually has a large effect on hydrophobic interactions with the binding site. Because the binding site overlaps with hotspots involved in interconversion, these changes in ligand also manifest themselves as changes in conformational exchange, albeit to a lesser extent. For more dramatic changes in ligand structure, such as moving from a tetrahedral, $^{+}1$ ligand (e.g. TPP^{+}) to a planar, $^{+}2$ ligand (e.g. PP^{2+}), changes in the helix tilt have a clearer impact on the interconversion hotspots.

My thesis work has focused on the conformational interconversion of EmrE when bound to a polyaromatic cation substrate, as this is the step that moves the drug across the membrane barrier and provides the most insight into multidrug recognition. However, the proton side of the transport cycle is key to understanding how EmrE couples the efflux of drug to its energy source. We are currently working to fill in the mechanistic details of the full transport cycle (**Fig. 1**).

Further investigation into the mechanism of multidrug transport: Drug binding is coupled to proton antiport.

The proton gradient across the inner membrane is the energy source for polyaromatic cation drug efflux by EmrE. The TM helices of integral membrane proteins are largely hydrophobic to stabilize interactions with neighboring TM helices and the surrounding lipid membrane. However, transporters of ions and charged compounds require polar and charged residues to coordinate these substrates along the translocation pathway[8]. EmrE only has one charged residue within the TM helices—the highly conserved glutamate 14, which binds proton or polyaromatic cation substrate. The other seven charged amino acids are found in loop regions or ends of helices and can be mutated to cysteine without affecting function[9,10]. The Schuldiner lab has shown via mutagenesis and reactivity with the carbodiimide DCCD, which inactivates the protein, that E14 is critical for transport activity [9,10]. E14 is the basis of the proton-drug coupling mechanism of the single-site alternating-access model of transport.

Based on data published to date, EmrE has been thought to bind *either* two protons *or* one substrate molecule[8,11] and to have a strict $2H^+$:1 polyaromatic cation transport stoichiometry[12]. Drug binding and transport activities are strongly dependent on pH. The tightest drug binding occurs at high pH where there are fewer competing protons[13]. Substrate binding stimulates proton release, and rates of substrate binding and substrate-induced release of protons are faster at higher pH[14].

Understanding how substrates with a charge of $^+1$ vs. $^+2$ are transported will help to understand how proton and drug transport are coupled. Based on assays carried out on EmrE in *E. coli* and reconstituted into liposomes, Schuldiner and co-workers claim that transport stoichiometry is always $2H^+$:1 drug, regardless of substrate charge[12] (**Fig. 2A**). EmrE provides resistance to *E. coli* against both TPP$^+$ and methyl viologen^{2+} (MV^{2+}) in the presence of a pH gradient[12]. However, when the pH gradient is replaced by an electric potential, EmrE only provides resistance against the $^+$1 ligand[12]. Similarly, in liposomes, EmrE can transport TPP$^+$ but not MV^{2+} when the driving force is an electric potential[12]. Schuldiner and co-workers claim that these results imply that transport of TPP$^+$ is electrogenic but transport of MV^{2+} is electroneutral[12]. However, just because something *can* happen, doesn't mean that it *must* happen. One could envision that the two E14 residues of an EmrE dimer could coordinate: 1 × $^+$2 ligand, 1 × $^+$1 ligand, 1 × $^+$1 ligand + 1 × H$^+$, or 2 × H$^+$ (**Fig. 2A, B**).

I have performed ΔpH-driven PP^{2+}- and TPP$^+$-transport assays on EmrE reconstituted into liposomes (**Fig. 3**). If transport were electrogenic, a charge gradient would quickly build up that would halt transport. Addition of the K$^+$-ionophore valinomycin would dissipate this gradient and re-start transport. However, in my assays, ΔpH-driven transport of both the $^+$1 and $^+$2 charged ligand proceeded independently of valinomycin. Thus, an electric potential was not built-up during the transport of TPP$^+$. Perhaps EmrE can transport a $^+$1 charged ligand electroneutrally (1H$^+$:1 drug stoichiometry) or electrogenically (2H$^+$:1 drug stoichiometry), depending on which driving forces are present.

Future experiments are planned that will employ ITC in order to probe the linkage between proton and TPP$^+$ binding. We will perform ITC titrations of TPP$^+$ binding to EmrE at a range of pH values. Proton-linked equilibria are challenging to study because protons also bind buffers. In order to tease apart the binding of protons to buffer and protein, these titrations will be carried out in a range of buffers[15,16]. In the end, a combination of titrations performed at different pH values and buffer conditions will provide the intrinsic binding constants for TPP$^+$ and proton and determine whether a proton and TPP$^+$ are capable of binding EmrE simultaneously, as in **Fig. 2B**. The intrinsic binding constant for protons is of course related to the pK_a of E14.

The pK_a of E14 is elevated in EmrE in order to couple transport to the proton gradient at physiological pH values. Current estimates from the literature put the value between 7.3 and 8.5[13,14,17]. Canonical pK_a values for Asp and Glu lie in the range of 3.90 and 4.35, respectively, based on titrations on the blocked tripeptide Ac-Ala-Asp(Glu)-Ala-NH_2[18]. Measured pK_a values for surface-exposed acidic residues in the model soluble protein staphylococcal nuclease (SNase) are similar to those values, and some are even depressed[18]. How can the pK_a of E14 lie around physiological pH? The affect of burying an ionizable residue in the hydrophobic interior of a protein has been investigated in SNase. Elevated pK_a values were measured for glutamates buried at over 20 positions, with values ranging from 5.2-9.4 and an average of 7.7[19]. These acidic residues can be stably accommodated within the hydrophobic protein interior without causing any major structural changes by increasing the probability of protonation [19].

We will also attempt to measure the pK_a of E14 using NMR. The pH-dependent ITC experiments will provide the pK_a value(s) of EmrE, but NMR will allow us to directly observe E14. NMR determinations of pK_a come with their own challenges. If the resonances for E14 in states A and B are overlapped, we will not be able to analyze their chemical shifts. In addition, specifically labeled glutamate samples are expensive and difficult to make due to amino acid scrambling. With the high resolution that this technique affords, we will hopefully be able to determine whether the two E14 within the dimer are truly symmetric, as suggested in the literature[20]. I hypothesize that the two active-site E14 residues are asymmetric, but that both have highly elevated pK_a values.

Further investigation into the mechanism of multidrug transport: Drug binding.

One of my current aims is to further pursue the questions of multidrug transport brought up in **Chapter 4**. It is clear that binding affinity, the rate of the open-in to open-out conformational exchange, and transport rate all depend on the identity of the bound substrate. What is (are) the rate-limiting step(s) of transport? According to the single-site alternating-access model for antiport (**Fig. 1**), ligand association, ligand dissociation and conformational interconversion are candidates. Pre-steady-state kinetic studies of the binding of three different ligands to EmrE suggest that binding is diffusion-limited[14], which leaves ligand dissociation and the open-in to open-out transition. We used our substrate binding constants measured via ITC, in conjunction with ligand association rates based on Schuldiner's studies in detergent[14] and corrected for the temperature dependence of diffusion, to estimate dissociation rates for five tetrahedral ligands (**Chapter 4**). According to these calculations, dissociation rate is within an order of magnitude of the rate of conformational exchange for all but one ligand. Thus, both steps are likely to contribute to transport, and precise measurements of dissociation rates are required.

There are several processes involved in the transport mechanism of EmrE that could convolute an attempt to determine ligand association and dissociation rates, such as proton binding, dimerization, and conformational exchange process(es). Previous attempts at reproducing the stopped-flow experiments of Schuldiner and co-workers[14] for EmrE reconstituted into isotropic bicelles revealed that the data could not be fit to the simple mechanism of a single binding event. Attempts to push the system toward a fully-dimerized, fully-deprotonated state to focus on ligand on/off resulted in substrate binding reactions that were largely lost in the instrument deadtime.

My current approach is to take one of the competing process, protein dimerization, out of the equation. We are using methyl CPMG NMR experiments to measure ligand association and dissociation rates of MeTPP$^+$-EmrE at pH 7. This technique allows us to directly monitor natural-abundance ^{13}C of the ligand in the presence of unlabeled, fully-dimerized EmrE. We have collected data sets for 25 and 45°C at two ratios of free:bound ligand. Comparison of the ratio of off- and on-rates measured via methyl CPMG at 45°C to the dissociation constant measured via ITC under the same conditions will provide a check for the validity of this method.

The benefit of this NMR technique is that it allows us to directly follow the ligand. However, MeTPP$^+$ is the only substrate that can be studied using methyl CPMG NMR because it is the only ligand with an isolated methyl spin system. MeTPP$^+$ will be used to bridge the two techniques. We can use the CPMG data to establish a well-defined system for stopped-flow kinetics studies of fully-dimerized EmrE (determined from measurements of dimerization constant by S. Dutta) at pH 7 and 25°C. Once the system is established, we can proceed to measure the on/off rates of other ligands.

Conclusion.

The overall aim of my research is to understand the complete transport cycle of the small multidrug resistance transporter EmrE (**Fig. 1**). My thesis work focused on the global exchange between the inward- and outward-facing conformations of EmrE (**Fig. 1**, bottom row) when bound to diverse substrates. The remaining steps to be addressed are the association and dissociation of substrates (protons and polyaromatic cation) and the conformational exchange of protonated EmrE (**Fig. 1**, top row).

References:

1. Zhao, Y. *et al.* Single-molecule dynamics of gating in a neurotransmitter transporter homologue. *Nature* **465,** 188–193 (2010).
2. Zhao, Y. *et al.* Substrate-modulated gating dynamics in a Na+-coupled neurotransmitter transporter homologue. *Nature* **474,** 109–113 (2011).
3. Akyuz, N., Altman, R. B., Blanchard, S. C. & Boudker, O. Transport dynamics in a glutamate transporter homologue. *Nature* **502,** 114–118 (2013).
4. Fleishman, S. J. *et al.* Quasi-symmetry in the cryo-EM structure of EmrE provides the key to modeling its transmembrane domain. *J Mol Biol* **364,** 54–67 (2006).
5. Forrest, L. R. & Rudnick, G. The rocking bundle: a mechanism for ion-coupled solute flux by symmetrical transporters. *Physiology (Bethesda)* **24,** 377–386 (2009).
6. Shi, Y. Common Folds and Transport Mechanisms of Secondary Active Transporters. *Annu. Rev. Biophys.* **42,** 51–72 (2013).
7. Korkhov, V. M. & Tate, C. G. Electron crystallography reveals plasticity within the drug binding site of the small multidrug transporter EmrE. *J Mol Biol* **377,** 1094–1103 (2008).
8. Yerushalmi, H. & Schuldiner, S. A model for coupling of H(+) and substrate fluxes based on ‘time-sharing’ of a common binding site. *Biochemistry* **39,** 14711–14719 (2000).
9. Yerushalmi, H. & Schuldiner, S. An essential glutamyl residue in EmrE, a multidrug antiporter from Escherichia coli. *J Biol Chem* **275,** 5264–5269 (2000).
10. Yerushalmi, H., Mordoch, S. S. & Schuldiner, S. A single carboxyl mutant of the multidrug transporter EmrE is fully functional. *J Biol Chem* **276,** 12744–12748 (2001).
11. Yerushalmi, H. & Schuldiner, S. A common binding site for substrates and protons in EmrE, an ion-coupled multidrug transporter. *FEBS Lett* **476,** 93–97 (2000).
12. Rotem, D. & Schuldiner, S. EmrE, a multidrug transporter from Escherichia coli, transports monovalent and divalent substrates with the same stoichiometry. *J Biol Chem* **279,** 48787–48793 (2004).
13. Muth, T. R. & Schuldiner, S. A membrane-embedded glutamate is required for ligand binding to the multidrug transporter EmrE. *EMBO J* **19,** 234–240 (2000).
14. Adam, Y., Tayer, N., Rotem, D., Schreiber, G. & Schuldiner, S. The fast release of sticky protons: kinetics of substrate binding and proton release in a multidrug transporter. *Proc Natl Acad Sci USA* **104,** 17989–17994 (2007).
15. Kozlov, A. G. & Lohman, T. M. Large contributions of coupled protonation equilibria to the observed enthalpy and heat capacity changes for ssDNA binding to Escherichia coli SSB protein. *Proteins* **Suppl 4,** 8–22 (2000).
16. Armstrong, K. M. & Baker, B. M. A comprehensive calorimetric investigation of an entropically driven T cell receptor-peptide/major histocompatibility complex interaction. *Biophysical Journal* **93,** 597–609 (2007).
17. Soskine, M., Adam, Y. & Schuldiner, S. Direct evidence for substrate-induced proton release in detergent-solubilized EmrE, a multidrug transporter. *J Biol Chem* **279,** 9951–9955 (2004).
18. Castañeda, C. A. *et al.* Molecular determinants of the pKa values of Asp and Glu residues in staphylococcal nuclease. *Proteins* **77,** 570–588 (2009).
19. Isom, D. G., Castañeda, C. A., Cannon, B. R., Velu, P. D. & García-Moreno E, B. Charges in the hydrophobic interior of proteins. *Proc Natl Acad Sci USA* **107,** 16096–16100 (2010).

20. Schuldiner, S. EmrE, a model for studying evolution and mechanism of ion-coupled transporters. *BBA - Proteins and Proteomics* 1–15 (2009). doi:10.1016/j.bbapap.2008.12.018

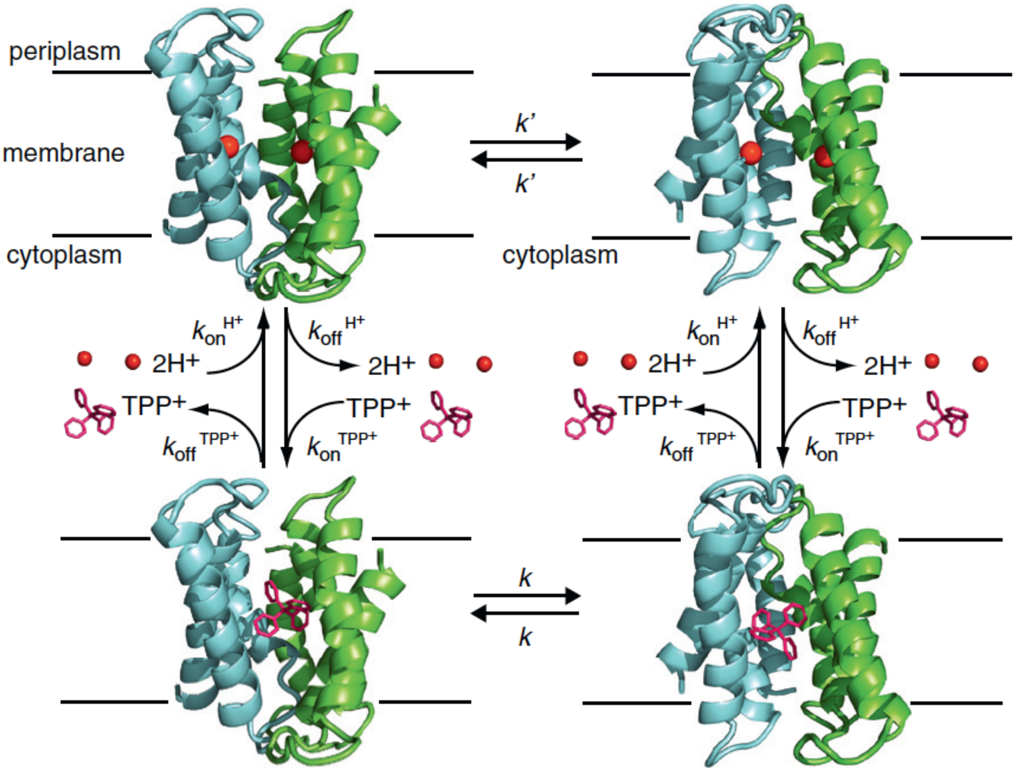

Figure 1. Transport cycle for EmrE. EmrE interconverts between outward- and inward-facing states when bound to substrate (proton, top or drug, bottom). The two states have equal populations, thus, the forward and reverse rates are identical when a given substrate is bound. Either two protons or a single polyaromatic cation binds EmrE at one time. Figure from Henzler-Wildman, K. A. *Curr Opin Struct Biol* **22,** 38-41 (2012).

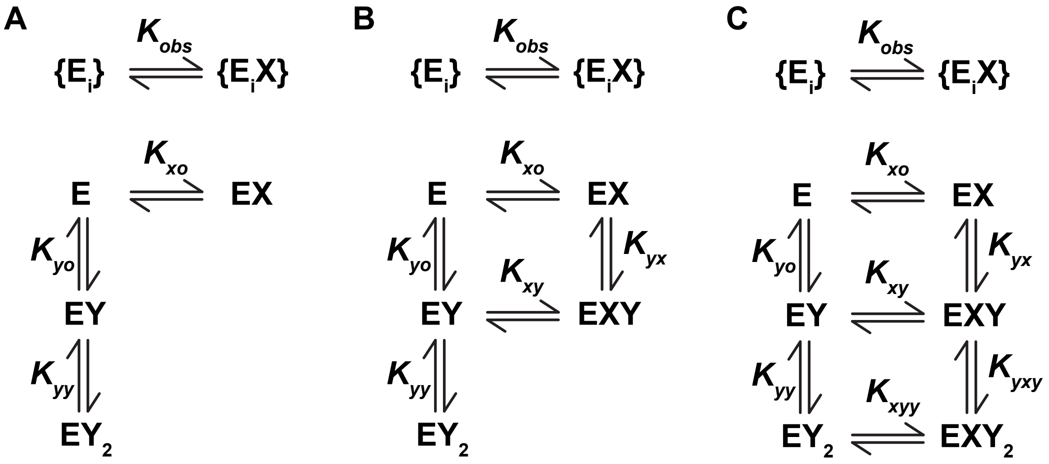

Figure 2. Possible schemes for the binding of two different ligands (X or Y) to protein (E, the EmrE dimer). The Schuldiner lab proposes that only two protons (Y) or one polyaromatic cation (X) can bind, independent of substrate charge, supporting scheme (**A**). However, my data suggests that scheme (**A**) or (**B**) may be possible for EmrE, depending on whether the competing ligand is a $^{+}2$ or $^{+}1$ compound, respectively. There is no support for scheme (**C**), a scheme that allows for the simultaneous binding of two protons and one drug molecule.

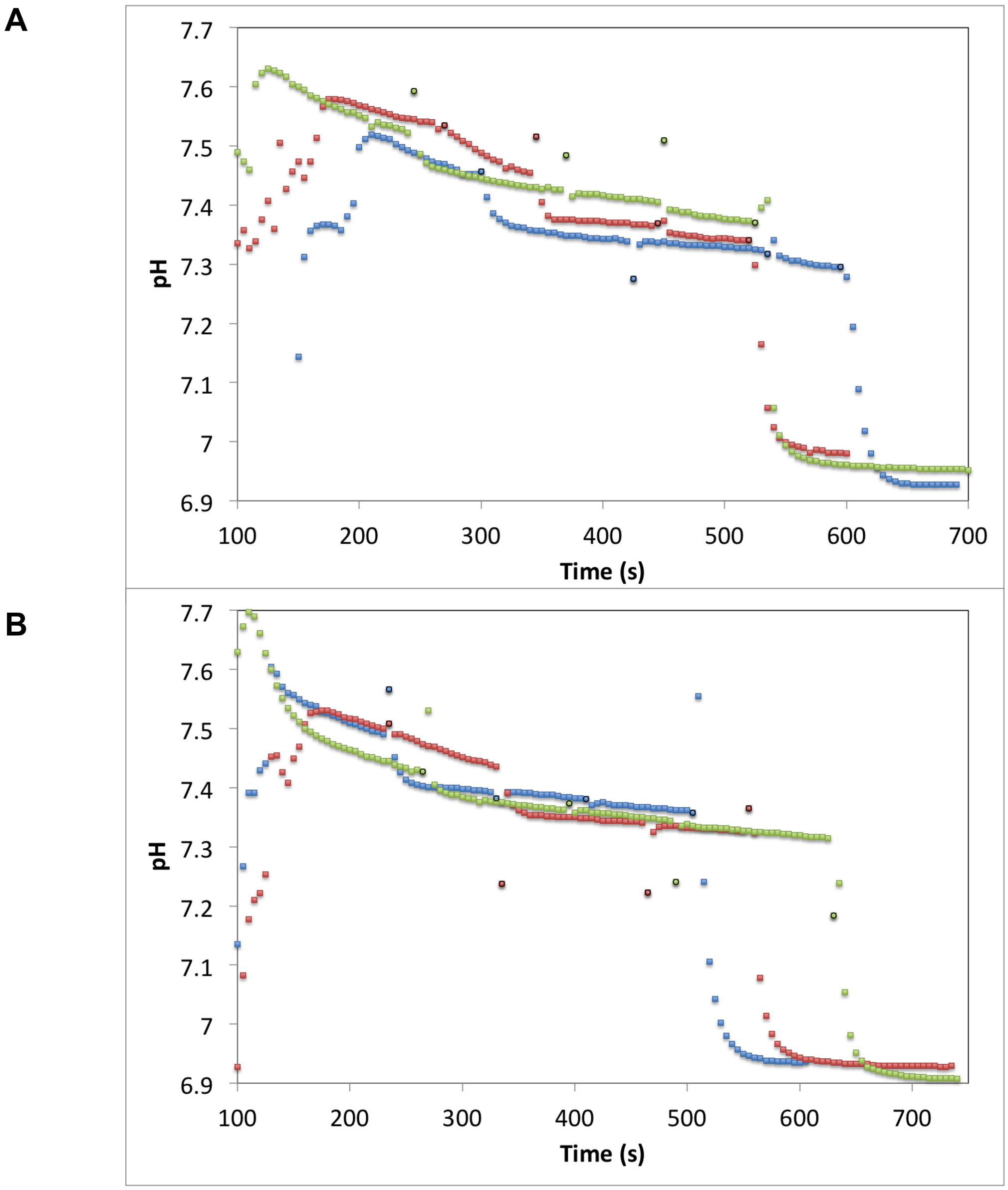

Figure 3. Transport by EmrE is electroneutral. Transport is not electrogenic for either a $^{+}1$ or $^{+}2$ charged ligand, under the conditions of the assay. EmrE (26 μM) was reconstituted into 20 mg/mL POPE/POPG 3:1 (wt/wt) liposomes. The pH of the bulk solution was monitored over time. A pH gradient was introduced across the liposome between the weakly buffered exterior solution (1 mM KPi, 300 mM KCl, pH ~7.6) and the strongly buffered interior volume (20 mM KPi, 300 mM KCl, pH 6) by addition of base. The affect of the order of addition on transport was tested by adding: (i) ~40 μM ligand, 1 μg/mL valinomycin, ~40 μM ligand, and 1 μg/mL FCCP (blue traces) or (ii) 1 μg/mL valinomycin, ~40 μM ligand, ~40 μM ligand, and 1 μg/mL FCCP (red traces) for both PP^{2+} (**A**) and TPP^{+} (**B**). Black circles mark each addition. For both substrates, transport was initiated by the addition of ligand, independent of whether the K^{+}-ionophore valinomycin was present. Pre-incubation with an 8-fold excess of the carbodiimide DCCD over protein greatly inhibits transport (green traces, compounds added according to (i)), indicating that this assay is monitoring transport by EmrE. The addition of the protonophore FCCP demonstrates that a pH gradient was held across the liposomes.